1977

Determination of subcritical reactivity in a liquid-metal-cooled fast breeder reactor by the coherence function method

Norman Hai-Ming Koo
Iowa State University

Determination of subcritical reactivity in a liquid-metal-cooled fast breeder reactor by the coherence function method

by

Norman Hai-Ming Koo

A Dissertation Submitted to the

Graduate Faculty in Partial Fulfillment of

The Requirements for the Degree of

DOCTOR OF PHILOSOPHY

Department: Chemical Engineering and Nuclear Engineering
Major: Nuclear Engineering

Approved:

Signature was redacted for privacy.

In Charge of Major Work

Signature was redacted for privacy.

For the Major Department

Signature was redacted for privacy.

For the Graduate College

Iowa State University
Ames, Iowa
1977

TABLE OF CONTENTS

NOMENCLATURE

Symbols	Descriptions	Units
English		
$a(t)$	detection network response at time t	picocoulomb/ detection
$A(\omega)$	detection network transfer function at frequency ω	picocoulomb-sec/detection
$B(x,\omega)$	coefficient matrix (of TASK code) at space point x and frequency ω	cm^{-1}
C	number of counts in interval T	counts
$\dot{C}$	count rate	counts/sec
C'	correction factor of the modified relation for subcritical reactivity	dimensionless
C_i	concentration of the i-th group delayed neutron precursor	$nuclei/cm^3$
C_ω	polarity correlation of signals at frequency ω	+1 or -1
D	Diven factor of Pu-239	dimensionless
D'	Diven factor of Pu-240	dimensionless
F	total fission rate of the whole reactor	fissions/sec
F_{nf}	neutron induced fission rate	fissions/sec
F_{sf}	spontaneous fission rate	fissions/sec
g_N	probability of N neutrons released in the starting event (of a fission chain) by a Pu-240 spontaneous fission or a delayed neutron induced fission of Pu-239	dimensionless
$g(r_n,t)$	response function of the neutron multiplication and detection system	picocoulomb/ fission

Symbols	Descriptions	Units
$G(\omega)$	transfer function of the neutron multiplication and detection system	picocoul-sec/ fission
$G(\Delta x, \omega)$	scattering matrix/response matrix (of TASK code) for slab thickness of Δx and at frequency ω	dimensionless
$G_{12}(\Delta x, \omega)$ $G_{21}(\Delta x, \omega)$	reflection matrix (of TASK code) for slab thickness Δx and at frequency ω	dimensionless
$G_{11}(\Delta x, \omega)$ $G_{22}(\Delta x, \omega)$	transmission matrix (of TASK code) for slab thickness Δx and at frequency ω	dimensionless
$h(t)$	response function of the neutron population to the injection of one prompt neutron into the system	dimensionless
$H(\omega)$	reactor transfer function at frequency ω	sec
$<\|I_p(\omega)\|^2>$	power spectral density of the pile noise (chain-related counts) at frequency ω	$\text{picocoul}^2\text{-sec}$ or $\text{picoamp}^2/\text{sec}$
$<\|I_w(\omega)\|^2>$	power spectral density of the white noise (uncorrelated counts) at frequency ω	$\text{picocoul}^2\text{-sec}$ or $\text{picoamp}^2/\text{sec}$
K_{eff}	effective multiplication factor	dimensionless
K_{pi}	prompt multiplication factor of subcritical state or near critical state i	dimensionless
ℓ	neutron life time	sec
ℓ_p	prompt neutron life time	sec
m_i	rate of reaction of type i	reactions/sec
n_o	steady state neutron density	neutrons/cm^3

Symbols	Descriptions	Units
$<\|n(\omega)\|^2>$	power spectral density of the neutron density at frequency ω	neutrons^2-sec/cm^6
$p(x), p(y)$	probability density function of random variable x,y	dimensionless
$p(x,y)$	joint probability density function of random variables x and y	dimensionless
p_i	probability of i fissions occurring in the first generation of the fission chain	dimensionless
$P_c(t_1,t_2)$	probability of coincidence counts (due to the same fission chain) at time t_1 and t_2	dimensionless
$P_D(t)$	probability of a detection at time t	dimensionless
$P_R(t_1,t_2)$	probability of random counts (due to all fission chains) at time t_1 and t_2	dimensionless
q	electric charge released per neutron detection	picocoulomb/detection
Q	Bennett factor, $\overline{q^2}/\overline{q}^2$	dimensionless
$Q_n(\omega)$	ratio of correlated to uncorrelated noise contribution (signal-to-noise ratio) for channel n and at frequency ω	dimensionless
$Q_{n,i}$	maximum signal-to-noise ratio for channel n and at state i	dimensionless
R	neutron yield ratio between Pu-240 and Pu-239, ν'/ν	dimensionless
$\underline{S}$	volumetric source vector (of TASK code)	neutrons/cm^3-sec
S_o	extraneous neutron source strength	neutrons/sec
$<\|S_o\|>$	noise equivalent source (NES)	neutrons^2/sec

Symbols	Descriptions	Units
T	sampling interval of detection network	sec
V	velocity of prompt neutron	cm/sec
$\underline{\underline{V}}^{-1}$	inverse velocity matrix (of TASK code)	sec/cm
W_i	detector efficiency of sub-critical state or near critical state i	detection/ fission
$Z(x,\omega)$	source vector (of TASK code) at space point x and at frequency ω	neutrons/cm^3-sec
Greek		
α	prompt neutron decay constant (break frequency; roll-off frequency)	sec^{-1}
β_i	total delayed neutron fraction of subcritical state or near critical state i	dimensionless
η	standardized variable	dimensionless
ε	detector efficiency ratio, W_2/W_1	dimensionless
λ_i	decay constant of the i-th group delayed neutron precursor	sec^{-1}
$\Lambda^{(1)}(\Delta x,\omega)$	transfer matrix (of TASK code) for slab thickness Δx and at frequency ω	cm
ν	number of neutrons released in a Pu-239 fission	neutrons
ν'	number of neutrons released in a Pu-240 spontaneous fission	neutrons
$\$_i$	reactivity of state i $\left(\$_i = \frac{K_i - 1}{K_i} \times \frac{1}{\beta_i}\right)$	dollar, \$
ϕ_o	steady state neutron flux	neutrons/cm^2-sec

Symbols	Descriptions	Units
$\phi(\omega)$	neutron flux at frequency ω	neutrons/cm^2-sec
$\phi^*(\omega)$	complex conjugate of neutron flux at frequency ω	neutrons/cm^2-sec
$\chi(x,\omega)$	state vector at space point x and at frequency ω	neutrons/cm^2-sec
$\Phi_{xx}(\omega), \Phi_{yy}(\omega)$	auto power spectral density of random variable x,y at frequency ω	neutrons^2-sec, picocoulomb^2-sec or picoamp^2/sec
$\Phi_{xy}(\omega)$	cross power spectral density of random variables x and y at frequency ω	neutrons^2-sec, picocoulomb^2-sec or picoamp^2/sec
ρ_c	coherence function at delayed critical	dimensionless
ρ_f	probability of fission in the reactor when a neutron is released from the starting event of a delayed neutron induced fission or a spontaneous fission	dimensionless
ρ_i	coherence function of sub-critical state or near critical state i	dimensionless
Σ_a	macroscopic absorption cross section	cm^{-1}
Σ_c	macroscopic capture cross section	cm^{-1}
Σ_d	macroscopic detection cross section	cm^{-1}
Σ_f	macroscopic fission cross section	cm^{-1}
Σ_s	macroscopic scattering cross section	cm^{-1}

Symbols	Descriptions	Units
δ_1	standard deviation of the correlated count rate	counts/sec
δ_2	standard deviation of the random count rate	counts/sec
δ_c	standard deviation of the total count rate	counts/sec
$\delta_{\$_i}$	standard deviation of the sub-criticality of state i	dollar, \$
δ'_F	standard deviation of the fission rate of all fission chains	fissions/sec
δ_F	standard deviation of a chain-related fission rate	fissions/sec
δ_N	standard deviation of the number of fissions in a Pu-239 delayed neutron initiated fission chain	fissions
δ_x	standard deviation of the number of fissions in a Pu-240 spontaneous fission initiated fission chain	fissions
δ'_N	standard deviation of the number of first generation fission in a fission chain	fissions
δ''_N	standard deviation of the number of fissions following i first generation fissions	fissions
ω	frequency	radian/sec

I. INTRODUCTION

A. Background

For purposes of operational safety and efficiency during shutdown and refueling, it is necessary to obtain kinetic information such as rod worth and the subcritical state of a reactor. In particular, the reliable determination of subcritical reactivity for a Liquid-Metal-Cooled Fast Breeder Reactor (LMFBR) is required in the United States Atomic Energy Commission (USAEC) LMFBR program plan [1].

One of the techniques for determination of subcritical reactivity is by neutron noise analysis. The term "neutron noise" is used because the "birth" and "death" of neutrons due to the various reactions result in random fluctuation. By studying a collection of neutron noise data in the time or frequency domain, such reactor kinetics quantities as the power spectral density (PSD), the prompt neutron decay constant (α), and the coherence function (ρ) may be determined. The subcriticality of the reactor can then be deduced from these reactor kinetics quantities.

The determination of subcriticality by means of the coherence function is one of the promising methods of neutron noise analysis techniques. A pair of neutron detectors are utilized to measure the coherence functions. The coherence function can be defined as the ratio of the cross-power

spectral density (CPSD) and the square root of the respective auto-power spectral densities (APSD). In neutron noise measurement, the CPSD may be viewed as the signal and the APSD the sum of the signal and the white noise. For the core locations where detector efficiency is high and the reactor is near critical, the signal dominates the white noise and the coherence function approaches unity. As the reactor becomes increasingly subcritical (due to fuel depletion or control rod insertion, e.g.), the white noise becomes comparable to the signal and the coherence function decreases in magnitude. With the knowledge of the subcriticality of a calibrated state, the reactivity of another state can be inferred from the coherence functions of the two states.

Most studies of coherence function reactivity were made with the pair of neutron detectors located at the core center. This was done to obtain a high signal-to-noise ratio. However, the deployment of neutron detectors may be limited to ex-core locations in an operating LMFBR plant. It is not clear whether the coherence function reactivities determined by the ex-core detectors are the same as those determined by the core-centered detectors. The proper interpretations of the effect of detector placement on the coherence function reactivity is not well known.

B. Purpose of Study

The purpose of this investigation is to study, experimentally and numerically, the space dependent sensitivity of the coherence function reactivity. Specifically, the effect of detector placement on the coherence function reactivity is examined.

Spatial measurements of the polarity coherence function were made in the Zero Power Plutonium Reactor (ZPPR). Subcritical reactivities were inferred from these measurements. Coherence functions were also calculated by numerical simulation of the neutron detector response. The corresponding subcriticalities were inferred accordingly. The validity of the inference relation for the coherence function reactivity was also examined.

Determination of subcritical reactivities by measurements of polarity coherence functions has been done successfully on various experiemtnal reactors [2, 3]. Application of this method was made on ZPPR, a fast critical assembly operated by Argonne National Laboratory (ANL) [4, 5, 6]. In this investigation, the measurements were made with pairs of lithium-6 neutron detectors located at the core center and the blanket. The space dependency of the polarity coherence function method was studied experimentally.

Calculation of the theoretical coherence function requires the solution of the neutron flux in the frequency domain. The technique of transfer and scattering kinetics (TASK) has been shown to be suitable for solution of the neutron transport equation in the frequency domain. In this study, the TASK technique was applied for different cases of space dependent calculations of the coherence function reactivity for the Zero Power Plutonium Reactor.

This study can be divided into three areas, namely:

1. An experimental investigation of the space dependency of the polarity coherence function and its effect on the inferred reactivity.
2. A numerical computation of the coherence functions at different spatial locations and an investigation of its effect on the inferred reactivity.
3. An examination of the accuracy and validity of the inference relation for the subcritical reactivity.

II. REVIEW OF LITERATURE

Various techniques for reactivity measurement in a fast breeder reactor have been used [7, 8]. These techniques fall into four categories:

1. Subcritical source multiplication method.
2. Neutron noise analysis of break frequency and/or coherence function.
3. Inverse kinetics by rod drop or source jerk.
4. Pulse neutron transient analysis.

The first two techniques are nonperturbing to the reactor. The inverse kinetics and pulse neutron method utilize the sudden removal and introduction of neutron absorbers or sources to the reactor to measure the subcritical reactivities.

With regard to far subcriticality measurement, the only proven reliable method is the subcritical source multiplication method. This method was first developed by Serber [9] in Los Alamos Scientific Laboratory. It is based on the point kinetics model and does not account for the spatial effects of neutron flux perturbations at various subcritical states. Recently, two dimensional diffusion calculations were used to correct the source multiplication method for this reactor spatial effect which caused departure from fundamental mode behavior. One of the "corrected" source multiplication methods was developed and used in the ZPPR facility. The correction

was made by applying a calculated correction factor to the measured subcriticality. The correction factor was obtained from 2-dimensional diffusion calculation of the real flux with an inhomogeneous source equivalent of the Pu-240 spontaneous fission source, and the adjoint flux from a lamda mode calculation [10]. The correction factor accounts for the change in detector efficiency and source worth for different subcritical states. In addition, there is another "corrected" method known as the modified source multiplication method (MSM). This method was tested in the Hanford Engineering Development Laboratory and will be applied to the Fast Flux Test Facility and future LMFBR's [11]. In this method, a configuration factor is applied to correct the measured subcriticality. The configuration factors are inferred from representative 2-dimensional source mode diffusion calculations for different detector placements [12, 13].

Inverse kinetics by rod drop or source jerk have been applied to several fast critical assemblies [14, 15, 16]. Results indicated that the method is accurate for slightly subcritical state measurements ($\$ > -2.0$) but unreliable at far subcritical states ($\$ \sim -30$) [17]. It is used as a technique for calibration of control rods and reference subcriticality in ZPPR [18].

The pulse neutron method was applied to the Zero Power Reactor-III (ZPR-3) by Lehto [19]. Due to the higher mode

contamination and high background neutron source, the measurement became impractical for more than five dollars subcritical. In addition, because of the fact that a neutron generator is required to introduce neutron into the reactor, this method, while suitable for experimental study, is not seriously considered for fast breeder reactor application.

Neutron noise generally refers to the fluctuation in the neutron density due to the probabilistic nature of the various nuclear reactions, e.g. fission, capture, scattering etc. Neutron noise measurement techniques can be microscopic or macroscopic in nature. Microscopic measurements are those in which the detection counts, whether triggered by a fission chain or individual nuclear interaction, are studied by statistical techniques. The Rossi-Alpha [20, 21] and Feymann's variance-to-mean techniques [22] are examples of microscopic measurement. Macroscopic measurement, on the other hand, are based on the composite system response. The neutron noise is viewed as the reactor "output" due to the "input" of random driving functions which exhibit the statistical nature of nuclear interaction. Correlation, spectral density and coherence function measurement are example of macroscopic measurement. For fast breeder reactor application, the macroscopic techniques show great promise for determination of reactor physics parameter, reactor safety monitoring and anomaly detection.

There are many ways of applying the macroscopic neutron noise analysis technique to the measurement of subcritical reactivity [23, 24]. These techniques can be classified according to the type of input signals: internal or external. Balcomb [25], Stern [26] and Valat [27] used externally applied signals; while Cohn [28], Danofsky et al. [6] and Seifritz [2] utilized the natural stochastic process of fission, capture, scattering, etc. as the random "noise equivalent source" with no externally applied input. This is the basis for the "noise equivalent source" [28]. Neutron noise techniques can also be classified according to the domain of analysis: time or frequency. Boardman [29], Dragt [30], and Rajagopal [31] performed experiments in the time domain. Bradgley and Urig [32], Seifritz [2] and Danofsky et al. [6] conducted investigation in the frequency domain. Finally, neutron noise techniques can be grouped according to the number of detection channels employed. Early experiments by Balcomb et al. [33], Cohn [28] and Rajagopal [31] employed one detection channel to determine the output signal. The use of only one detection channel has the inherent constraint of required high detector efficiency. This requirement is necessary in order to insure that the reactor noise signal is observable above the random detection noise. For measurements with two detector channels, the detector efficiency could be lowered. In general, an approximate factor of 20 improvement over the single detector

measurement was observed.

The polarity coherence function method was first applied to the thermal neutron assembly STARK 4 and the fast neutron assembly SNEAK 4A by Seifritz [2]. In the polarity correlation process only the signs of the signals (with respect to their mean values) are correlated. The advantage of this technique is fourfold: (1) it is nonperturbing, (2) accuracy is not very sensitive to power level, (3) the results of this technique do not depend on the instrument transfer function and (4) on-line analysis can be easily implemented.

The polarity coherence function method was applied to ZPPR to determine the subcritical reactivity by Lehto [5] and Danofsky et al. [6]. The results of this technique indicated good agreement with other methods (source multiplication and inverse kinetics by rod drop or source jerk) except in the far subcritical range. These measurements and corresponding calculations were done with the lithium-6 neutron detector located at the core center. The space dependency of the polarity coherence function method and its effect on the inferred subcriticality was not well known.

The coherence function reactivity (usually written as $\$_2$) is calculated by using the conventional inference relation (Equation 3, p. 14). The relation accounts for a nonconstant detector efficiency (W) and delayed neutron fraction (β) [34, 6]. The validity of this inference relation was first

examined by Carpenter [35]. A modified form of the inference relation for the coherence function reactivity was consequently proposed.

This study investigates experimentally and numerically the space dependency of the subcritical reactivity obtained by the polarity coherence function method. The inference relation for the coherence function reactivity is examined and several modifications presented.

III. GENERAL THEORY

A. Definition of the Coherence Function

The coherence function is a stochastic quantity that describes the relative magnitude of the noise and signal. The signal from a neutron detection system of a nuclear reactor consists of the detection of neutrons from fission chains. The noise may be due to uncorrelated neutrons (e.g. extraneous neutronic sources) or electrical signal contamination (especially at 60 hz). The coherence function for a two-detector cross-correlation measurement, $\rho(\omega)$, is defined as the ratio of the effective cross power spectral density, CPSD, and the square root of the product of the respective auto power spectral densities, APSD. Thus,

$$\rho(\omega) = \frac{\left|\Phi_{xy}(\omega)\right|}{\{\Phi_{xx}(\omega)\ \Phi_{yy}(\omega)\}^{1/2}} \tag{1}$$

where $\Phi_{ii}(\omega)$ = auto power spectral density of random signal i at frequency ω; i = x,y

$\Phi_{xy}(\omega)$ = cross power spectral density of random signal x and y at frequency ω.

The coherence function indicates how well two random variables, in the presence of noise, are correlated. It serves the same purpose in the frequency domain as the

coefficient of correlation does in the time domain. It can be viewed as a normalized cross power spectral density.

The coherence function also illustrates the linear dependency of the two random variables. If the two random variables are linearly dependent and their normalized fluctuations (standard variables) are the same, then they are completely coherent and their coherence function is unity. If the two random variables are statistically independent, then they are uncorrelated and their coherence function is null. For the case where the two random variables are partially correlated, then they are partially coherent and their coherence function is between zero and one.

Consider two correlated normal random signals, $x(\omega,t)$[1] and $y(\omega,t)$[1]. Assume that these two signals are of zero mean and that their joint probability density function is Gaussian, i.e. bivariate distribution. Then, it can be shown that the coherence function is given by [2]:

$$\rho(\omega) = \sin \frac{\pi}{2} \overline{C_{\omega}(t)} \qquad (2)$$

---

[1]The symbols of the normal random signals, $x(\omega,t)$ and $y(\omega,t)$ mean that they have been passed through an adjustable band pass filter at the center frequency of . The resulting signals, $x(\omega,t)$ and $y(\omega,t)$ are still a time dependent function.

where $\overline{C_\omega(t)}$ = time average of the polarity correlation at frequency ω,

$C_\omega(t)$ = polarity correlation at frequency ω

= product of the sign of the two signals

= [sign $x(\omega,t)$] [sign $y(\omega,t)$].

In this investigation, Equation 1 was utilized to numerically calculate the coherence function for different locations in the reactor. For experimental measurements, the coherence function was obtained by using Equation 2 since polarity correlation measurements were made.

It should be noted that the coherence functions are different for different locations of neutron detectors at the same subcritical state. This phenomena, namely, the space dependency of the coherence function [36], is caused partly by the change of detector efficiency. Consequently, change of detector efficiency (due to different detector placements or control rod pattern) would lead to change of coherence function. In addition, there is a possible space dependent effect other than the detector efficiency change that could take place.

B. The Inference Relation of Coherence Function Reactivity

The conventional inference relation for coherence function reactivity used by various investigators [6, 34] is

$$\$_2 = 1 - (1 - \$_1)\left(\frac{W_2}{W_1}\right)^{1/2}\left(\frac{\beta_1}{\beta_2}\right)\left[\frac{1 - \rho_2}{\rho_2} \times \frac{\rho_1}{1 - \rho_1}\right]^{1/2} \qquad (3)$$

where $\$_i$ = reactivity of state i in dollar

ρ_i = coherence function of state i

W_i = detector efficiency of state i in detection/fission

β_i = total delayed neutron fraction of state i

i = 1, 2.

Equation 3 can be derived from the basic definitions of the spectral densities and the coherence function [2]. Details of the derivation are shown in Appendix A. It should be mentioned that a modification factor for Equation 3 is needed when the measured state 2 is far subcritical (e.g. $\$_2 < -30$) [35].

C. Theory of Calculation

As indicated in Equations 1 and 3, computation of the various detector auto and cross power spectral densities would yield the subcritical reactivity of the reactor. For theoretical neutron flux detection calculation, the power spectral density can be defined as:

$$\Phi_{xy}(\omega) = \sum_{g=1}^{G} \{[\Sigma_d \times \phi(x,\omega)]_g \times [\Sigma_d \times \phi^*(y,\omega)]_g\} \qquad (4)$$

= detector response at spatial position x and frequency ω · the complex conjugate of detector response at spatial position y and frequency ω,

where Σ_d = macroscopic detector cross section,

$\phi(x,\omega)$ = Fourier transform of the neutron flux at spatial position x and frequency ω,

$\phi^*(y,\omega)$ = the complex conjugate of the neutron flux at spatial position y and frequency ω,

and G = total number of neutron energy groups.

The zero frequency neutron flux is the steady state flux and the frequency dependent neutron flux can be interpreted as the Fourier transform of the fluctuating part of the flux.

Computation of the coherence function, according to Equations 1 and 4, requires the solution of the neutron flux in the frequency domain. However, the conventional finite difference neutronic codes, such as the ARC system code [37] and the ANISN code [38], solve for the steady state neutron flux and the detector response. Calculation of the frequency dependent flux can be obtained indirectly by modifying the neutron diffusion equation into a frequency domain form [39]. This approach of converting the steady state code into a frequency domain form has been shown to result in an inherent difficulty of numerical convergence. The technique of

transfer and scattering kinetics, TASK [40], has been shown to be suitable for solution of the neutron flux in the frequency domain. It employs the concept of a noise equivalent source in calculating the frequency dependent neutron flux. The noise equivalent source (NES) is a term that describes the fluctuations of neutrons of the various reaction rates (fission, capture etc.). It was defined [41] in the form of a spectral density as:

$$<|S_o|^2> = \sum_i \overline{q_i'^2}\, m_i \qquad (5)$$

where $<|S_o|^2>$ = noise equivalent source in neutron^2/sec

q_i' = number of neutrons produced (or lost) in a reaction of type i

m_i = rate of reaction type i.

By substitution of the square root of the NES into the frequence dependent one-dimensional transport equation, the transmission and reflection matrix can be formed. The neutron flux as a function of space, energy and frequency can then be solved. The manipulation of the various matrices were done internally in the TASK code. Details of its algorithm are described in Appendix B.

In this investigation, the TASK technique was employed to calculate the spatially dependent neutron flux, $\phi(x,\omega)$ and

$\phi^*(y,\omega)$ in the frequency domain. These spatial and frequency dependent fluxes were then folded with the detection cross section to obtain the detector response and the coherence function by using Equation 4. From the coherence function, the subcritical reactivity was then inferred using Equation 3.

Figure 1 illustrates the above procedures in a flow chart. It shows the steps taken in obtaining the numerical solution of the subcritical reactivity in this study.

As a first step, the fine group cross sections of different reactor materials from the Evaluated Nuclear Data File B, Version II were collapsed into a 6-group structure by using appropriate energy spectrum weighting. For each phase of the ZPPR assembly, the geometry and the atom densities of the various reactor materials are known. Thus the macroscopic cross sections of each region (inner core, radial blanket, etc.) can be calculated. This process of reducing the raw, fine group microscopic cross section data into the ZPPR regionwise 6-group macroscopic cross sections was achieved by using the codes ARC-MC^2 [42] and CCSX/TOPSY [43]. These regionwise cross sections were input into the TASK code. In addition, as the distribution of the core materials (including the extraneous neutron source) is fixed, the noise equivalent source can be obtained analytically. The square root of the NES was input into the TASK code as the source term.

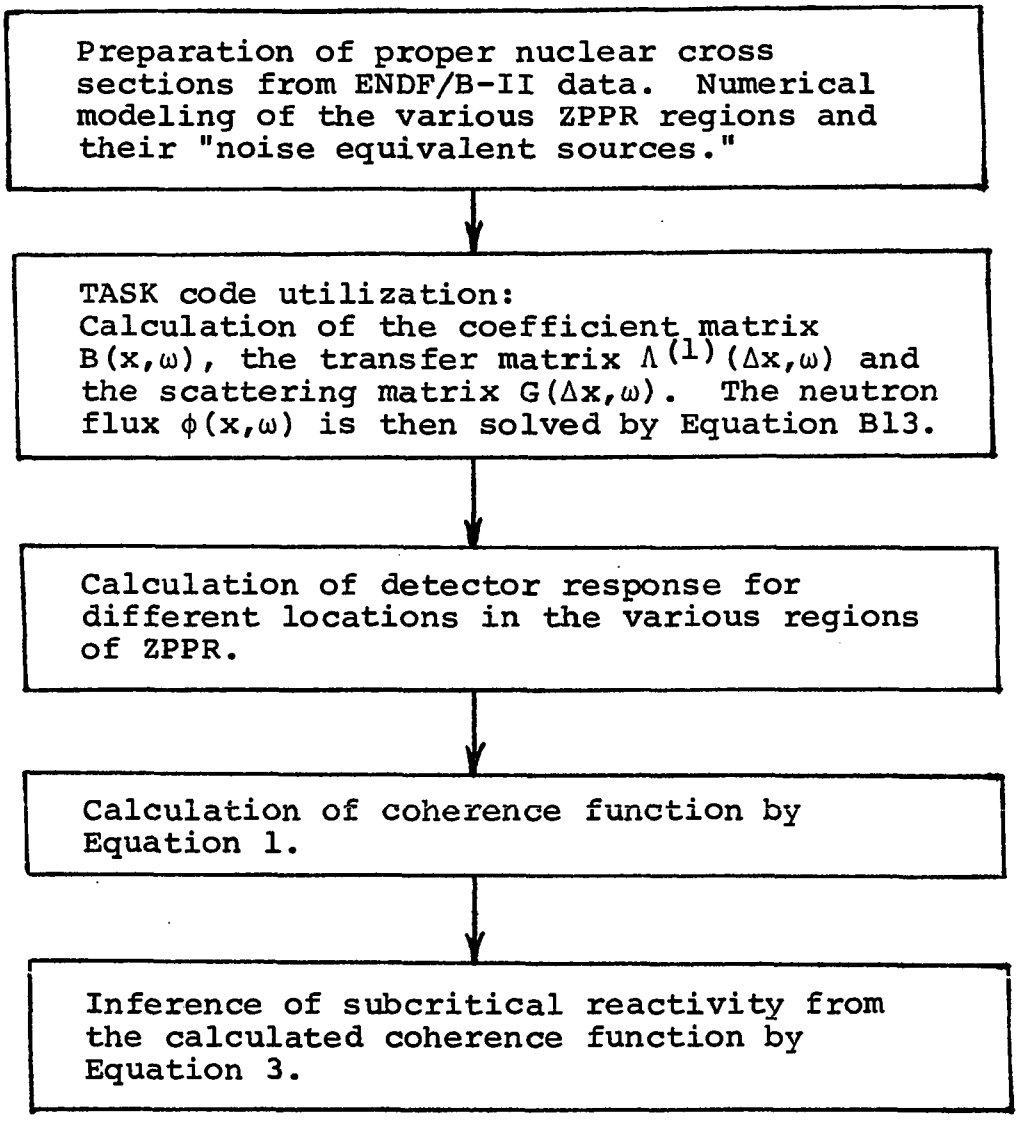

Figure 1. Calculational procedures for numerical solution of subcritical reactivity

With the information of the regionwise macroscopic cross sections and the NES, the TASK code was used to compute the coefficient matrix $B(x,\omega)$, the transfer matrix $\Lambda^{(1)}(x,\omega)$ and the scattering matrix $G(\Delta x,\omega)$. These matrices are defined in Appendix B. Having defined these three matrices for each reactor region, the frequency dependent neutron fluxes $\phi(x,\omega)$ and $\phi^*(y,\omega)$ were solved using Equation B13.

In this study, the spatial and frequency dependent neutron fluxes at 100 Hz were obtained. Since the amount of lithium-6 in the neutron detector is known from the product specifications, the macroscopic detection cross section, Σ_d, can be defined. With the TASK-computed neutron flux and the detection cross sections, the detector response and the coherence function were calculated by means of Equations 4 and 1. Given the knowledge of the necessary parameters (delayed neutron fraction ratio and detector efficiency ratio), the inference of the subcritical reactivity can then be obtained by using Equation 3.

D. Theory of Measurement

The coherence function was experimentally obtained from Equation 2 using measured polarity correlation functions. The measurement of the polarity correlation function depends only on the fraction of time that the random variable signals are above or below their mean, i.e. their polarities. Two

separate but identical neutron detection channels were employed. The polarity of the two random variable signals from these two channels were sampled and used to form the correlation output, $C_{\omega}(t)$. After repetitive sampling of the two signals (usually on the order of 10^5 samples/sec), the time average correlation output $\overline{C_{\omega}(t)}$, was formed. The coherence function was then calculated according to Equation 2 by an on-line minicomputer. It should be noted that the amplitude of the power spectral densities were not involved in this measurement technique.

The detection system used in this study is shown in a block diagram in Figure 2.[1] A pair of lithium-6 glass scintillation detectors (Nuclear Enterprise model 905) were placed inside the reactor. They are viewed by RCA 6199 photomultiplier. For purpose of easy identification, one detection channel is labeled the X channel and the other the Y channel. The instrumentation of these two channels are identical.

Referring to Figure 2, consider a neutron incidents on the detector. The neutron is captured by the lithium-6 atom and undergoes the reaction:

---

[1] In recent ZPPR experiments [44], four separate and identical neutron detection channels were employed. The detection systems of these experiments were essentially the same as Figure 2 except two more independent channels were added.

Figure 2. Polarity coherence function measurement system in ZPPR

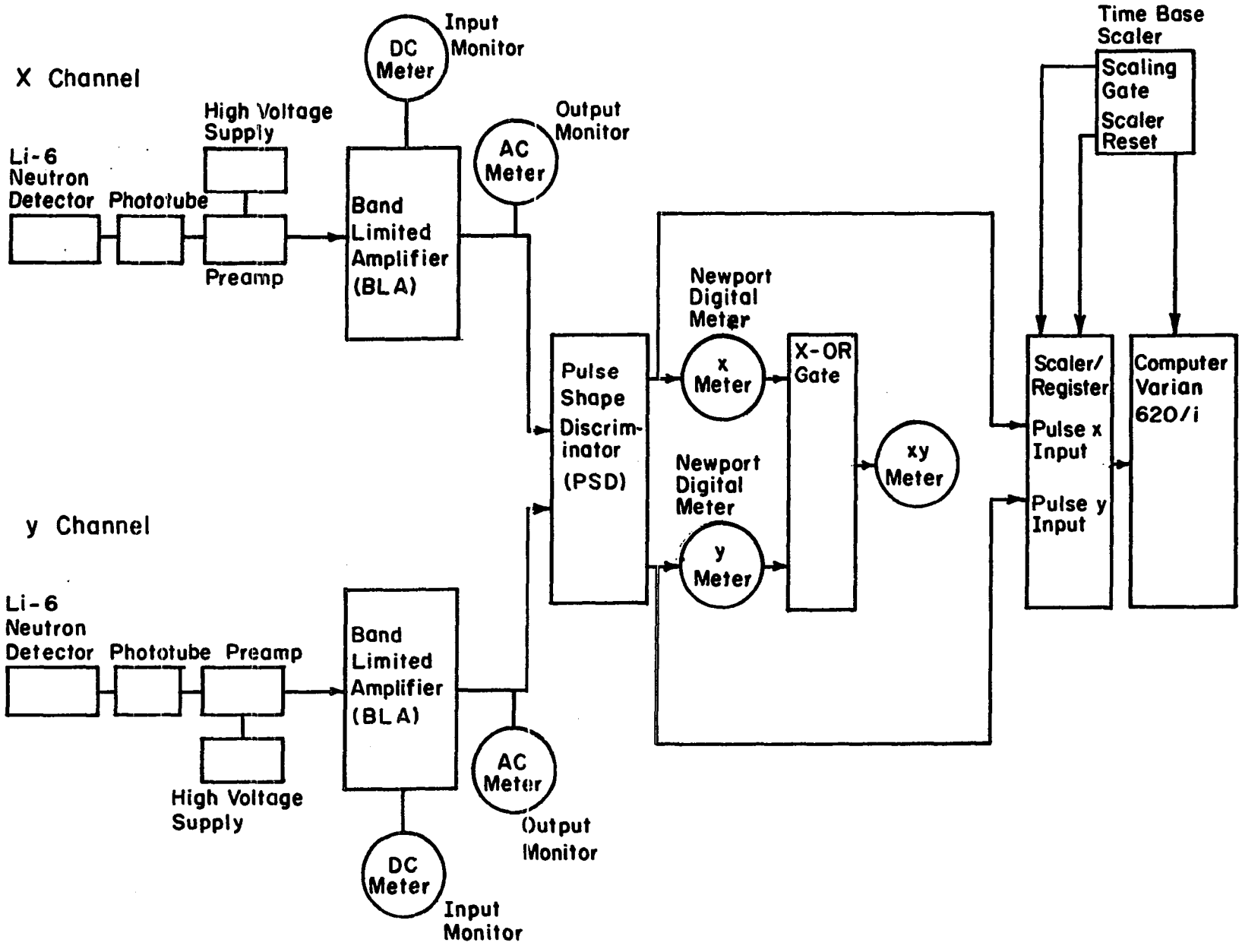
X Channel
DC Meter
Input Monitor
High Voltage Supply
Output Monitor
AC Meter
Li-6 Neutron Detector
Phototube
Preamp
Band Limited Amplifier (BLA)
Time Base Scaler
Scaling Gate
Scaler Reset
Newport Digital Meter
x Meter
X-OR Gate
Pulse Shape Discrim-inator (PSD)
xy Meter
Scaler/ Register
Pulse x Input
Pulse y Input
Computer Varian 620/i
y Channel
Newport Digital Meter
y Meter
Li-6 Neutron Detector
Phototube
Preamp
Band Limited Amplifier (BLA)
High Voltage Supply
AC Meter
Output Monitor
DC Meter
Input Monitor

$$^{6}_{3}L_{i} + ^{1}_{o}\eta \rightarrow ^{3}_{1}H + ^{4}_{2}H_{e} \ .$$

One of the product, $^{4}_{2}H_{e}$, is a positively charged particle (α particle). As it traverses the glass scintillator (cerium matrix glass or zinc sulphide crystal), a photon pulse signal is developed. The photon pulse, due to the variations in the detection process, is a fluctuating quantity. Typically, the sampling bandwidth is 10-200 Hz and the fast neutron generation time is approximately 10^{-7} sec. Thus, each sampling of the photon pulses is the result of many neutrons of different generations arriving at the detector within a time interval comparable to the inverse bandwidth. The fluctuating nature of the number of neutrons being detected in each sampling results in the photon pulse fluctuation.

The photon pulse from the scintillator is converted into a current pulse upon entering the photomultiplier. The current pulse is then fed into the pre-amplifier. For measurement of the polarity coherence function, one is interested in the signals of low frequency (10-200 Hz). Thus, the current signals from the pre-amp are processed by the band-limited-amplifier (BLA). The meters at the input and output of the BLA is for on-line monitoring purpose. For reliable operation, the high voltage supply should be adjusted such that the DC meter display (input to BLA) is between 60 to 90% full scale. The coarse and fine gain of the BLA should be set

such that the AC meter displays (output of BLA) are also between 60% and 90% full scale. Too high a reading in the input, i.e. current through the photomultiplier, would damage the system. Too low a reading from the output would result in significant noise contamination (a low signal-to-noise ratio). The current pulse signals x, y from the BLAs are then fed into the pulse shape discriminator (PSD). By setting the potentiometers of the PSD to the mean voltage of the current pulse signals x and y, those signals that are below their mean voltage level would be stopped (discriminated) from proceeding in the circuit any further. Those signals that are above their mean voltage (i.e. discriminator pot setting) would then be recorded in the register. The discriminated signals x and y also go to X-OR gate. The X-OR gate samples the signals and forms their product. The outputs from the PSD are displayed on the three Newport digital meters. The xy meter will read the fraction of the time that the x and y signals are above or below their average at the same time. If the reading is +1000. they are completely correlated. If the reading is 0000, they have no correlation and if -1000 they are completely anticorrelated. The x and y meters display the fraction of the time that x and y channels have reading above their discriminator settings. A reading of 000 indicated a correct setting of 50% of the time above and 50% below, a 1000 indicates always above and -1000 always below. At the

register, the random variable signals x and y are recorded according to their polarity. Any signal that is above the mean is positive and any below is negative. By correlating these pairs of polarity signal at repetitive time, the average correlation, $\overline{C_\omega(t)}$, can be determined. With the aid of an on-line mini-computer (Varian model 620/i), the polarity signals are stored at the rate of 125,000 pairs per second. Utilizing a standard program in the mini-computer, the coherence function is calculated from the average correlation using Equation 2. With the proper input of the reference state data of $\$_1$ and ρ_1, determined earlier from a calibration test, the subcritical reactivity is then inferred using Equation 3.

It is appropriate at this point to illustrate the behavior of the coherence function as a function of frequency and subcriticality. Applying the prompt point reactor kinetic model for a two-detector cross-correlation experiment, the following expression for the coherence function can be obtained,

$$\rho(\omega) = \left(\frac{Q_x \quad Q_y}{(1 + Q_x)(1 + Q_y)} \right)^{1/2} \tag{6a}$$

where $Q = \dfrac{Q^c}{(1 - \$)^2 + \left(\frac{\omega}{\alpha}\right)^2}$ = ratio of correlated to uncorrelated noise contributions (signal-to-noise ratio)

$Q^c = \frac{DW}{R\beta^2}$ = maximum signal-to-noise ratio at critical

W = detector efficiency in detection/fission

D = Devin's factor

R = Bennet's factor

$\alpha = \frac{\beta}{\ell_p}$ = prompt neutron decay constant

ℓ_p = prompt neutron life time

β = total delayed neutron fraction

and subscripts x and y refer to the two detector channels.

It should be pointed out that implicit in Equation 6a, the effect of delayed neutrons is neglected. Furthermore, it is observed that the coherence function is only dependent on the correlated to uncorrelated noise contributions, Q_x and Q_y. Figure 3 shows some typical ZPPR coherence function curves. These curves were inferred from measurements made by pairs of adjacent lithium-6 neutron detectors placed in the same inner core location. Therefore, the detector efficiencies of these subcritical states are approximately equal.

As can be observed from Figure 3, the coherence function exhibits a plateau between the largest delayed neutron break frequency ($\frac{\lambda}{2\pi}$) and the prompt neutron break frequency ($\frac{\omega_{BF}}{2\pi}$), namely between roughly 0.5 Hz and 800 Hz. This is the frequency range corresponding to the time span that is long enough to cover the history of a single fission chain and short enough to preclude the emergence of the delayed

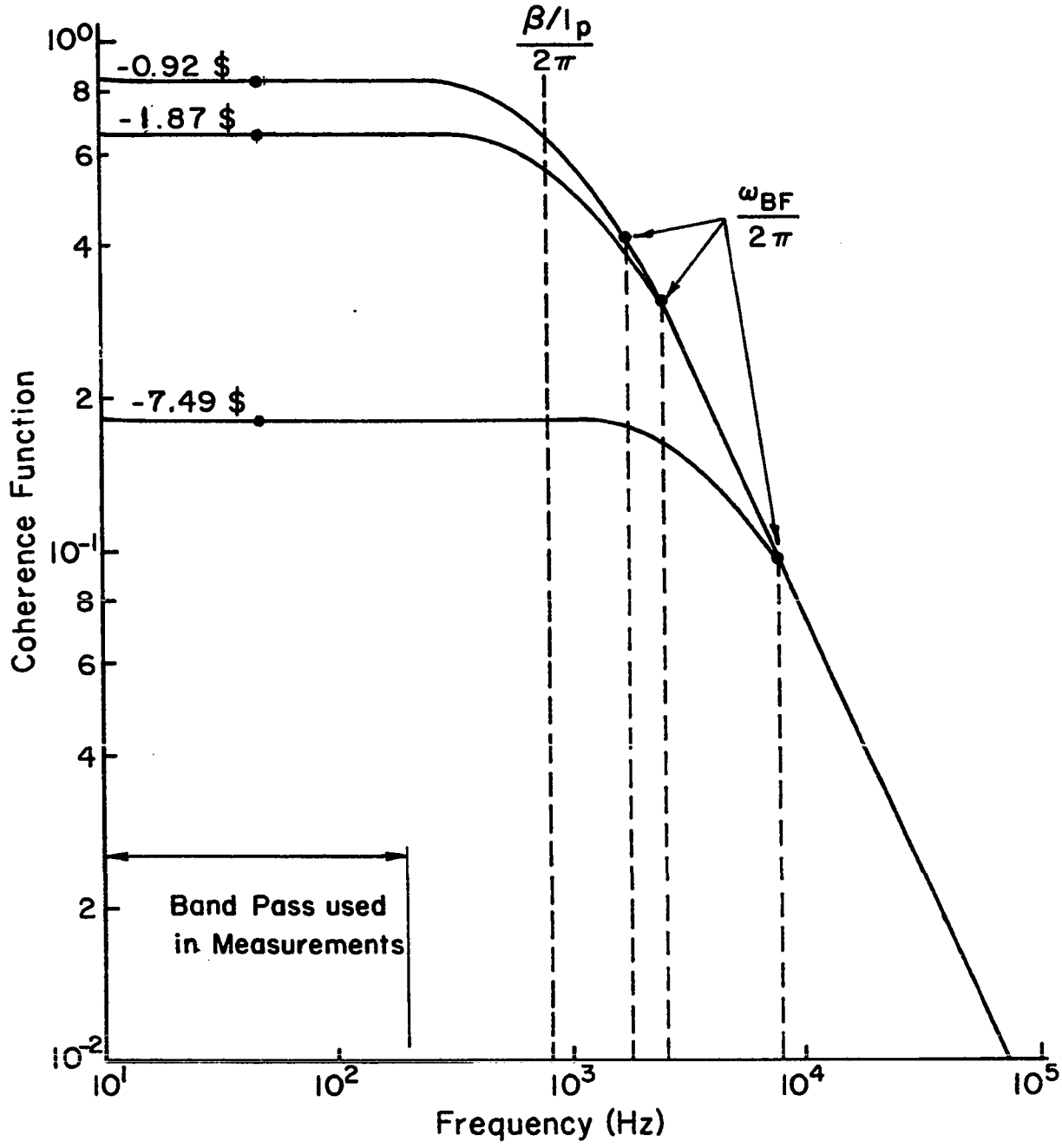

Figure 3. Frequency behavior of coherence function

neutron. (The former contributes to the correlated count rate whereas the latter increases the uncorrelated count rate.) It is on this plateau (10-200 Hz) that experimental measurements and numerical calculation of coherence functions were done for this study.

Figure 3 indicates that as the reactivity decreases, the coherence function decreases also. This reduction of the coherence function can be explained in terms of the signal-to-noise ratio, i.e. the quantity Q in Equation 6a. At low frequency ($\omega << \alpha$), the quantity Q decreases with increasing subcriticality. As a result, the coherence function displays a decrease in magnitude also.

It is shown in Figure 3 that the prompt neutron break frequency increase as the reactivity decreases. The break frequency is defined as the frequency where the magnitude of the coherence function has decreased by a factor of one-half. From Equation 6a, the upper break frequency is governed by the expression

$$\omega_{BF} = \frac{\beta}{\ell_p} [(1 - \$)^2 + Q^c]^{1/2} \qquad (6b)$$

where ω_{BF} = prompt neutron break frequency, and the rest of the symbols of Equation 6b are the same as in Equation 6a.

For a near subcritical state ($\sim$ -1\$), Q^c is about 4.0-0.13 for ZPPR, depending on the detector location. Thus, as shown by Equation 6b, the prompt neutron break frequency at the subcritical state is almost dominated by the term $\frac{\beta}{\ell_p}$ (1 - \$). Hence, the increase of prompt neutron break frequency is observed for decreased reactivity.[1]

To summarize the coherence function behavior, the following points can be made:

1. The coherence function is almost constant at the plateau frequency range of $\frac{\lambda}{2\pi} << f << \frac{\omega_{BF}}{2\pi}$, where λ and ω_{BF} are the largest delayed neutron precursor decay constant and the prompt neutron break frequency in radian/sec respectively, and f is the plateau frequency in Hz. Experimental measurements and numerical calculations of coherence functions were done on this plateau frequency range.
2. Increased subcriticality results in a reduction of the signal-to-noise ratio and therefore a decrease of the coherence function.
3. The prompt neutron break frequency increases as the reactivity decreases.

---

[1] In Figure 3, the coherence function behavior at high frequency is based on the assumption that detector efficiencies are the same for all three subcritical states.

IV. EXPERIMENTAL FACILITY

The measurements of the coherence function in this study were conducted in the Zero Power Plutonium Reactor (ZPPR) of the Applied Physics Division of Argonne National Laboratory (ANL) in Idaho. The following is a brief description of the ZPPR facility, its function and use [45].

The Zero Power Plutonium Reactor is the largest fast reactor critical assembly in the world. Its primary function is to study the physics characteristics of plutonium-fueled power breeder reactors for central power station. For physics studies of the 500 Mw(e) core, normal core loading consisted of approximately 1200 Kg of plutonium. The power level during the experiments are quite low, usually less than 50 watts. The heat generated in the reactor, due to plutonium fissioning and radioactive decay, is removed by forced convection of air. There is no provision for circulation of liquid sodium coolant as in the real liquid metal cooled fast breeder reactor.

The Zero Power Plutonium Reactor is a split-table critical assembly, i.e. the reactor core is assembled in two halves on two separate tables. Each half is 10 x 10 x 4 feet. They are slowly brought together to complete the core. Final criticality can be reached by slowly inserting fuel-bearing control rods with the two halves of the core together.

Figures 4 and 6 show the ZPPR when the two halves are apart. Each half of the reactor consists of arrays of matrix tubes. Drawers loaded with simulated reactor materials (e.g. Pu, Na, B) are inserted into the matrix tubes to assemble a given reactor design. Figure 7 is a cross sectional drawing of one of the core design. The drawer has nominal inside dimensions of 2 by 2 inches and varies in length from 18 to 36 inches. Figures 8 to 10 show typical drawers used in ZPPR.[1]

Recent experiments in the ZPPR facility were performed on a mockup core to yield benchmark data for theoretical calculations in support of the LMFBR program. The geometric dimension of the reactor for these experiments (ZPPR assembly 2 and 3) were 10 by 10 by 8 feet. Additional experiments (assembly 5) enlarged the reactor to 14 by 14 by 8 feet. It was used for simulation studies of the core characteristics of the LMFBR demonstration plant.

Considerable neutron noise measurement have been made in ZPPR to simulate the kinetics, control and safety features of the LMFBR. In particular, Lehto [5], Danofsky et al. [6] and Carpenter [35, 44] investigated the use of the coherence function to determine the subcritical reactivity. This research is a continuation of the past effort.

---

[1]For purpose of identification of the various locations of the two split-tables, each ZPPR half is labelled in cartesian coordinates of the matrix numbers. These coordinate numbers are displayed on the side of the split-tables and are visible in Fig. 5 and 6. Thus, the location of each drawer can be characterized by its coordinates. For example, the center drawer at half-1 is at matrix location 137-57.

Figure 4. View of the ZPPR with halves separated

Figure 5. A close up view of half 1 of ZPPR

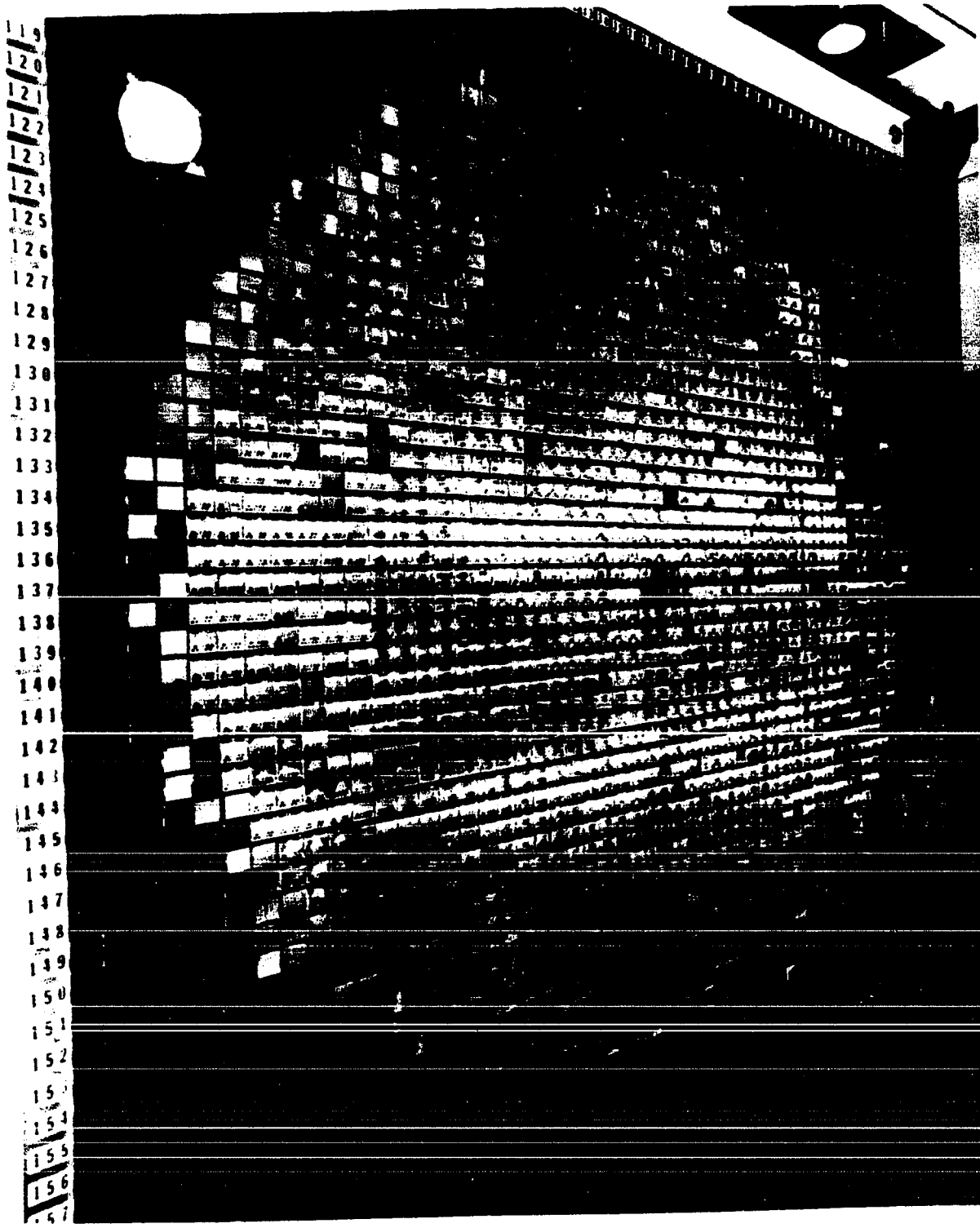

Figure 6. A close up view of half 2 of ZPPR

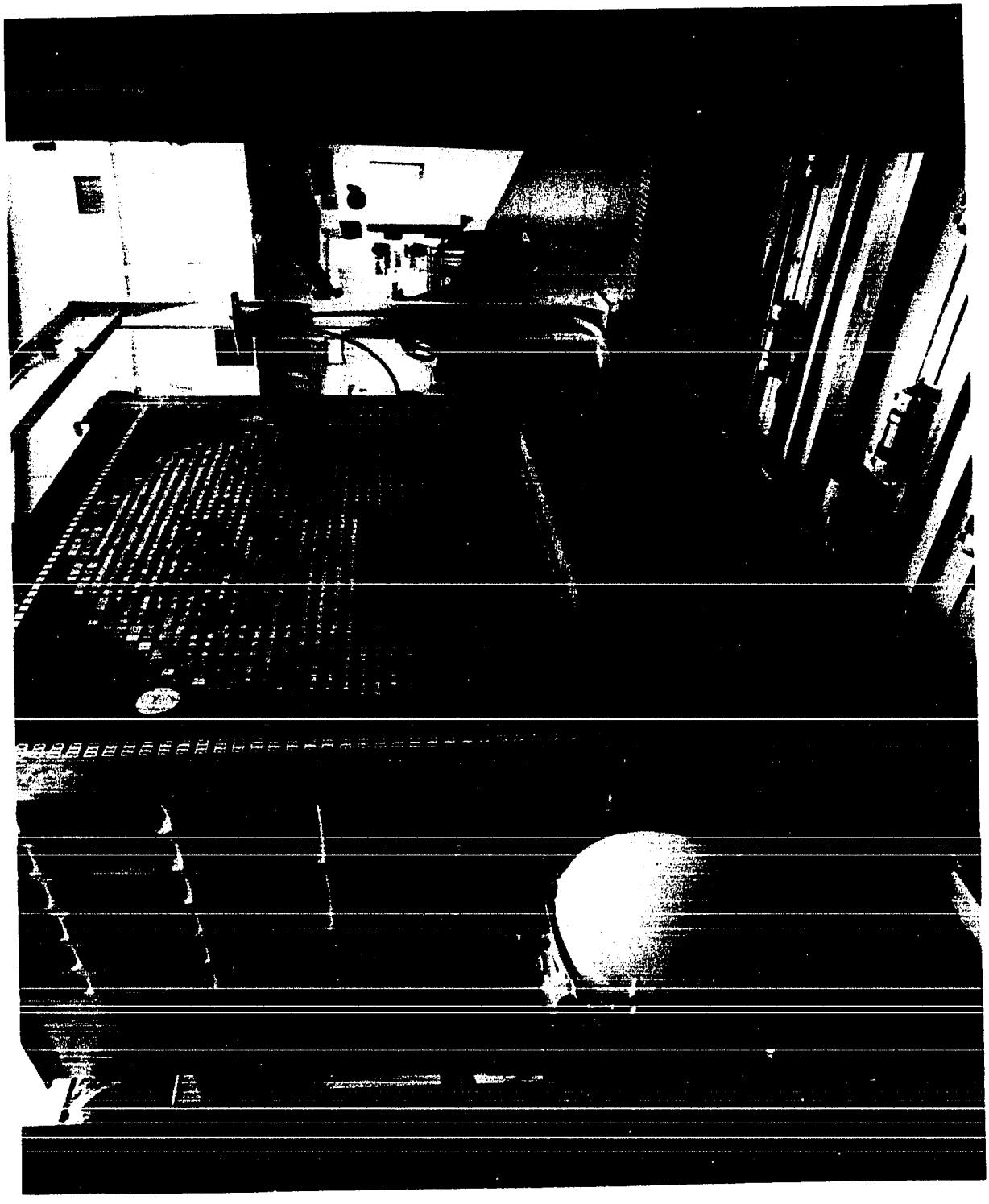

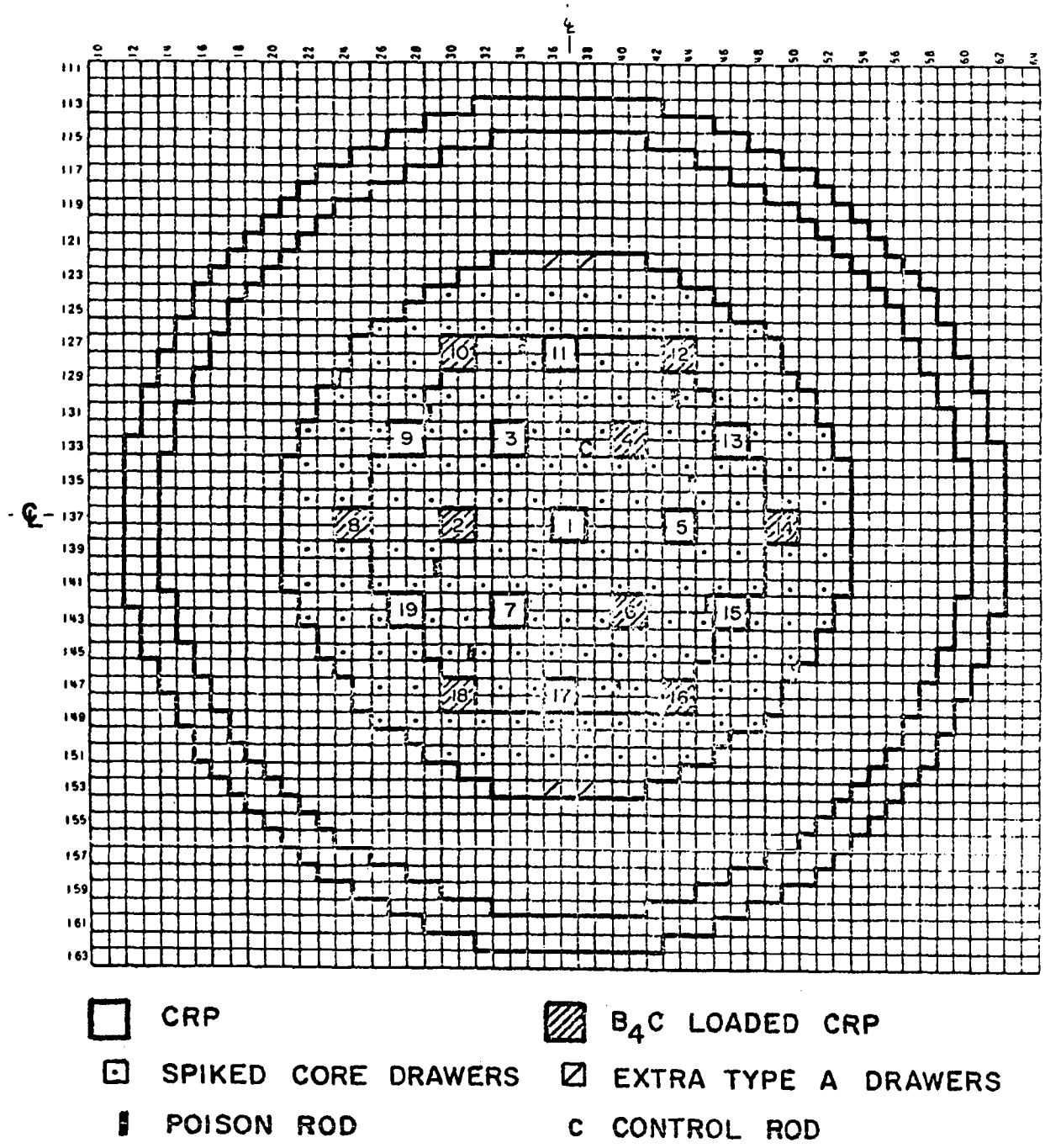

Figure 7. Cross section of ZPPR Assembly 3

Figure 8. Fuel drawer and calandria tube of ZPPR

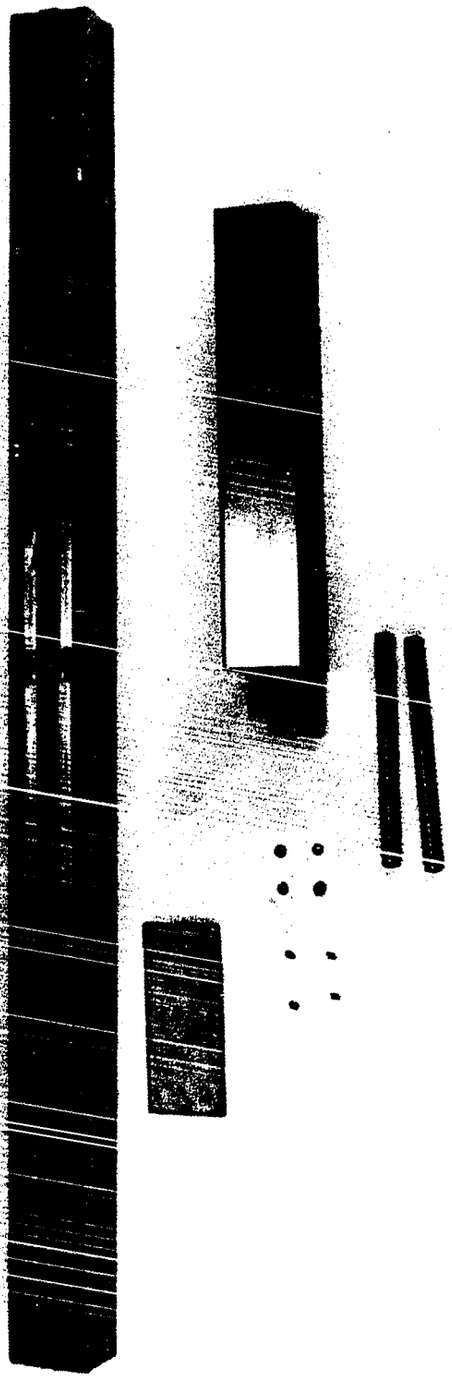

Figure 9. A close view of fuel drawer and calandria tube of ZPPR

Figure 10. Cross sections of fuel drawers in ZPPR

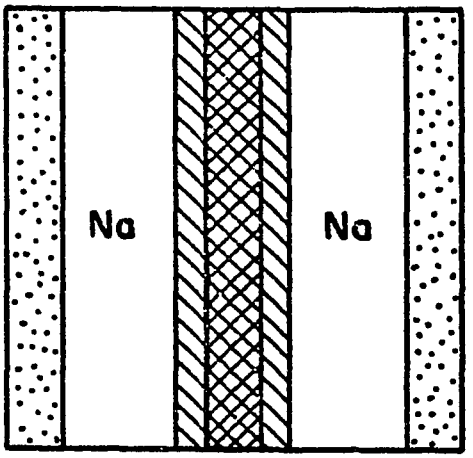

a. STANDARD FUEL-SECTION LOADING OF INNER CORE DRAWERS

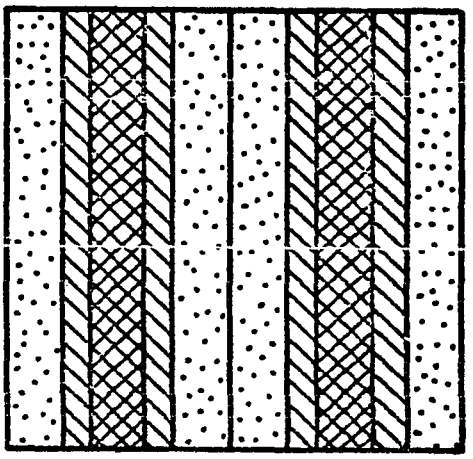

b. SLUMPED-FUEL ARRANGEMENT FOR DRAWERS IN CENTRAL "SUBASSEMBLY"

LEGEND: Pu-U-Mo; U_3O_8; Fe_2O_3; Na

V. RESULTS AND DISCUSSION

A. Experimental

The coherence function method was used to determine the subcriticality of ZPPR assembly 3 for various experimental conditions. Previous measurements were made with one pair of lithium-6 glass scintillation detector located in two adjacent drawers. For example, the control rod group worth of the ZPPR assembly 3, phase 3 core was measured with the pair of Li-6 detectors in the center drawers, matrix positions 137-37, 138-37 [46]. The single rod worth measurements in the sodium voided core of assembly 3 were made with the Li-6 detector pair in the blanket drawers, matrix number 146-21, and 147-22 [47]. This study investigated the space dependent nature of the coherence function by using two pairs of neutron detectors. Specifically, the coherence function subcriticality as a function of detector placement was studied.

It is shown by Equation 4 that the detector response is dependent on the distribution of neutron flux. For all practical purposes, the neutron flux is nonuniformly distributed inside the reactor. Therefore, it is evident that the detector placement would affect the detector response. From Equations 4 and 1, it can be observed that the coherence function may depend on the detector locations also, i.e. space dependent. It is therefore suspected that the subcriticality

determined by the polarity coherence function method may also be dependent on detector placement.

Experiments were conducted in phase 3 cores of ZPPR assembly 3 to investigate the space dependence of the coherence function and polarity coherence reactivity [48]. Two pairs of Li-6 neutron detectors were deployed. In the sodium-voided core experiment, the two detector pairs were located in the blanket at midplane (matrix Nos. 148-19, 194-20, 146-22, 147-23). These two detector pairs are about 2 and 10 inches from the outer-core boundary. Table 1 summaries the results of the measurements. Figure 11 shows the locations of the 4 detectors (detector A, B, C, D) used for these measurements. In the hexagonal-core experiment, one detector pair (detector E, F) was in the inner core (matrix Nos. 137-43, 138-43) and the other pair (detector G, H) in the radial blanket (matrix Nos. 137-57, 138-57). The results of the measurements obtained by detector E, F, G, H are summarized in Table 2 [48] and the detector locations are shown in Figure 11. In both experiments, an external neutron source of Californium-252 was used. The strength of the Cf-252 source was about the level of the Pu-240 spontaneous fission in the ZPPR core, approximately 1.9×10^8 n/sec. The Cf-252 source was in the inner-core region when it was at the "in" position (6" inches from midplane) and in the axial blanket region at the "out" position (30 inches from midplane). It was observed that the

Table 1. Measurement of polarity coherence function and the polarity coherence subcritical reactivity in a sodium voided core of ZPPR assembly 3 phase 3 by detector pairs of different positions (Results uncorrected for detector efficiency changes.) [48]

Run	^{252}Cf Source[a]	Adjacent detector pair				Cross detector pair			
		CD		AB		AD		CB	
		$\rho \pm \delta_\rho$	$\$ \pm \delta_\$$	$\rho \pm \delta_\rho$	$\$ \pm \delta_\$$	$\rho \pm \delta_\rho$	$\$ \pm \delta_\$$	$\rho \pm \delta_\rho$	$\$ \pm \delta_\$$
610	out	0.25587 ±0.00227	-1.6080[b] ±0.0020	0.48420 ±0.00180	-1.6080[b] ±0.0020	0.36264 ±0.00212	-1.6080[b] ±0.0020	0.34135 ±0.00220	-1.6080[b] ±0.0020
610	in	0.25571 ±0.00257	-1.6091 ±0.031	0.48725 ±0.00072	-1.5921 ±0.026	0.35980 ±0.00275	-1.5645 ±0.0317	0.34679 ±0.00294	-1.6129 ±0.0385
613	out	0.21598 ±0.00261	-1.9137 ±0.0362	0.42643 ±0.00207	-1.9306 ±0.0278	0.31323 ±0.00228	-1.8858 ±0.0343	0.29964 ±0.00225	-1.9300 ±0.0396
613	in	0.21711 ±0.00350	-1.9040 ±0.0412	0.42575 ±0.00240	-1.9346 ±0.0287	0.31223 ±0.00223	-1.9139 ±0.0452	0.29680 ±0.00220	-1.9451 ±0.0390
614	out	0.24253 ±0.00239	-1.7027 ±0.0317	0.46090 ±0.00175	-1.7328 ±0.0251	0.34465 ±0.00196	-1.7136 ±0.0317	0.36267 ±0.00213	-1.7319 ±0.0322
614	in	0.24155 ±0.00242	-1.7099 ±0.0319	0.46227 ±0.00206	-1.7253 ±0.0257	0.34408 ±0.00202	-1.7267 ±0.0314	0.32288 ±0.00242	-1.7295 ±0.0242
619	out	0.08680 ±0.00239	-3.9615 ±0.0893	0.20035 ±0.00215	-4.0482 ±0.0547	0.13949 ±0.00248	-3.9991 ±0.0813	0.12627 ±0.00272	-4.0502 ±0.0834
619	in	0.08592 ±0.00229	-3.9855 ±0.0876	0.20395 ±0.00253	-3.9922 ±0.0576	0.13899 ±0.00233	-3.7750 ±0.0863	0.12797 ±0.00260	-3.7770 ±0.0871
620[c]	out	0.0200 ±0.0025	-9.7529 ±0.6619	0.0536 ±0.0018	-9.6746 ±0.2099	--	--	--	--
620[c]	in	0.0226 ±0.0018	-9.1010 ±0.4053	0.0579 ±0.0018	-9.2476 ±0.1832	--	--	--	--

[a]Source strength: $S = 1.9 \times 10^8$ n/sec. "Out" position: axial blanket, 30 in. from midplane. "In" position: axial inner core, 6 in. from midplane.

[b]Reference calibration by rod drop inverse kinetics.

[c]All PSRs were inserted in.

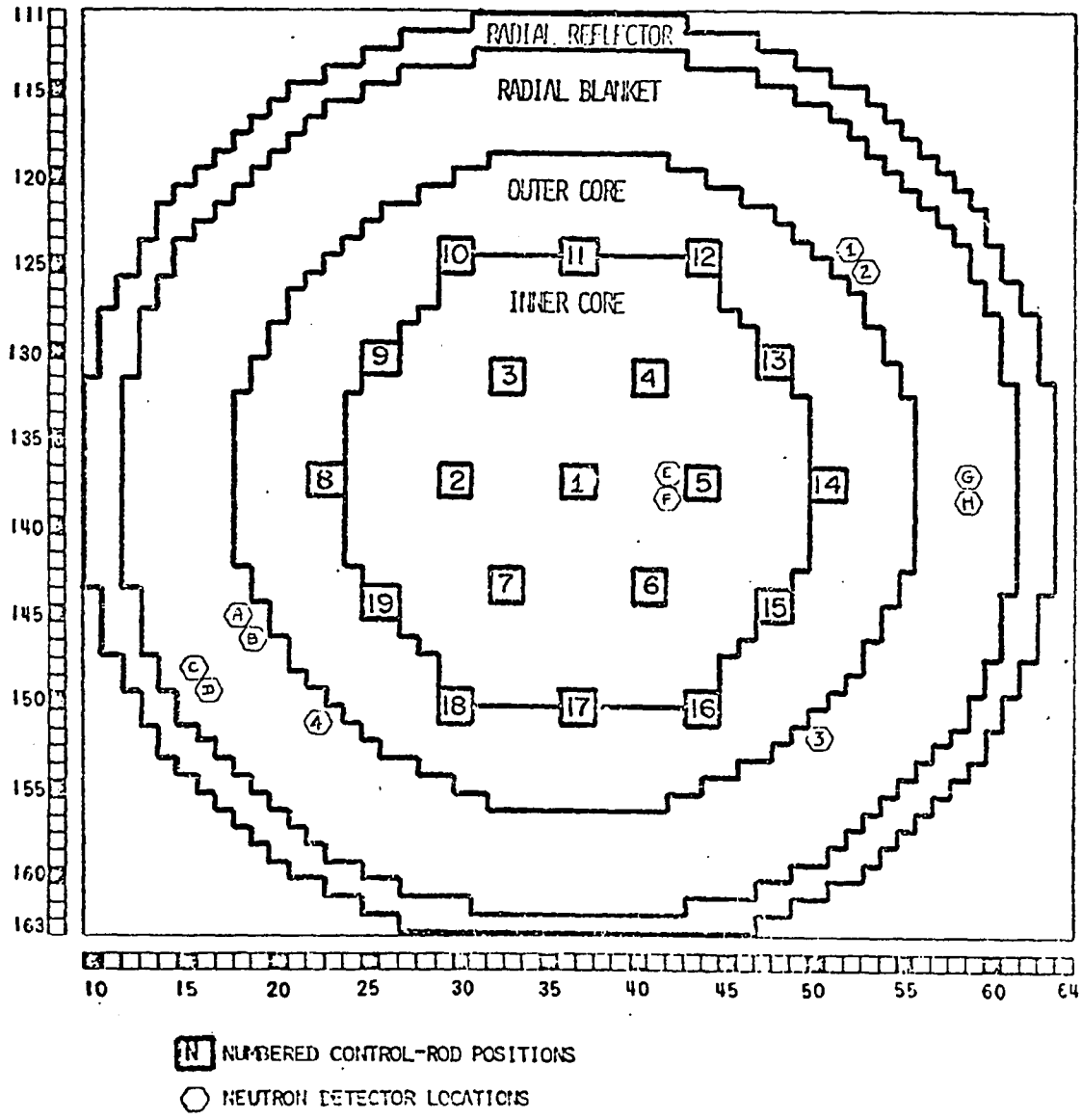

Figure 11. A cross-sectional view of detector and control rod locations in ZPPR

Table 2. Measurement of polarity coherence function and the polarity coherence subcritical reactivity in a hexagonal core of ZPPR assembly 3 phase 3 by detector pairs of different positions (Results uncorrected for detector efficiency changes.) [48]

Run	^{252}Cf Source[a]	Adjacent detector pair EF $\rho \pm \delta_\rho$	Adjacent detector pair EF $\$ \pm \delta_\$$	Adjacent detector pair GH $\rho \pm \delta_\rho$	Adjacent detector pair GH $\$ \pm \delta_\$$	Cross detector pair EH $\rho \pm \delta_\rho$	Cross detector pair EH $\$ \pm \delta_\$$	Cross detector pair FG $\rho \pm \delta_\rho$	Cross detector pair FG $\$ \pm \delta_\$$
684	out	0.66674 ±0.00144	-1.8714 ±0.0152	0.29785 ±0.00147	-1.7121 ±0.0541	0.43794 ±0.00193	-1.8434 ±0.0357	0.44195 ±0.00205	-1.8188[b] ±0.0384
684	in	0.66876 ±0.00168	-1.8584 ±0.0164	0.29938 ±0.00267	-1.7022 ±0.0555	0.44313 ±0.00207	-1.8138 ±0.0576	0.44367 ±0.00234	-1.8105 ±0.0413
684	out	0.45750 ±0.00263	-3.4228 ±0.0313	0.15254 ±0.00243	-3.1635 ±0.0918	0.25494 ±0.00181	-3.4665 ±0.0712	0.25544 ±0.00277	-3.4603 ±0.0291
684[c]	out	0.18614 ±0.00256	-7.4927 ±0.0870	0.06070 ±0.00235	-5.9485 ±0.2136	0.09318 ±0.00282	-6.7223 ±0.1677	0.09861 ±0.00241	-6.4804 ±0.1542
685	out	0.80106 ±0.00100	-1.0240 ±0.0105	0.45079 ±0.00204	-0.9497 ±0.0385	0.59609 ±0.00162	1.0330 ±0.0294	0.59567 ±0.00187	-1.0349 ±0.0328
685	in	0.80215 ±0.00113	-1.0171 ±0.0112	0.45262 ±0.00512	-0.9425 ±0.0454	0.60000 ±0.00124	-1.1053 ±0.0315	0.59570 ±0.00415	-1.0346 ±0.0373
686	out	0.81606 ±0.00142	-0.9283 ±0.0127	0.47703 ±0.00182	-0.8495 ±0.0363	0.61643 ±0.00233	-0.9411 ±0.0276	--	--
686	in	0.81778 ±0.00098	-0.9172 ±0.0102	0.48281 ±0.00210	-0.8282 ±0.0362	0.62285 ±0.00270	-0.9097 ±0.0373	0.62833 ±0.00158	-0.8860 ±0.0347
686[c]	out	0.22105 ±0.00231	-6.6440 ±0.0648	0.07493 ±0.00233	-5.2065 ±0.1698	0.11490 ±0.00210	-5.8740 ±0.1734	0.11237 ±0.00221	-5.9627 ±0.1862

[a]Source strength: $S = 1.9 \times 10^8$ n/sec. "Out" position: axial blanket, 30 in. from midplane. "In" position: axial inner core, 6 in. from midplane.

[b]Coherence signal was possibly contaminated by 60 cps line signal.

[c]All PSRs (except Nos. 5 & 12) were inserted in.

insertion of the Cf-252 source into the axial inner core has negligible effect on the coherence function and hence on the polarity coherence subcriticality.

Of particular significance of all the measurements is run 620 in Table 1 and runs 684, 686 in Table 2. These runs showed distinctly that the adjacent pair of detectors farther away from the core center displayed a lower coherence function than the adjacent pair nearer to the core center. The two cross pairs showed an intermediate value of the coherence function compared to the two adjacent pairs. In addition, the subcriticalities determined in these runs (all cases with all poison safety rods in) are dependent on which adjacent pair of detectors are used. Specifically, for run 684 and 686 in Table 2, the inferred $\$_2$ values by pair GH of the radial blanket are 21% and 22% lower (less subcritical) than those of pair EF of the inner core.

It is observed that there are no significant differences in the subcriticalities determined by the different adjacent and cross pairs of detectors when the reactor was not more than 2$ subcritical. Considerable differences showed up around -7$. In general, the adjacent pair that was closer to the core center showed a more subcritical reactivity. This is in agreement with the calculations done by Kryter et al. [49] and the measurements by the source multiplication method in phase 1B [50] and phase 2 [46].

Before discussing another experiment, some detailed explanations of Tables 1 and 2 are in order. As shown in the tables, the subcritical reactivities $\$ \pm \delta_{\$}$ were calculated for the adjacent detector pair and the cross detector pair. For the adjacent detector pair (where the detectors are of the same efficiency), $\$$ was calculated from the inference relation of Equation 3. Its standard deviation, $\delta_{\$}$, is calculated according the relation:

$$\delta_{\$_2} = \frac{1 - \$_2}{2} \left[\frac{\delta^2_{\rho_1}}{\rho_1^2(1 - \rho_1)^2} + \frac{\delta^2_{\rho_2}}{\rho_2^2(1 - \quad_2)^2} \right]^{1/2} \tag{7}$$

where $\delta_{\$_2}$ = standard deviation of subcritical reactivity of $\$_2$

δ_{ρ_i} = standard deviation of polarity coherence function ρ_i

$i = 1, 2.$

The derivation of the above equation is explained in detail in Appendix C. It supplements the expression defined by Hess and Albrecht [51].

For the cross detector pairs, the inference relation of Equation 7 is not applicable because of the different detector efficiency, i. e. $W_x \neq W_y$. To obtain $\$_2 \pm \delta_{\$_2}$ for the cross detector pair, the following equations were used. Their derivations are discussed in detail in Appendices D and E.

$$\$_2 = 1-(1-\$_1)\left(\frac{\beta_1}{\beta_2}\right)\left(\frac{W_{y2}}{W_{y1}}\right)^{\frac{1}{2}}\left\{\rho_1\frac{(1+\varepsilon_1)\rho_1+[(1-\varepsilon_1)^2\rho_1^2+4\varepsilon_1]^{\frac{1}{2}}}{2\varepsilon_1(1-\rho_1^2)}\right.$$

$$\left.x\ \frac{[(1-\varepsilon_2)^2\rho_2^2+4\varepsilon_2]^{\frac{1}{2}}(1+\varepsilon_2)\rho_2}{2\rho_2}\right\}^{\frac{1}{2}} \qquad (8)$$

where W_{yi} = efficiency of detector y at subcritical state i

$\varepsilon_i = \frac{W_{xi}}{W_{yi}}$ = detector efficiency ratio at subcritical state i

$i = 1, 2,$

$$\delta_{\$_2} = \left(\left(\frac{1-\$_2}{1-\$_1}\right)^2 \delta^2_{\$_1} + \left(\frac{\partial\$_2}{\partial\rho_1}\right)^2\delta^2_{\rho_1} + \left(\frac{\partial\$_2}{\partial\rho_2}\right)^2 \delta^2_{\rho_2}\right.$$

$$\left. + \left(\frac{\partial\$_2}{\partial\varepsilon_1}\right)^2 \delta^2_{\varepsilon_1} + \left(\frac{\partial\$_2}{\partial\varepsilon_2}\right)^2 \delta^2_{\varepsilon_2}\right)^{\frac{1}{2}} \qquad (9)$$

where $$\frac{\partial\$_2}{\partial\rho_1} = (1-\$_2)\left(\frac{1}{\rho_1}\ \frac{1}{(1-\varepsilon_1)\rho_1+[(1-\varepsilon_1)^2\rho_1^2+4\varepsilon_1]^{\frac{1}{2}}}\right)x$$

$$\left(\frac{\rho_1(1+\varepsilon_1)[(1-\varepsilon_1)^2\rho_1^2+4\varepsilon_1]^{\frac{1}{2}} + (1-\varepsilon_1)^2\rho_1^2+2\varepsilon_1(1+\rho_1^2)}{(1-\rho_1^2)^2[(1-\varepsilon_1)^2\rho_1^2+4\varepsilon_1]^{\frac{1}{2}}}\right),$$

$$\frac{\partial \$_2}{\partial \rho_2} = (1-\$_2)\ x$$

$$\left[\frac{2\varepsilon_2}{\rho_2[(1-\varepsilon_2)^2\rho_2^2+4\varepsilon_2]^{\frac{1}{2}}}\right] x \left[\frac{1}{[(1-\varepsilon_2)^2\rho_2^2+4\varepsilon_2]^{\frac{1}{2}}-(1+\varepsilon_2)\rho_2}\right],$$

$$\frac{\partial \$_2}{\partial \varepsilon_1} = \frac{(1-\$_2)}{2}\ x$$

$$\left[\frac{\varepsilon_1}{(1+\varepsilon_1)\rho_1+[(1-\varepsilon_1)^2\rho_1^2+4\varepsilon_1]^{\frac{1}{2}}}\right]$$

$$\left[\frac{2-\rho_1[(1-\varepsilon_1)^2\rho_1^2+4\varepsilon_1]^{\frac{1}{2}}-2(1-\varepsilon_1)^2\rho_1^2-4\varepsilon_1}{\varepsilon_1^2[(1-\varepsilon_1)^2\rho_1^2+4\varepsilon_1]^{\frac{1}{2}}}\right],$$

and

$$\frac{\partial \$_2}{\partial \varepsilon_2} = \frac{(1-\$_2)}{2}\ x$$

$$\left[\frac{1}{[(1-\varepsilon_2)^2\rho_2^2+4\varepsilon_2]^{\frac{1}{2}}-(1+\varepsilon_2)\rho_2}\right]\left[\frac{2-(1-\varepsilon_2)\rho_2^2}{[(1-\varepsilon_2)^2\rho_2^2+4\varepsilon_2]^{\frac{1}{2}}}-\rho_2\right].$$

Recent experiments were conducted at Argonne National Laboratory [44] to further investigate the effect of detector placement on the inferred subcriticality of the polarity coherence function method. Four detectors were deployed in

the radial blanket. They were situated such that they all had approximately the same efficiency in the reference state. One pair was placed in adjacent drawers and the other two widely separated. Their locations are shown in Figure 11. The results of the measurements are shown in Table 3. With no correction for detector efficiency change in the inference relation of Equation 3, it was found that when the control rod was in position CRP-17 (Figure 11), the measured result by detector pair 34 was more subcritical than pair 12. This is reasonable since detector pair 34 was in a lower neutron flux and hence had a lower detector efficiency, i.e. detections per fission. When the control rod was in position CRP-1 (the core center) the measurements obtained from the different pairs showed little difference since they experienced almost the same magnitude of neutron flux. With the control rod in position CRP-7 detector 4 is neutronically shadowed. Therefore, the results of the measurements by detector pairs without detector 4 were less subcritical than the pairs with detector 4.

The above measurements showed that the detector efficiency, and hence detector response, is dependent on the detector location inside the reactor. Placement of a detector in a neutronically shadowed area would result in a decrease of the detector efficiency. If this change of detector efficiency is unaccounted for in the inference relation (Equation 3), the

Table 3. Subcriticality, in dollars, as measured by polarity coherence[a] (results uncorrected for detector-efficiency changes) [44]

Reactor condition	Detector pair					
	12	13	14	23	24	34
1. Reference	1.67	1.67	1.67	1.67	1.67	1.67
2. Ref. with Shims out	1.34	1.32	1.30	1.31	1.26	1.30
3. N1 in CRP-17	1.84	1.88	1.88	1.88	1.84	1.93
4. N1 in CRP-7	2.45	2.50	2.59	2.43	2.55	2.47
5. N1 in CPR-1	3.13	3.06	3.07	2.94	3.02	2.93
6. M in CRP-1	4.36	4.48	4.44	4.40	4.29	4.25
7. E1 in CRP-1	4.46	4.48	4.47	4.39	4.49	4.24
8. E2 in CRP-1	4.55	4.56	4.59	4.52	4.44	4.35
9. M in CRP-7	3.35	3.41	3.69	3.37	3.65	3.66
10. M in CRP-17	2.43	2.53	2.53	2.51	2.52	2.62
11. E2 in CRP-17	2.44	2.58	2.60	2.56	2.56	2.71

[a]Statistical uncertainties about 1%.

inferred subcritical reactivity would be less than the true value. Under the condition of using the uncorrected efficiency ratio for an azimuthally neutronically shadowed location, the inferred reactivity would be erroneously more subcritical.

To summarize, the following conclusions can be drawn from experimental measurements in ZPPR:

1. Practically no space effect was observed in the inferred subcriticality at not more than 2$ subcritical.
2. Spatial effect due to detector placement in neutronically shadowed area would cause the inferred subcriticality to differ from the true value. This effect was observed to start around -3$ and become quite significant at -7$ ($\sim$7% $\$_2$) discrepancy.

In addition, inner core measurements showed an inferred $\$_2$ values about 22% more subcritical than those of the radial blanket at ∿-6$.

3. The introduction of an extraneous neutron source has little effect on the numerical result of the coherence function and the inference of the subcriticality.

B. Calculational

The computer code TASK was utilized to compute the neutron detector response at steady state and at low frequency (100 Hz). From the detector response, three quantities were calculated: the cross power spectral density (CPSD), the detector white noise (due to random detection of the steady state flux), and the auto power spectral density (APSD). Substituting the result of the CPSD and APSD into Equation 1, the coherence function can be calculated. By using the inference relation of Equation 3, the coherence function reactivity in $\$_2$ can be obtained.

There are many possible candidate materials for neutron detectors in a fast breeder reactor. Among the more common ones are lithium-6, uranium-235, uranium-238, and plutonium-240. Their detection cross sections in a 6-group structure are shown in Table 4. Figure 12 is a simplified graph of detector cross section vs. energy for different detection materials. It can be observed from this graph that lithium-6 has the highest detection cross section among all the

Figure 12. Detector cross sections for different neutron energies

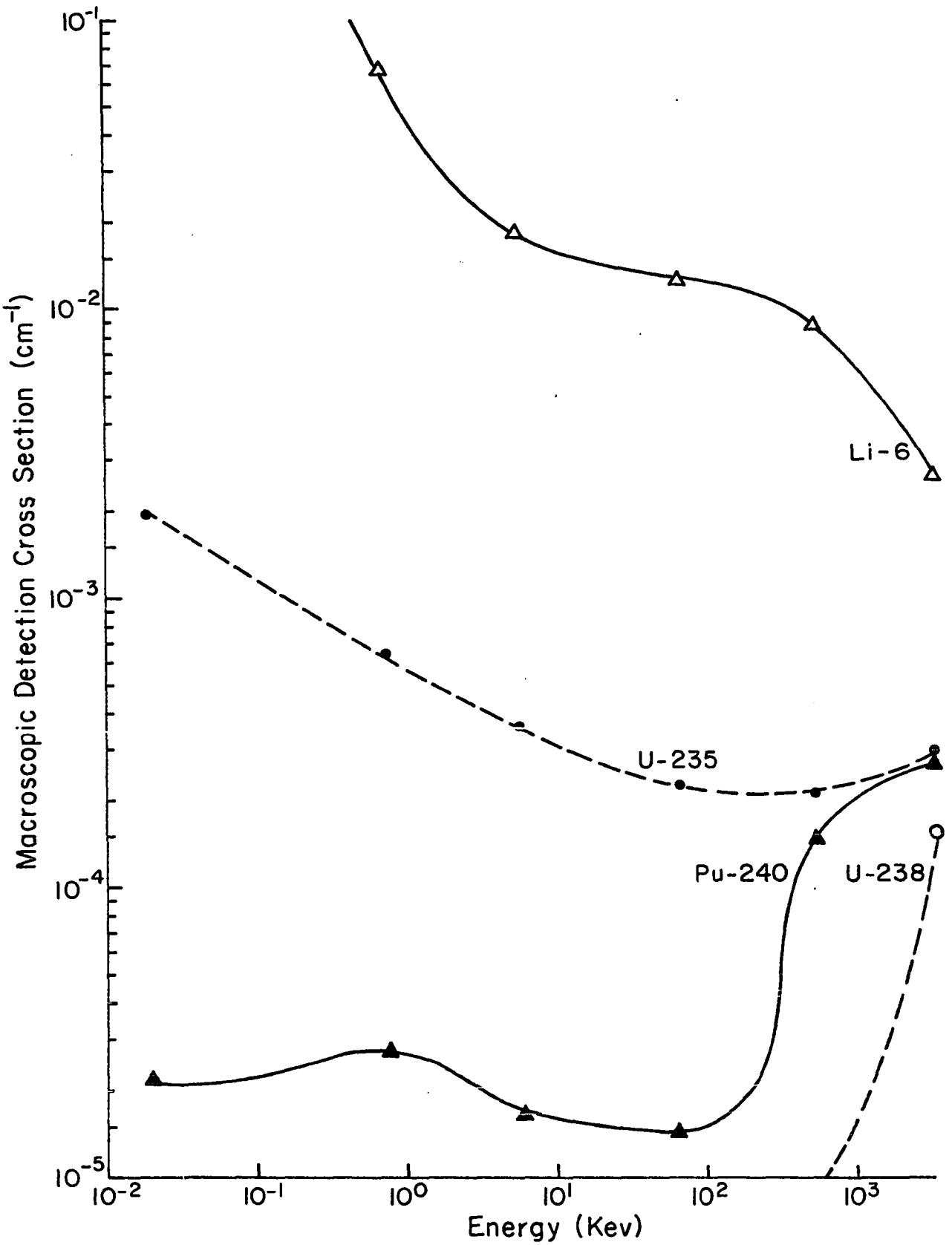
Macroscopic Detection Cross Section (cm⁻¹)
10⁻¹
10⁻²
10⁻³
10⁻⁴
10⁻⁵
10⁻²
10⁻¹
10⁰
10¹
10²
10³
Energy (Kev)
Li-6
U-235
Pu-240
U-238

Table 4. Macroscopic detector cross section of various materials

Energy group	Neutron velocity (cm/sec)	Upper energy boundary, E_U	Lower energy boundary, E_L	Lethargy[a] interval, ΔL	Li-6 (cm^{-1})	U-235 (cm^{-1})	U-238 (cm^{-1})	Pu-240 (cm^{-1})
1	2.0072+9	10 Mev	1.35 Mev	2	2.69-3	2.95-4	1.53-4	2.78-4
2	8.2740+8	1.35 Mev	186 Kev	2	8.80-3	2.12-4	3.34-6	1.49-4
3	3.4212+8	186 Kev	24.7 Kev	2	1.23-2	2.26-4	9.35-9	1.46-5
4	1.3241+8	24.7 Kev	3.35 Kev	2	1.81-2	3.61-4	-0-	1.61-5
5	4.2005+7	3.35 Kev	0.275 Kev	2.5	6.80-2	6.23-4	-0-	2.78-5
6	1.1384+7	0.275 Kev	0	∞	1.01-0	1.96-3	-0-	2.16-5

[a] $\Delta u = \ln\left(\frac{E_U}{E_L}\right)$.

candidates. It should be noted that lithium-6 and uranium-235 are low-energy-sensitive detector material while uranium-238 and plutonium-240 are high-energy-sensitive detector material. In ZPPR the neutron energy spectrum is relatively soft, i.e. the bulk of the neutron flux is in the Kev range from the second to the fourth group of a 6-group structure (Table 4). The use of a low energy sensitive detector is more appropriate for purpose of increasing detector efficiency. The lithium-6 detector is numerically simulated in this study.

The nuclear cross section of each nuclide used in the calculation was obtained from the Evaluated Nuclear Data File B, Version II (ENDFB/II) of Argonne National Laboratory in Idaho. They were used in all the calculations for simulation of ZPPR in this study.

With the proper input of nuclear cross sections for each region, the ZPPR was modeled numerically in the radial direction. Figure 13 shows the reactor configuration studied. Although the reactor configuration is two-dimensional in nature, the TASK code can only handle one-dimensional problems. For the radial calculation, an axial buckling term was used for each region to account for the effect of the finite axial dimension.[1]

---

[1]The one-dimensional numerical model has limited capability in describing azimuthal heterogeneity. See Appendix F for detail discussion.

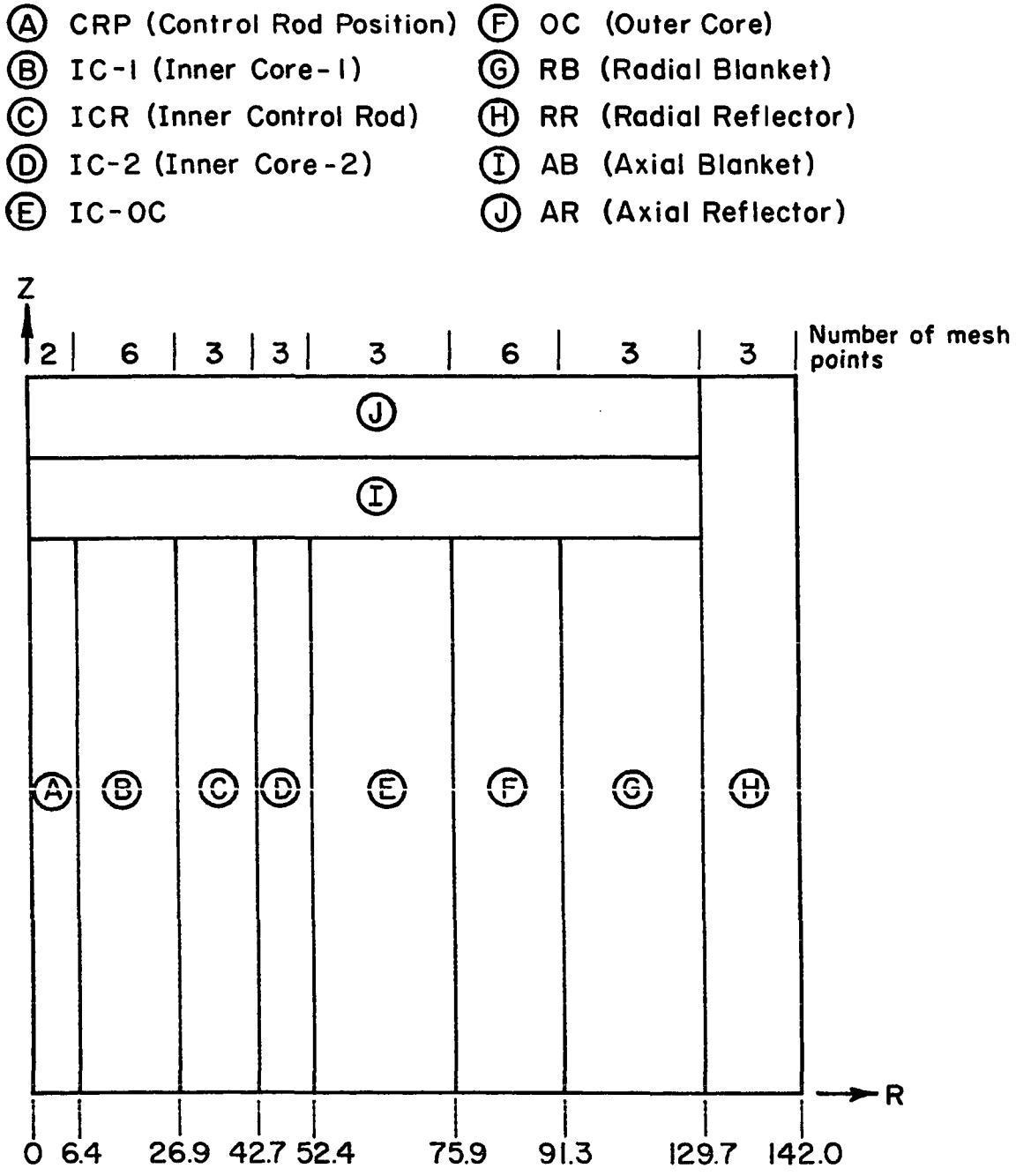

Figure 13. The RZ model of ZPPR assembly 3 phase 1B (all dimensions in cm)

For each reactor phase core studied, the steady state case ($\omega = 0$) was first solved. The detector white noise (due to random detection of the steady state flux) was then calculated. Specifically, the following relation was employed:

$$\sum_{g=1}^{G} [\Sigma d_g \phi_{og}]_i = \text{detector white noise at position } i$$

where Σd_g = detector cross section of energy group g

ϕ_{og} = steady state neutron flux of energy group g

G = number of energy groups.

The detector white noise is due to the statistics of the detection process, since the steady detection rate in the neutron detector chamber is made up of many reactions produced by randomly arriving neutrons [41].

The neutron flux at 100 Hz was solved next. The detector response was calculated by the following expressions:

$$\sum_{g=1}^{G} [\Sigma d_g \phi_g(\omega)]_i = \text{Detector response at position i and frequency } \omega$$

where $\phi_g(\omega)$ = neutron flux at frequency ω of energy group g.

The power spectral densities can now be obtained by means of the results of the frequency-dependent detector response and the detector white noise. In particular, it can be

written:

$$\Phi_{ij}(\omega) = \sum_{g=1}^{G} [\Sigma d_g \phi_g(\omega)]_i \times [\Sigma d_g \phi_g^*(\omega)]_j \qquad (10)^2$$

$$\Phi_{ii}(\omega) = \sum_{g=1}^{G} \left([\Sigma d_g \phi_g]_i + \left| [\Sigma d_g \phi_g(\omega)]_i \right|^2 \right) \qquad (11a)$$

and

$$\Phi_{jj}(\omega) = \sum_{g=1}^{G} \left([\Sigma d_g \phi_{og}]_j + \left| [\Sigma d_g \phi_g(\omega)]_j \right|^2 \right) \qquad (11b)$$

In the case where the two detection systems are identical and the detectors are situated in adjacent drawers, position i are essentially the same as position j. Therefore, the equation for the coherence function becomes:

$$\rho(\omega) = \frac{\left| \Phi_{ij}(\omega) \right|}{\left(\Phi_{ii}(\omega) \Phi_{jj}(\omega) \right)^{\frac{1}{2}}} = \frac{\sum_{g=1}^{G} \left| [\Sigma d_g \phi_g(\omega)]_i \right|^2}{\sum_{g=1}^{G} \left([\Sigma d_g \phi_{og}]_i + \left| [\Sigma d_g \phi_g(\omega)]_i \right|^2 \right)} \qquad (12)$$

---

[2]The superscript * denotes the complex conjugate of the frequency dependent flux.

Before proceeding to the calculational result, it would be informative to examine the meaning of Equation 12. If the detector white noise, $\Sigma_d\phi_o$, is small compared to the cross power spectral density, $|[\Sigma_d\phi(\omega)]|^2$, then the coherence function, $\rho(\omega)$, approaches unity and the system is highly coherent (correlated). This is the case of the near critical states where the signal, i.e. $|[\Sigma_d\phi(\omega)]|^2$, dominates the detector white noise, $\Sigma_d\phi_o$. If the detector white noise is higher in magnitude as compared to the power spectral density, then the coherence function becomes small. Such is the case of far subcritical states where the detector white noise dominates the signal.

In Section V, the subject of "chain-related" (correlated) counts and "random" counts is discussed. It is sufficient to indicate here that the cross power spectral density, $|[\Sigma_d\phi(\omega)]|^2$, represents the "chain-related" counts and the detector white noise, $\Sigma_d\phi_o$, represents the "random" (uncorrelated) counts. In near critical states, there are only a few fission chains (of long chain-life) and therefore the "chain-related" counts dominates the "random" counts. As a result, the coherence function approaches unity in these states. In the far subcritical states, there are many fission chains (of short chain-life) and therefore the random (uncorrelated) counts are comparable or greater than the "chain related" counts. Consequently, the coherence function

decreases in magnitude in these states.

A 6-group model was used for the numerical study of the ZPPR assembly 3 phase 1B core. A static flux calculation was done for the critical state. This was done in order to solve for the fundamental mode (lambda mode) neutron flux distribution. For TASK code, this would mean an input of zero frequency and zero distributed source. The result of a TASK-computed neutron flux profile was compared with the static ARC (Argonne Reactor Computation) [37] diffusion calculation. Close agreement was observed between the TASK and ARC results. Figures 14 and 15 show the flux distributions from the two calculations. This is in agreement with the computational test done by Dodd et al. [40].

It should be noted that because of different normalization schemes in the computer codes TASK and ARC, the magnitude of the neutron flux calculated from each code is different. Consequently, only the profile can be meaningfully compared in Figures 14 and 15.

A near critical state of -1.51$ was first studied. Two neutron flux distributions for the ZPPR assembly 3 phase 1B core were calculated by using the TASK code. One calculation is for the solution of the static neutron flux (i.e. zero Hz) and the other the low frequency flux (the Fourier transform of the neutron flux at 100 Hz). For near critical states, the effect of the extraneous neutron source on the flux distribu-

Figure 14. Steady state flux distribution TASK computation of ZPPR assembly 3 phase 1B at critical

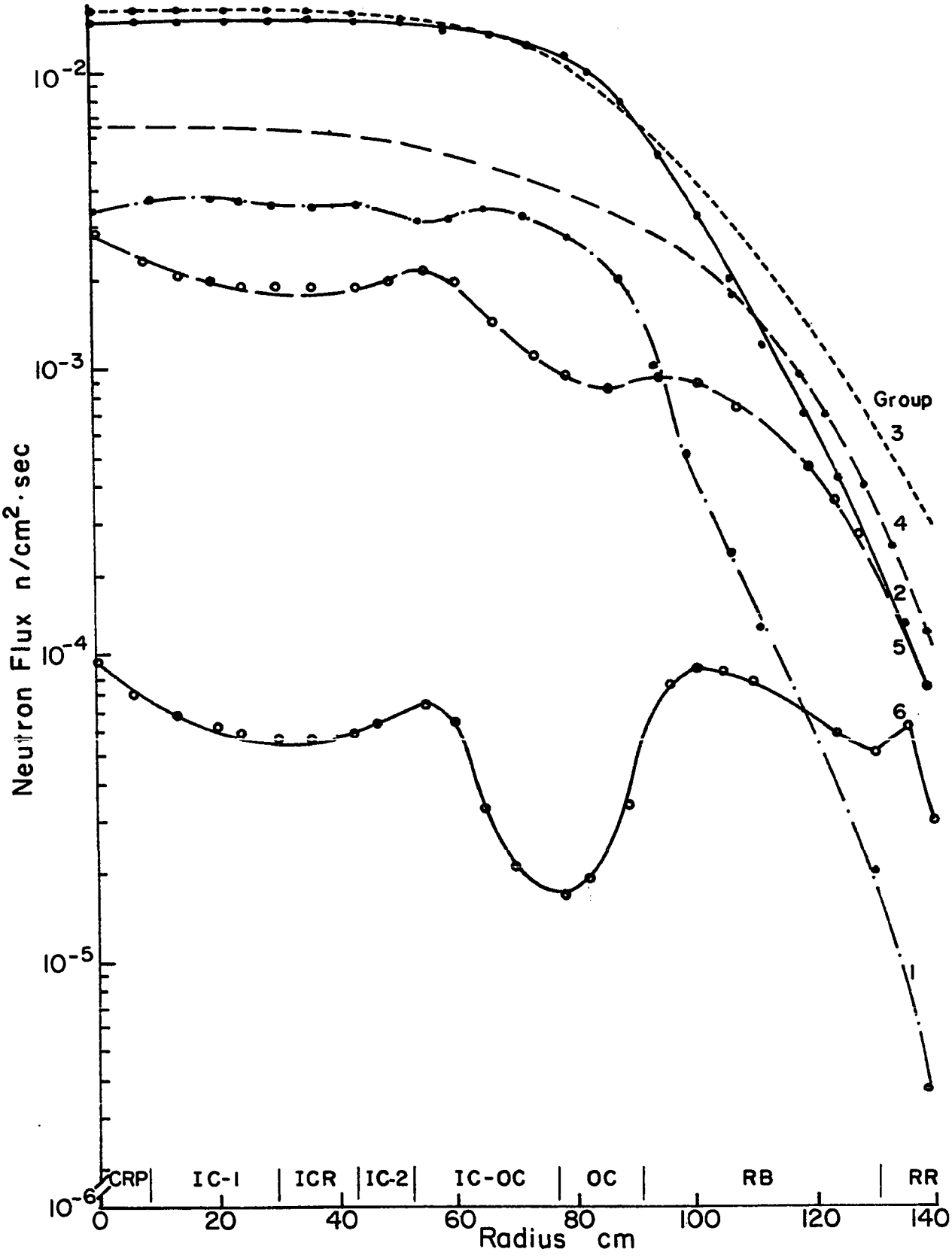
Neutron Flux n/cm^2·sec
10^{-2}
10^{-3}
10^{-4}
10^{-5}
10^{-6}
Group
3
4
2
5
6
1
CRP
IC-1
ICR
IC-2
IC-OC
OC
RB
RR
0
20
40
60
80
100
120
140
Radius cm

Figure 15. Steady state flux distribution ARC computation of ZPPR assembly 3 phase 1B at critical

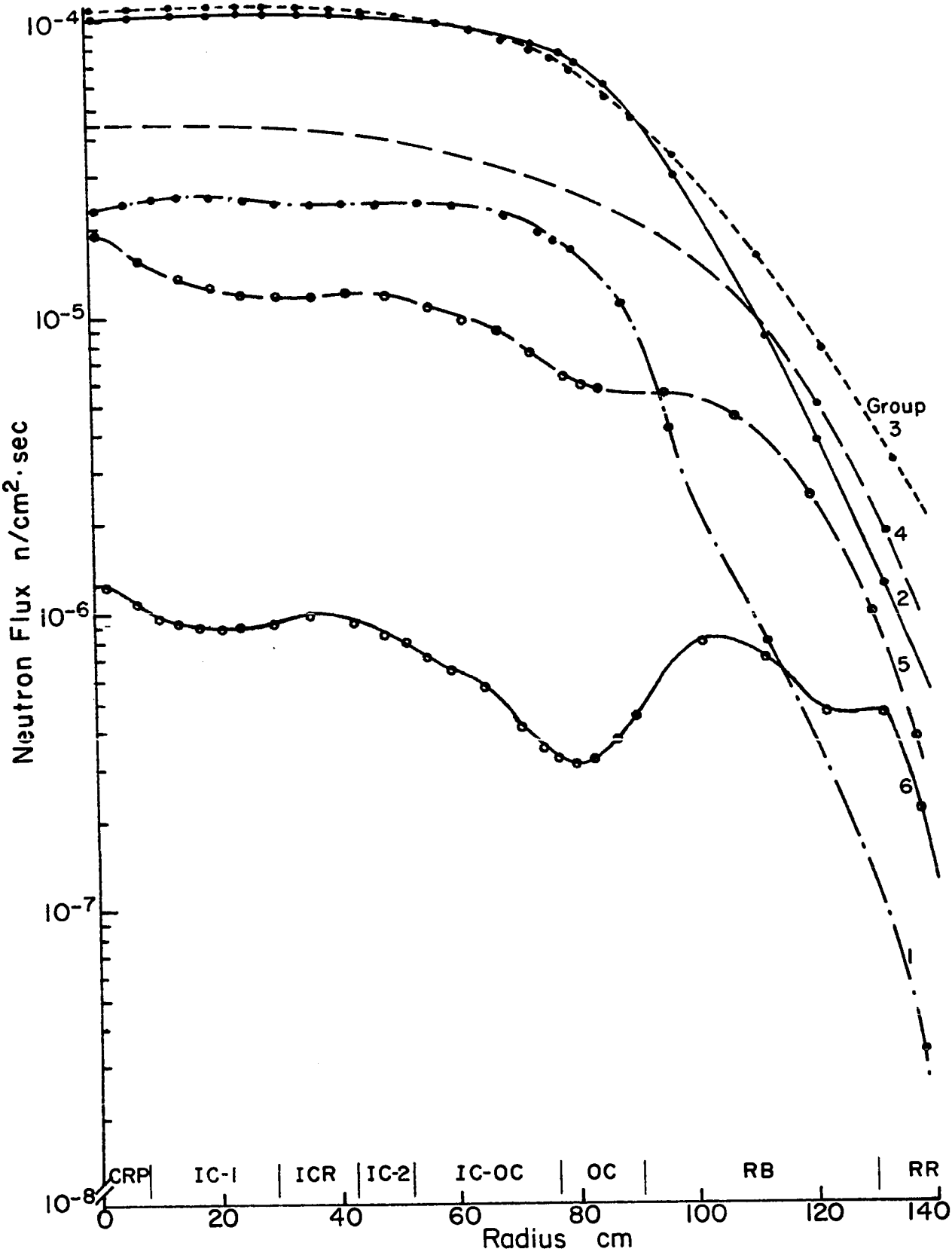
Neutron Flux n/cm².sec
10⁻⁴
10⁻⁵
10⁻⁶
10⁻⁷
10⁻⁸
Group
3
4
2
5
6
1
CRP
IC-1
ICR
IC-2
IC-OC
OC
RB
RR
0
20
40
60
80
100
120
140
Radius cm

tion is minimal [12,13]. Therefore, the source free eigenvalue (lambda mode) calculation was adequate for the solution of the static flux. With the static flux, the low frequency flux at 100 Hz of the same near critical state was computed next. First, the driving function in the form of a distributed neutron source for this frequency state has to be calculated. The distributed neutron source input to TASK was obtained by taking the square root of the noise equivalent source [40, 52] as defined by Cohn [41] and Sheff and Albrecht [53]. Specifically, the following expression was used to describe the region dependent noise equivalent source for the ZPPR assembly 3 cores:

$$\langle |S_o|^2 \rangle_g = (\Sigma_a \phi_o)_g \; [k \; \nu \; D + \delta k] + S_g \qquad (13)$$

where $\langle |S_o|^2 \rangle_g$ = noise equivalent source (NES) of energy group g

ϕ_o = static neutron flux

Σ_a = macroscopic absorption cross section

k = multiplication factor

δk = k - 1

D = Diven's factor

ν = number of neutrons emitted per fission

S_g = extraneous source strength of energy group g

Referring to Equation 13, the static neutron flux, ϕ_o, was obtained from the previous eigenvalue calculation at the near critical state of -1.51$. In addition, the contribution of the extraneous source term Sg (primarily due to the Pu-240 spontaneous fission) to the NES is negligible at this near critical state. Consequently, Sg can be left out in computing the noise equivalent source at -1.51$ subcritical. This practice is consistent with the computational procedures used by Dodd et al. [40]. With the noise equivalent source calculated, its square root was used as the distributed source input to the TASK code for the computation of the low frequency (100 Hz) flux.

Having computed the static and low frequency (100 Hz) fluxes, the various detection rates can be obtained. The different power spectral densities can be computed by Equations 10 and 11. Using Equation 12, the coherence function at each reactor region was obtained. They are shown in Figure 16 and Table 5.

A subcritical case of -14.26$ was next investigated. Unlike the near critical state, the static flux distribution in this case is highly biased by the extraneous source (primarily that of Pu-240). Therefore, the eigenvalue calculation, which does not account for the source effect, is not suitable to describe the static flux distribution. (The eigenvalue calculation is still quite accurate in converging on the solution

Figure 16. Calculated coherence function distribution at -14.26$ and -1.51$

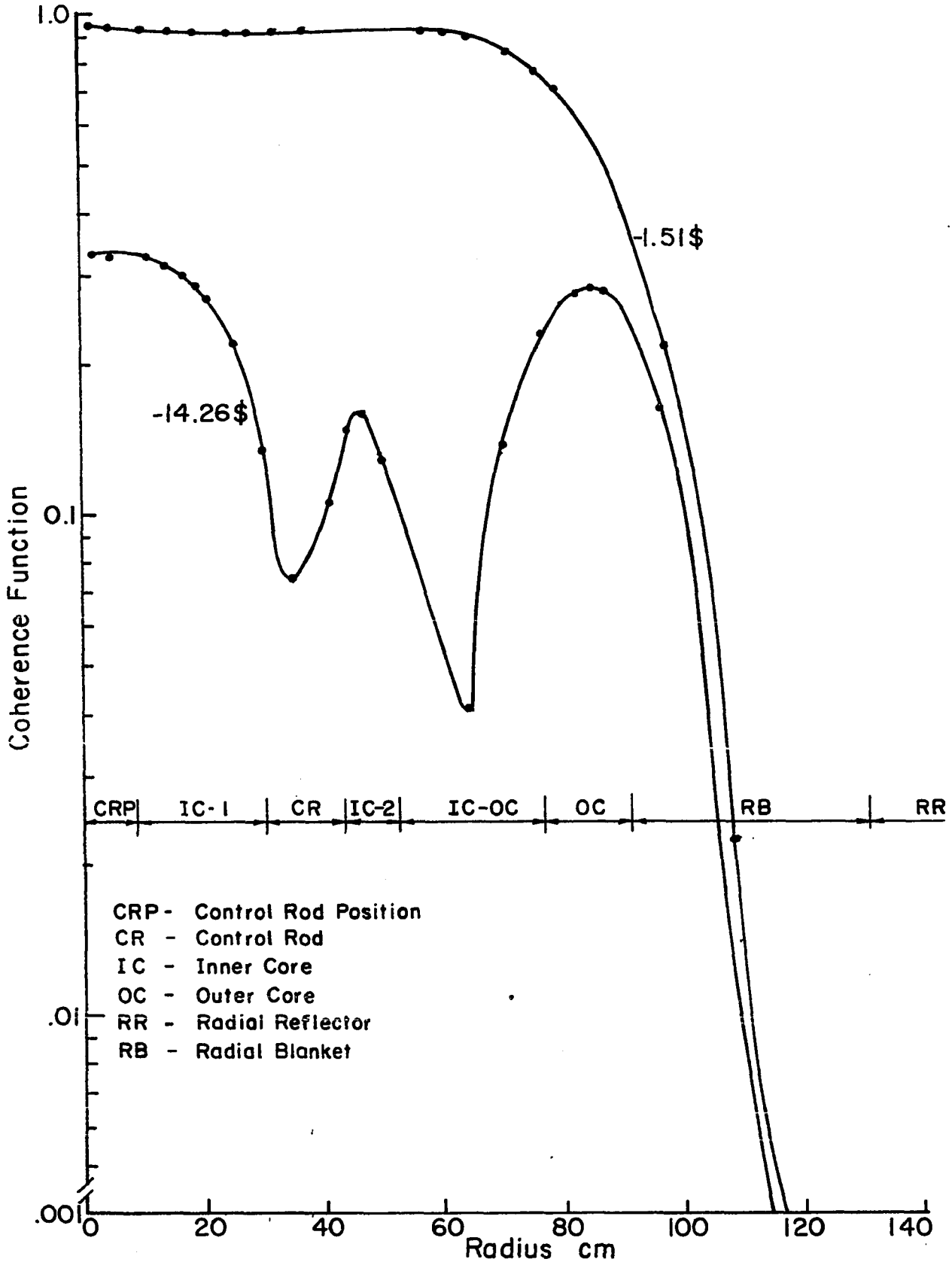
1.0
0.1
.01
.001
Coherence Function
-1.51$
-14.26$
CRP
IC-1
CR
IC-2
IC-OC
OC
RB
RR
CRP- Control Rod Position
CR - Control Rod
IC - Inner Core
OC - Outer Core
RR - Radial Reflector
RB - Radial Blanket
0
20
40
60
80
100
120
140
Radius cm

Table 5. The inferred subcritical reactivities for the spatially dependent coherence function of ZPPR assembly 3 phase 1B

Location (distance from core center)	Region	Detector efficiency ratio, $\frac{W_2}{W_1}$ [c]	ρ_1	$\$_1$ [a]	ρ_2	$\$_2$ [b]
1.594 cm	CRP	---	0.9595	-1.51	0.3390	-15.52
8.091 cm	IC 1	---	0.9431	-1.51	0.3323	-12.98
25.230 cm	IC 1	---	0.9051	-1.51	0.2220	-12.95
47.520 cm	IC 2	---	0.9051	-1.51	0.1416	-11.76
72.000 cm	IC-OC	---	0.8072	-1.51	0.1339	-11.52
110.500 cm	RB	---	0.2160	-1.51	0.0103	-11.36

[a] Lambda-mode reactivity. Obtained from source-free eignevalue calculation.

[b] The lambda-mode reactivity for this state is -14.26$. Delayed neutron fraction ratio, $\left(\frac{\beta_1}{\beta_2}\right)$, is 1.0.

[c] Detector efficiency ratio taken as 1.0.

of the eigenvalue of the subcritical state, i.e. the lambda mode reactivity).

The source mode calculation was employed in such cases. With the proper input of the extraneous source, the static flux (zero frequency) was calculated for the -14.26$ subcritical state of ZPPR assembly 3 phase 1B. The low frequency flux at the same subcritical state can be solved next. First, Equation 13 was used to find the noise equivalent source. The static flux from the source mode calculation was applied to Equation 13. The magnitude of the extraneous source term is no longer negligible for this subcritical state. Therefore, both the reaction rate term and the extraneous source term (due to Pu-240 spontaneous fission) have to be accounted for in Equation 13 at -14.26$ subcritical. With the noise equivalent source computed, its square root was used as the input driving function for the solution of the low frequency flux at 100 Hz.

Accordingly, the static (zero frequency) and the low frequency (100 Hz) neutron flux distribution at -14.26$ subcritical were calculated by TASK. The neutron fluxes were folded with the Li-6 detector cross section to obtain two quantities: the detector white noise and the "signal" (square modulus of the low frequency detector response). The coherence functions were then computed by using the white noise and the signal according to Equation 12. The coherence

function at -14.26$ of each spatial point is shown in Figure 16. It is observed that the coherence function is highly space dependent. In general, it displayed a high value at a high flux region (e.g. the inner core and outer core region) and a diminishing value in the low flux area, e.g. the blanket. The calculated results of this spatial behavior of the coherence function are in general agreement with the experimental measurements shown in Table 1 and 2 (pp. 47 and 49).

It should be noted from Figure 16 that the coherence function undergoes significant decrease in the vicinity of the control rod region. Specifically, the depression of neutron flux by the control rod material reduces the coherence function very drastically.

The detector efficiency ratios at different reactor locations were calculated next. The detector efficiency is the ratio between the detection rate and the reactor fission rate. Both the detection rate and the reactor fission rate are directly proportional to the magnitude of the neutron flux, i.e. the flux scaling factor. Thus, the calculated detector efficiency is independent of the flux normalization factor. Consequently, the flux (or power) normalization scheme in the neutronic code has no affect on the computation of the detector efficiency.

For the two subcritical states of -1.51$ and -14.26$ and at the core center location, the detector efficiency ratio of

0.9377 was obtained. This was obtained by using the static flux distributions of the respective subcritical states. By folding the steady state neutron fluxes with the Li-6 macroscopic cross-section, the detector efficiency for each location at these two subcritical states were obtained. The changes of detector efficiency ratios calculated in this way are observed to be less than 6%.

With the delayed neutron fraction ratio and the pertinent parameters from reference [54] and previous data, the subcriticality corresponding to the calculated coherence functions was inferred by using Equation 3. Table 5 shows the inferred subcriticalities obtained from these calculations.

From the calculational results of $\$_2$ in Table 5, the following few points were observed:

(1) The inferred subcritical reactivity near the core center agreed with the lamda-mode reactivity[1] within 8%.

(2) In the low flux locations such as the control rod and the blanket regions, the coherence functions are quite small as compared with those near the core center. The inferred subcritical reactivities at

---

[1]The lambda-mode reactivity is based on the eigenvalue of the neutron diffusion (or transport) equation describing the whole reactor. It is a gobal quantity and therefore space independent.

these locations are about 26% less subcritical than those of the core center.[2]

(3) Traversing in the radial direction from the core center to the radial reflector, the coherence function generally decreases. In addition, the inferred subcriticality becomes smaller in magnitude, i.e. less subcritical, in moving away from the core center.[2]

It should be noted that the above observations of the calculated spatial behavior for coherence functions and their inferred subcriticality are in good agreement with experimental results, e.g. run 684 and 686 of Table 2 (p. 47). Specifically, both sets of data indicate a more subcritical inferred $\$_2$ value in the core center than the blanket region. This trend has been observed independently using other reactivity measurement methods (e.g. Table 6, 7 on pp. 82,83).

It should be pointed out that the underestimation of the inferred subcriticality (i.e. erroneously less subcritical) at the radial blanket region has two significant implications. In the case of measurement of shutdown subcriticality by ex-core neutron detectors (e.g. blanket detectors or radial shield monitors) this underestimation would add a safety margin during shutdown and refueling. On the other hand, in

---

[2]This observation is in agreement with the experimental results of runs 684 and 686 in Table 2. Specifically, the effect of detector efficiency ratio on the spatial dependence of $\$_2$ is secondary as compared to that of the coherence function.

the approach-to-critical case, the underestimation of the control rod worth for control rod and safety rod withdrawal would lead to an erroneously low reactivity. Thus, a set of correction factor for adjustment of spatial effects are needed for the correct interpretation of the coherence function reactivity.

To summarize, it has been shown numerically that the coherence function is spatially dependent. The spatial dependence effect becomes more pronounced with the presence of the neutron absorber, such as control rod insertion. The inferred subcriticalities showed a varying range of 26% at different locations. It is observed that both the experimental data and the computational results show the following trend: at far subcritical range, the farther the detector pair is located away from the core center, the lower (less subcritical) the $ value is (pp. 50 and 78). Thus, when comparing with the lambda-mode reactivity, the most accurate coherence function reactivity is likely to be at the core center. It should also be noted that the results in Table 5 suggest that there may be a space dependent effect other than the detector efficiency effect which may cause the discrepancies between the results of different detector locations.

VI. MODIFICATION OF THE INFERENCE RELATION FOR SUBCRITICAL REACTIVITY FROM THE COHERENCE FUNCTION

Various reactivity measurements have been made in the ZPPR critical assembly for different phases of the core. The methods used to make measurements of more than -7$ subcritical are the source multiplication method and the coherence function method.

Intercomparison of the experimental results of these two methods revealed a consistent discrepancy. The source multiplication method showed a higher degree of subcriticality than the coherence function method. This discrepancy remained even after the proper calculational correction in detector efficiency and delayed neutron fraction for Equation 3.

Tables 5, 6 and 7 show the experimental results of subcriticality measurements by the different methods. They illustrate that as the degree of subcriticality becomes greater, the discrepancy between the source multiplication method and the polarity coherence function method increases. Figure 17 shows the positions of control rods and neutron detectors for these measurements.

The observed discrepancy of the results between the coherence function method and the source multiplication method shows up at moderate to far-subcritical ranges. For example, consider the measurements made at the core center by these two

Table 5. Multiple-rod configuration worth measurements in phase 1A of ZPPR assembly 3

Run	Control-rod positions loaded with B_4C rods	Uncorrected noise $	W_2/W_1	β_1/β_2	Corrected noise $[a]	Source mult. $	Inverse kinetics $
1	2	1.37	0.98	1.00	1.36 ±1	1.34	1.39
2	8	1.38	1.01	1.00	1.39 ±1	1.41	1.41
3	8, 14	3.36	1.02	1.00	3.40 ±1	3.37	3.20
4	9	1.12	1.00	1.00	1.12 ±1	1.14	1.17
5	2, 5	3.12	0.95	1.01	3.05 ±1	2.98	2.93
6	2, 4, 6	4.81	0.92	1.01	4.64 ±1	4.52	4.04
7	2, 4, 6, 10, 14, 18	9.29	0.95	1.01	9.11 ±1	9.42	NA
8	All 18	22.5	0.93	1.03	22.3 ±3	30.2	NA
9	outer ring	14.7	1.08	1.01	15.5 ±2	18.8	NA
10	8, 10, 12, 14, 16, 18	8.80	1.04	1.01	9.10 ±1	9.90	NA

[a] Uncertainties are in %.

Table 6. Multiple-rod configuration worth measurements in phase 1B of ZPPR assembly 3

Run	Assembly configuration: Control-rod positions loaded with B_4C rods	Net configuration worth, $, relative to reference phase 1B configuration			
		Polarity coherence; detectors at core center	Inverse multiplication		
			Fission counter at core center	BF_3 proportional counters outside axial reflector	BF_3 ion chambers outside radial reflector
1	9	-1.95 ± 0.01	-1.93 ± 0.01	-1.98 ± 0.01	-2.05 ± 0.01
2	2,9	-3.60 ± 0.02	-3.69 ± 0.02	-3.71 ± 0.02	-3.75 ± 0.02
3	2,8,9	-4.74 ± 0.02	-4.94 ± 0.02	-5.01 ± 0.03	-4.90 ± 0.02
4	2,8	-3.55 ± 0.02	-3.62 ± 0.02	-3.67 ± 0.02	-3.58 ± 0.02
5	8,9	-3.31 ± 0.02	-3.41 ± 0.02	-3.56 ± 0.02	-3.55 ± 0.02
6	8	-1.90 ± 0.01	-1.93 ± 0.01	-2.00 ± 0.01	-1.99 ± 0.01
7	2	-2.04 ± 0.01	-2.03 ± 0.01	-2.03 ± 0.01	-2.05 ± 0.01
8	2,5	-4.29 ± 0.02	-4.34 ± 0.02	-4.15 ± 0.02	-4.17 ± 0.02
9	8,14	-4.40 ± 0.03	-4.16 ± 0.02	-4.36 ± 0.02	-4.28 ± 0.02
10	2,4,6	-6.44 ± 0.04	-6.44 ± 0.04	-6.36 ± 0.03	-6.45 ± 0.04
11	2,3,4,5,6,7,10,14,18	-18.61 ± 0.40	-20.53 ± 0.14	-19.16 ± 0.11	-18.54 ± 0.09
12	2,3,4,5,6,7,8,10,12,	-24.39 ± 0.69	-29.28 ± 0.21	-26.71 ± 0.17	-26.30 ± 0.13
13	14,16,18				
14	All except CRP-1	-31.45 ± 0.80	-43.58 ± 0.30	-37.97 ± 0.24	-36.40 ± 0.18
15	2,4,6,9,10,11,13,14,	-23.77 ± 0.40	-28.33 ± 0.20	-25.91 ± 0.18	-25.13 ± 0.14
16	15,17,18,19				
17	8,9,10,11,12,13,14,	-23.20 ± 0.22	-27.47 ± 0.17	-25.70 ± 0.17	-25.92 ± 0.14
18	15,16,17,18,19				
19	8,10,12,14,16,18	-13.63 ± 0.11	-14.88 ± 0.08	-14.64 ± 0.08	-15.22 ± 0.08
20	2,4,6,8,10,12,14,	-19.76 ± 0.31	-22.20 ± 0.14	-20.99 ± 0.14	-21.16 ± 0.11
21	16,18				
22	2,4,6,10,14,18	-14.80 ± 0.18	-14.01 ± 0.07	-13.59 ± 0.07	-13.44 ± 0.07

Table 7. Multiple-rod configuration worth measurements in phase 2 of ZPPR assembly 3

Run	Assembly configuration: Control-rod positions loaded with B_4C rods	Net configuration worth, $, relative to reference phase-2 configuration			
		Polarity-coherence measurement, detectors at core center	Results of multiplication measurements		
			Fission counter at core center	BF_3 proportional counters outside axial reflector	BF_3 ion chambers outside radial reflector
1	2,4,6,9,10,14,18	-1.76 ± 0.01	-1.73 ± 0.01	-1.79 ± 0.01	-1.81 ± 0.01
2	2,3,4,5,6,7,10,14,18	-5.84 ± 0.03	-5.76 ± 0.04	-5.73 ± 0.03	-5.67 ± 0.03
3	2,4,6,8,10,12,14,16 18	-7.73 ± 0.05	-7.40 ± 0.05	-7.48 ± 0.05	-7.88 ± 0.05
4	8,9,10,11,12,13,14, 15,16,17,18,19	-14.05 ± 0.11	-13.01 ± 0.09	-12.99 ± 0.08	-13.77 ± 0.08
5	2,3,4,5,6,7,8,10, 12,14,16,18	-13.46 ± 0.17	-13.88 ± 0.10	-13.47 ± 0.08	-13.72 ± 0.08
6	2,4,6,9,10,11, 13,14,15,17,18,19	-12.50 ± 0.09	-13.03 ± 0.09	-12.67 ± 0.09	-12.71 ± 0.08
7	All except CRP-1	-23.05 ± 0.40	-27.43 ± 0.19	-25.53 ± 0.19	-25.36 ± 0.15

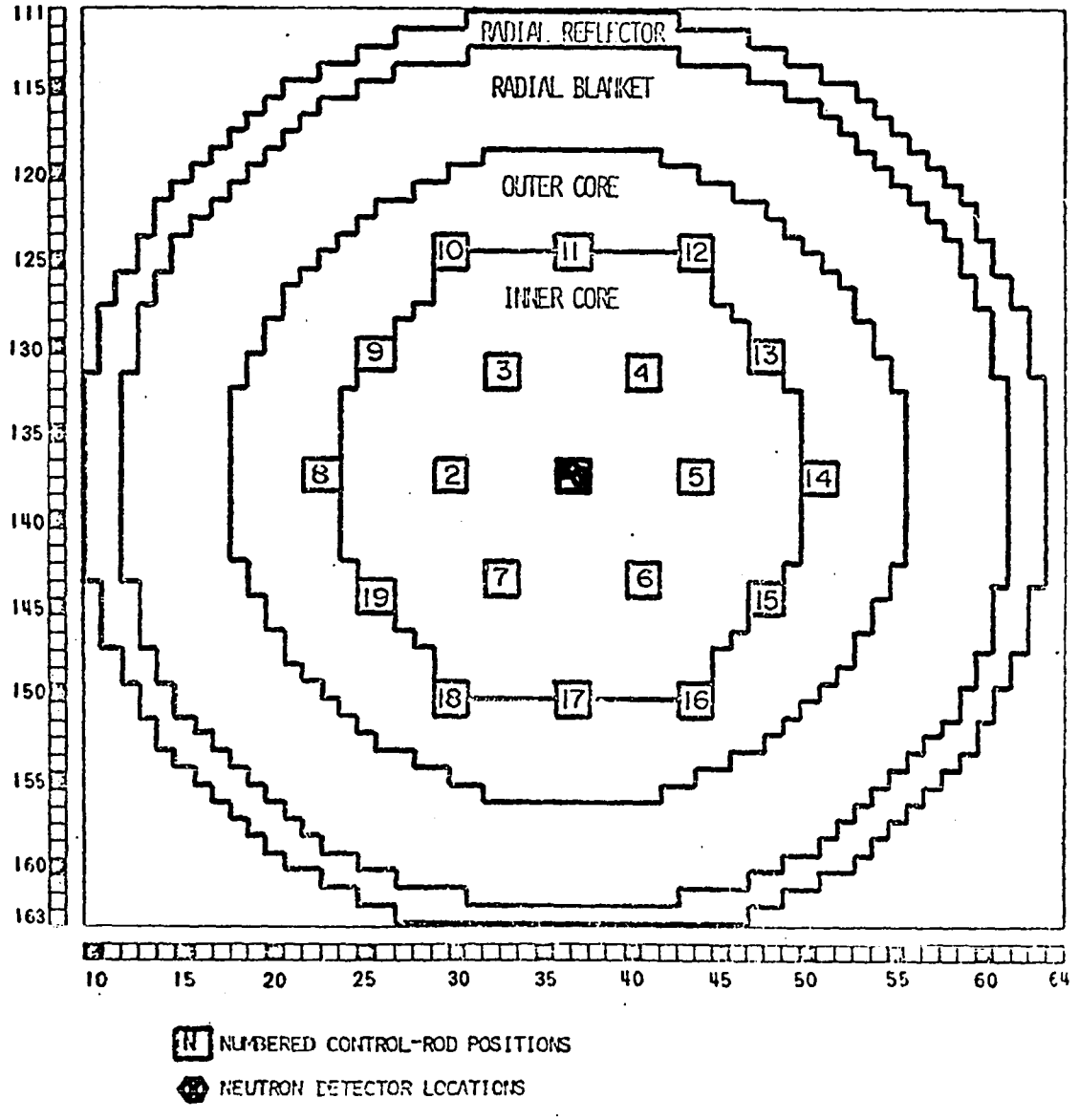

Figure 17. The ZPPR control rod positions

methods. At -9.90$, the results of the coherence function method is 3.33% less subcritical compared to the source multiplication method (run 10, Table 5). At -20.53$, the result of the former is 9.35% less subcritical than the latter (run 11, Table 6). At -27.43$, the result of the former is 15.97% less subcritical than the latter (run 7, Table 7). Starting around -9$, the discrepancy between the measurements of these two methods shows up consistently.

Since the modified source multiplication method is considered to be more reliable and accurate [12], it is necessary to identify the source of error of the coherence function method to account for the discrepancy of the two methods.

Various possible sources of error were investigated. It was found by Carpenter [35] that the experimental aspects of these possible sources of error were insignificant. It was concluded that electronic noise pickup, improper discriminator settings (i.e. the mean voltage signal is not zero), non-Gaussian count distribution, signal distortion, unequal detector efficiencies, and improper bandwidth settings could not account for the discrepancy. The analytical aspect of the coherence function method is likely to be the source of error. In particular, the inference relation to obtain the subcriticality from the coherence function for a pair of equal efficiency detectors, namely:

$$\$_2 = 1 - (1 - \$_1)\left(\frac{\beta_1}{\beta_2}\right)\left(\frac{W_2}{W_1}\right)^{\frac{1}{2}}\left(\frac{1 - \rho_2}{\rho_2} \times \frac{\rho_1}{1 - \rho_1}\right)^{\frac{1}{2}} \qquad (14)$$

was found to be inadequate for the far subcritical cases. Specifically, a correction factor is needed for the second term on the R.H.S. of Equation 14. The following are four independent ways to arrive analytically at the correction factor for Equation 14.

A. The Fission Probability Approach

Application of the fission probability concept to the derivation of the modified inference relation was first illustrated by Carpenter [35, 55]. In his original work, the relation between the fission variance and the fission probability in a source free system (e.g. a purely Pu-239 core) and a mixed system (e.g. Pu-239 mixed with Pu-240 and/or Cf-252) was defined. From the fission variance relation, the modified inference relation was ultimately obtained. Detail derivations of this approach are shown in Appendix G.

For purpose of concise representation, it is sufficient to state here that by accounting for all the variances in a fission chain, the modified inference relation in a source free system is

$$\$_2 = 1 - (1 - \$_1)\left(\frac{\beta_1}{\beta_2}\right)\left(\frac{W_2}{W_1}\right)^{\frac{1}{2}}\left(\frac{\rho_1}{1-\rho_1} \times \frac{1-\rho_2}{\rho_2}\right)^{\frac{1}{2}} C'^{\frac{1}{2}} \qquad (15)$$

where $$C' = \frac{\frac{\bar{\nu}^2 - \bar{\nu}}{\bar{\nu}^2} + \frac{1}{K_{p_2}^2} - 1}{\frac{\bar{\nu}^2 - \bar{\nu}}{\bar{\nu}^2} + \frac{1}{K_{p_1}^2} - 1}$$

ν = number of neutrons released per fission

K_{p_i} = prompt multiplication constant at state i

i = 1, 2.

According to the above equation, the degree of correction depends on the degree of subcriticality, i.e. $K_{p_2}^2$. For near critical measurements, $K_{p_1} \simeq K_{p_2} \simeq 1$, the correction factor $C^{\frac{1}{2}}$ is almost unity. Equation 15 therefore reduces to the more familiar form of the inference relation, Equation 14. If the measured state 2 is far subcritical (e.g. $K_{p_2} = 0.90$, $\$_2 \simeq 30$ for ZPPR), the correction factor $C'^{\frac{1}{2}}$ modifies the value of $\$_2$ by 14%.

B. The Binary Source Approach

In their original treatment of neutron noise analysis, Borgwaldt and Stegemamn [56] employed the concept of a binary source to define the neutron source input in a one-channel or two-channel frequency analysis experiment. The binary source

was considered as the input in a classical input-output transfer function. This source was written as:

$$S_2' = \int_E \frac{\overline{\nu(\nu - 1)}}{2} \Sigma_f(E')\phi(E')dE' \qquad (16)$$

where S_2' = binary source input to the reactor transfer function

$\Sigma_f(E')\phi(E')$ = fission rate at energy $E' = F(E')$

ν = number of neutron released per fission.

Equation 16 describes the number of neutron pairs generated at the fission rate of $F(E')$. The factor $\frac{\nu(\nu - 1)}{2}$ (i.e. $\frac{\nu!}{2!(\nu - 2)!}$), is the number of combination of two neutrons from a population of ν neutrons.

From this definition of a binary source, and with proper description of the reactor transfer function and the detection system transfer function, the detector response (and hence the power spectral densities) can be defined. The coherence function can subsequently be determined by Equation 1. The detail of the derivation were shown in ref. [56, 2]. It is sufficient to note here that the inference relation of $\$_2$ derived according to this treatment is identical to Equation 14, i.e. no correction factor is involved for far subcritical measurements.[1]

---

[1]The derivation of the inference reaction with the modified binary source as input is shown in detail in Appendix K.

Implicit in the definition of the binary source as defined in Equation 16 are the following two assumptions: (1) the detection system only "sees" ν neutrons at a time (i.e. one fission per sampling), and (2) there is no extraneous source (such as Pu-240 spontaneous fission) present. For a fast critical assembly such as the ZPPR, these two assumptions are not always valid.

The neutron lifetime in the fast ZPPR facility is about 5.7×10^{-7} sec. The sampling time of the neutron noise detection system is typically around 10^{-2} sec (determined mainly by the inverse of the narrow band filter frequency). Thus, within one sampling period, the detectors are exposed to many generations of neutrons and hence many fissions. (As will be seen in the Rossi-Alpha measurement, the detection system is purposely set to cover many generations of fissions.) Insofar as the binary source input to the reactor and detection transfer function in a fast reactor, it consists of not just one fission but many generations of fission. Equation 16 is applicable only to thermal reactor where the neutron lifetime ($\sim 10^{-3}$ sec) is comparable to the sampling time and hence only one generation of fission can be detected for each sampling.

The presence of an extraneous source would also change the composition of the binary source. In particular, at the far subcritical state of $K_p = 0.9$, $\$ \simeq -30$ for ZPPR, spontaneous fissions of Pu-240 account for 12.4% of the total

fission and the initiation of 96.8% of the fission chains. Equation 16 is applicable only at a near critical state where the effect of the extraneous source is negligible.

The following is an examination of the effect on the inferred subcriticality of $\$_2$ when the two implicit assumptions are not applicable.

1. Effect of sampling of multiple generation neutrons on the inferred subcriticality

Consider a purely Pu-239 system and assume that the sampling time is long enough to cover the whole span of the fission chain yet short enough to exclude the emergence of the delayed neutron. The shortest half-life of the delayed neutron precursors is approximately a fraction of a second. Thus, we are considering sampling intervals in the range of 10^{-5} to 10^{-2} sec.

There are a total of $(\frac{1}{1 - K_p})$ fissions in a chain. Each fission can contribute to the binary source as defined in Equation 16. It can also pair with the other fissions (from the same chain) to form an additional neutron pair as part of the binary source. This additional portion of the binary source due to the presense of more than one fission per sampling is:

$$S_2'' = \int_E \left(\frac{1 - K_p}{K_p}\right) \bar{\nu}^2 \frac{\Sigma_f(E')\phi(E')}{2} dE' \quad . \tag{17}$$

Equation 17 can be visualized as follows: For two different fissions (both of them from the same chain), there are a total of $\bar{\nu}^2$ pairs of neutrons for detection. There are $\left(\frac{K_p}{1 - K_p}\right)$ fission pairs in a chain. The number of chain per fission pair is therefore $\left(\frac{1 - K_p}{K_p}\right)$. The number of fission pairs generated per unit time is $\frac{\Sigma_f(E')\phi(E')}{2}$. Therefore, from Equation 17, it follows that

S_2'' = number of neutron pairs in the reactor formed by different fissions (of the same chain).

The modified binary source is the sum of the neutron source by pairing with itself (Equation 16) and by pairing with other chain-related fissions (Equation 17). The expression for the modified binary source becomes

$$S_2 = S_2' + S_2'' = \int_E \frac{\Sigma_f(E')\phi(E')}{2} \left[\frac{}{\nu(\nu-1)} + \bar{\nu}^2 \left[\frac{1-K_p}{K_p}\right]\right] dE' \tag{18}$$

Using Equation 18 as the definition of the binary source and following the derivation used by Borgwaldt and Stegemann [56], the following power spectral densities are obtained:

$$\Phi_{xy}(\omega) = \bar{q}^2 \frac{FW^2}{\beta^2(1-\$)^2} \left[D + \left(\frac{1}{K_p} - 1 \right) \right]$$

$$\Phi_{ii}(\omega) = \bar{q}^2 FWQ \left[1 + \frac{W}{Q} \times \frac{1}{\beta^2} \times \frac{1}{(1-\$)^2} \left[D + \frac{1}{K_p} - 1 \right] \right] \quad (19)$$

where $i = x, y$

W = detector efficiency (in detection per fission) for the x and y channel

q = charge released in detector per detection

$Q = \frac{\overline{q^2}}{\bar{q}^2}$ = Bennett factor

D = Diven factor of Pu-239 = $\frac{\overline{\nu(\nu-1)}}{\bar{\nu}^2}$

F = fission rate.

Referring back to the definition of the coherence function, Equation 1, and using the expression of Equation 19, the modified expression for the coherence function is obtained as

$$\rho = \frac{\frac{W}{Q\beta^2} \left[D + \frac{1}{K_p} - 1 \right]}{(1-\$)^2 + \frac{W}{Q\beta^2} \left(D + \frac{1}{K_p} - 1 \right)} \quad (20)$$

Applying Equation 20 to a reference state 1 and a measured state 2, and after proper rearrangement, it follows that

$$\$_2 = 1 - (1-\$_1)\,\frac{W_2}{W_1}\left(\frac{\beta_1}{\beta_2}\right)^{\frac{1}{2}}\left(\frac{\rho_1}{1-\rho_1} \times \frac{1-\rho_2}{\rho_2}\right)^{\frac{1}{2}} C'^{\frac{1}{2}} \qquad (21)$$

where $$C' = \frac{D + \frac{1}{K_{p_2}} - 1}{D + \frac{1}{K_{p_1}} - 1} .$$

Equation 21 is the modified form of the inference relation when the detector(s) "sees" all generations of fissions in each sampling. If the measured state is near critical, then $K_{p_2} \simeq K_{p_1} \simeq 1$ and the correction factor, C', reduces to unity. Equation 21 therefore becomes the more conventional form of Equation 14. If the measured state is around -30\$, then the correction factor can modified the result of $\$_2$ by 7%.

It should be pointed out that two assumptions have been made in the course of deriving Equation 21. They are (1) there is no extraneous source present, and (2) the fission rate is constant. In Equation G11 of the fission probability approach, the fission rate was not treated as constant. The effect of a fluctuating fission rate on the composition of the binary source (and hence the inferred subcriticality) is not well known.

2. Effect of the extraneous source on the inferred subcriticality in a mixed system of Pu-239 and Pu-240

Consider that a Pu-240 spontaneous fission takes place; a pulse of ν' neutrons is released in the reactor and causes

succeeding fissions of Pu-239. Each Pu-239 fissions releases ν neutrons. If the extraneous source strength of Pu-240 is S_o neutrons/sec, then the fission rates are:

$$F_{sf} = \frac{S_o}{\nu'}$$

$$F_{nf} = \frac{S_o K_p}{1 - K_p} \cdot \frac{1}{\nu}$$

$$F = F_{nf} + F_{sf} = S_o \left(\frac{K_p}{1 - K_p} \cdot \frac{1}{\nu} + \frac{1}{\nu'} \right) \qquad (22)$$

where F = total fission rate (fissions/sec)

F_{sf} = spontaneous fission rate of Pu-240

F_{nf} = neutron induced fission rate of Pu-239.

The binary source under the fission rate specified by Equation 22 is accordingly:

$$S_2'' = \frac{S_o K_p}{1 - K_p} \times \frac{1}{\nu} \times \frac{\overline{\nu(\nu-1)}}{2} + \frac{S_o}{\nu'} \frac{\overline{\nu'(\nu'-1)}}{2} . \qquad (23)$$

Using the corrected binary source as described above as the input to the reactor and detection transfer function, the expression for the coherence function can be derived in the same manner as shown in ref. [56, 41]. In accordance with this procedure, the power spectral densities are

$$\Phi_{xy}(\omega) = \bar{q}^2 \frac{W^2 S_o}{\beta^2 (1-\$)^2} \left(D \left[\frac{K_p}{1 - K_p} \cdot \frac{1}{\nu} \right] + \frac{1}{\nu'} \times D' \right)$$

$$\Phi_{ii}(\omega) = \bar{q}^2 W S_o Q \left(\left[\frac{K_p}{(1-K_p)\nu} + \frac{1}{\nu'} \right] + \frac{W}{(1-\$)^2 \beta^2 Q} \right.$$

$$\left. \left[D \left[\frac{K_p}{1-K_p} \cdot \frac{1}{\nu} \right] + \frac{1}{\nu'} \times D' \right] \right) \qquad (24)$$

where $i = x, y$

D' = Diven factor of Pu-240 = $\frac{\overline{\nu'(\nu'-1)}}{\bar{\nu}'^2}$

$R' = \frac{\nu'}{\nu}$.

With Equations 24 and 1, the proper ratio of the power spectral densities and the coherence function can be obtained. By making the reasonable assumption that the efficiency of the x channel and y channel detector are the same, the coherence function expression becomes

$$\rho = \frac{\frac{W}{\beta^2} \times \frac{1}{(1-\$)^2} \left(D \left[\frac{K_p}{1-K_p} \cdot \frac{1}{\nu} \right] + \frac{R}{\nu} \cdot D' \right)}{Q \left[\frac{K_p}{(1-K_p)\nu} + \frac{1}{\nu'} \right] + \frac{W}{\beta^2 (1-\$)^2} \left[D \left(\frac{K_p}{1-K_p} \cdot \frac{1}{\nu} \right) + \frac{R}{\nu} \times D' \right]} \qquad (25)$$

Applying Equation 25 for a reference state 1 and a measured state 2, and after proper combination of the results of these two equations, the inference relation for the subcritical

state 2 is

$$\$_2 = 1 - (1-\$_1)\left(\frac{W_2}{W_1}\right)^{\frac{1}{2}}\left(\frac{\beta_1}{\beta_2}\right)\left(\frac{\rho_1}{1-\rho_1} \times \frac{1-\rho_2}{\rho_2}\right)^{\frac{1}{2}} C'^{\frac{1}{2}}$$

where

$$C' = \frac{D\,K_{p_2} + (1-K_{p_2})D'R}{D\,K_{p_1} + (1-K_{p_1})D'R} \times \frac{1-K_{p_1}(1-R)}{1-K_{p_2}(1-R)} \quad . \tag{26}$$

If there is no extraneous source present, i.e. a purely Pu-239 system, then $\nu = \nu'$, $R = 1$ and $D = D'$. The correction factor C' defined above reduces to unity and Equation 26 becomes Equation 14. If $\nu' = 2.25$, $\nu = 2.87$, $K_{p_2} = 0.90$, $\$_2 \simeq -30$, the correction factor modified the result of $\$_2$ by 2.0%.

Correction for the extraneous source effect by Equation 26 is relatively small compared to that of the effect of sampling of multiple generation neutrons as given by Equation 21. The combined effect of the two causes, namely: (1) sampling of multiple generation neutrons, and (2) presence of the extraneous source, on the inference relation of the measured subcriticality can be obtained by defining the new binary source as:

$$S_2 = \frac{S_o}{1-K_p} \times \frac{K_p}{\nu} \times \frac{\overline{\nu(\nu-1)}}{2} + \frac{S_o}{\nu'}\frac{\overline{\nu'(\nu'-1)}}{2} + \frac{1}{2}\left(\frac{S_o}{1-K_p} \times \frac{1}{\nu}\right)\bar{\nu}^2\left(\frac{1-K_p}{K_p}\right) \tag{27}$$

The first term in Equation 27 is the number of neutron pairs for each neutron induced fission and the second term for that of the spontaneous fission. The third term describes the neutron pairing in each chain. Using the above expression as the input to the reactor and detection transfer function (in the same way as Equation 19 was derived), the following expression is obtained:

$$\$_2 = 1 - (1-\$_1)\left(\frac{W_2}{W_1}\right)^{\frac{1}{2}}\left(\frac{\beta_1}{\beta_2}\right)\left(\frac{\rho_1}{1-\rho_1} \times \frac{1-\rho_2}{\rho_2}\right)^{\frac{1}{2}} \quad C'^{\frac{1}{2}}$$

where

$$C' = \frac{D\,K_{p_2} + R(1-K_{p_2})D' + \left(\frac{1-K_{p_2}}{K_{p_2}}\right)}{D\,K_{p_1} + R(1-K_{p_1})D' + \left(\frac{1-K_{p_1}}{K_{p_1}}\right)} \times \frac{1-K_{p_1}(1-R)}{1-K_{p_2}(1-R)} \qquad (28)$$

For a purely Pu-239 system, i.e. $\nu' = \nu$, $D' = D$, $R = 1$, the correction factor C' becomes.

$$C' = \frac{D + \frac{1}{K_{p_2}} - 1}{D + \frac{1}{K_{p_1}} - 1}$$

and Equation 28 reduces to Equation 21. If one is treating a thermal neutron assembly where the emergence of more than one generation of fission in each sampling is highly unlikely, then the correction factor becomes:

$$C' = \frac{D\,K_{p_2} + (1-K_{p_2})D'R}{D\,K_{p_1} + (1-K_{p_1})D'R} \times \frac{1 - K_{p_1}(1-R)}{1 - K_{p_2}(1-R)} ,$$

and Equation 28 reduces to Equation 26.

Before conclusion of this discussion, it should be noted that at the ZPPR fast critical assembly, the neutron noise analysis experiment did sample multiple generations of fissions. In addition, there is an ever present source of Pu-240 and a movable source of Cf-252. The extraneous source effect is minor compared to the effect of sampling of multiple generations of fissions. This is in agreement with experimental observations where the removal and insertion of the strong Cf-252 source (ν = 3.87, D = 0.85, $S_o = 1.9 \times 10^8$ n/sec) have negligible effect on the inference of $\$_2$.

C. The Rossi-Alpha--Variance to Mean Method

It had been shown by Orndoff [20] that measurement of the time distribution of pairs of counts due to neutrons originating from a common ancestor in a neutron chain yields a value for the prompt neutron period of a near-critical system. Modification of this approach, supplemented by the variance-to-mean method, can be used to derive the inference relation for the subcritical reactivity. Similar to the binary source approach, this method is based on the point kinetics reactor equation and neglects delayed neutrons. In addition, the

success of this modified method rests on two criteria. They are:

(1) The fission rates must be such that there is no great overlapping of chains in the reactor. This requirement assures that time-correlated fission are not lost in the random background.

(2) The detector efficiency must be relatively high such that at the required fission rate, statistical precision can be obtained in a reasonable length of time.

The first criterion is used to meet the condition that the uncorrelated random fission rate does not dominate the chain-related fission rate. If there are many chains present in the reactor, then the random fission rate would be comparable to the chain-related fission rate in magnitude. As the reactor becomes far subcritical, there are increasingly more (and shorter) chains, the random fission rate therefore becomes dominate compared to the chain-related fission rate.

The second criterion addresses itself to the relative magnitude of the random count rate and the correlated count rate. As will be shown later, the variance of the random count rate is proportional to the detector efficiency whereas that of the correlated count rate is proportional to the square of the detector efficiency. If the detector efficiency is quite low (less than 10^{-5} detections per fission), then the

random count rate can be comparable or even dominate the correlated count rate. Such is the case when the reactor is far subcritical or the neutron detector is located in the vicinity of a control rod or near the edge of the reactor.

Assuming the above two criteria are met, consider the following sequence of events: A fission takes place at time t_o in dt_o. A detection count is registered at t_1 and dt_1, followed by a second detection count at t_2 in dt_2. All these three events pertained to the same chain. The probability that governs these three events are, respectively:

(1) Probability of a fission occurring at t_o in dt_o:

$$P(t_o)dt_o = F\ dt_o, \tag{29}$$

(2) Probability of a count at t_1 in dt_1 as a result of the fission at t_o in dt_o:

$$P_c(t_1)dt_1 = W\nu e^{-\alpha(t_1-t_o)}\ \frac{dt_1}{\Lambda}, \tag{30}$$

(3) Probability of a count at t_2 in dt_2 assuming the count at t_1 took place already:

$$P_c(t_2)dt_2 = W\ (\nu-1)e^{-\alpha(t_2-t_o)}\ \frac{dt_2}{\Lambda}, \tag{31}$$

where F = fission rate (of the whole reactor) in fissions per sec.

W = detector efficiency in counts per fission

ν = number of neutron released per fission

$\alpha = \frac{1-K_p}{\ell}$ = break frequency (roll-off frequency)

ℓ = neutron life-time = $\frac{1}{V\Sigma_a}$

Λ = neutron generation time = $\frac{1}{V\Sigma_f}$

V = velocity of prompt neutron in cm/sec.

Σ_a = macroscopic absorption cross section in cm^{-1}

Σ_f = macroscopic fission cross section in cm^{-1}

$K_p = \nu_p \frac{\ell}{\Lambda}$ = prompt multiplication constant.

Implicit in the above expressions for the probabilities of the counts are two assumptions:

(1) The neutron behavior follows the point kinetics equation and therefore displays an exponential decay of $\nu e^{-\alpha(t_1-t_o)}$ and $(\nu-1)e^{-\alpha(t_2-t_o)}$ at time t_1 and t_2 respectively,

(2) The fission rate is constant between the time $-\infty < t_o \leq t_1$.

To obtain the probability of coincidence counts at time t_1 and t_2 for all fissions of previous origins in the same chain (i.e. $-\infty < t_o \leq t_1$), take the product of the three individual probabilities and integrate with respect to time from $-\infty$ to t_1. Consequently, it follows that

$$P_c(t_1,t_2) = \int_{-\infty}^{t_1} P_c(t_1)dt_1\ P_c(t_2)dt_2\ F\ dt_o$$

$$= F\left(\frac{W}{\Lambda}\right)^2 \left(\frac{\overline{\nu(\nu-1)}}{2\alpha}\right) e^{-\alpha(t_2-t_1)}\ dt_1dt_2. \qquad (32)$$

The above equation describe the counts that pertain to the same chain. Superimposed on this chain-related counts are the so-called random counts that are due to all the fission chains in the reactor. The probability of random counts registered at time t_1 in dt_1 and time t_2 in dt_2 is:

$$P_R(t_1,t_2)dt_1dt_2 = (F\ W\ dt_1)(F\ W\ dt_2)$$

$$= (F\ W)^2dt_1dt_2. \qquad (33)$$

The total probability of coincidence counts due to random and chain-related origins is the sum of Equations 32 and 33. Accordingly, one obtains:

$$P(t_1,t_2)dt_1dt_2 = (F\ W)^2dt_1dt_2 + F\left(\frac{W}{\Lambda}\right)^2 \frac{\overline{\nu(\nu-1)}}{2\alpha} e^{-\alpha(t_2-t_1)}\ dt_1dt_2. \qquad (34)$$

It should be noted that in order to have coincidence counts, the fact that the first count was registered is a necessary condition. Thus, it follows that

$$F\ W\ dt_1 = 1. \qquad (35)$$

Furthermore, it is recognized that a fission must take place at time t_1 in order for the first count to be registered. This fission in turn released ν neutrons which decayed exponentially. The probability of this event happening and producing a second count is.

$$P_D(t)dt = W \nu e^{-\alpha t} \frac{dt}{\Lambda} . \tag{36}$$

Adding this effect described by Equation 36, i.e. the neutron released from the first count results in the second count, to Equation 34, the probability of coincidence counts due to all effects is

$$P(t_1,t_2)dt_1dt_2 = (FW)^2 dt_1dt_2 + F\left(\frac{W}{\Lambda}\right)^2 \left(\frac{\nu(\nu-1) + 2\nu\alpha\Lambda}{2\alpha}\right)$$

$$e^{-\alpha(t_2-t_1)} dt_1dt_2. \tag{37}$$

Let the number of counts in interval T be C. Then the number of pairs of counts for a two-detector measurement is:

$$\text{number of pairs of counts} = \frac{C!}{(C-2)!2!} = \frac{C(C-1)}{2} . \tag{38}$$

Equation 38 and the time integral of 37 are referring to the same physical quantity. Consequently, it follows that

$$\frac{\overline{C(C-1)}}{2} = \int_o^T \int_o^{t_2} FWdt_1 \left[FWdt_2 + \frac{W}{\Lambda^2} \times \frac{\overline{\nu(\nu-1)} + 2\nu\alpha\Lambda}{2\alpha} e^{-\alpha(t_2-t_1)} dt_2 \right]$$

$$= \frac{F^2W^2T^2}{2} + \frac{FW^2K_p^2 T}{2(1-K_p)^2} \left[\frac{\overline{\nu(\nu-1)}}{\bar{\nu}^2} + \frac{2(1-K_p)}{K_p} \right] \left[1 - \frac{1-e^{-\alpha T}}{\alpha T} \right].$$

If the sampling time, T, is much greater than the prompt neutron life-time but less than the half-lives of the delayed neutron precursors, then the factor $[1 - (1-e^{-\alpha T})/\alpha T]$ in Equation 39 reduces to unity. For example, for the ZPPR assembly 3 phase 1B core at $K_p = 0.90$, the following parameters indicate that this factor does become unity:

$$\ell = 5.796 \times 10^{-7} \text{ sec}$$

$$K_p = 0.90$$

$$\alpha = \frac{1-K_p}{\ell} = 1.73 \times 10^7/\text{sec}$$

$$T = 0.01 \text{ sec}$$

$$1 - \frac{1-e^{-\alpha T}}{\alpha T} = 1 - 9.9999 \times 10^{-11} \simeq 1.0.$$

Using the relation between the counts and the fission rate:

$$C = WFT$$

and applying it to Equation 39 yields

$$\frac{\overline{c^2} - \bar{c}}{2} = \frac{\bar{c}^2}{2} + \frac{\bar{c}}{2} \frac{W K_p^2}{(1-K_p)^2} \left[\frac{\overline{\nu(\nu-1)}}{\bar{\nu}^2} + \frac{2}{K_p} - 2 \right] . \qquad (40)$$

Rearranging Equation 40 yields the variance-to-mean expression

$$\frac{\bar{c}^2 - \bar{c}^2}{\bar{c}} = 1 + \frac{W}{\beta^2 (1-\$)^2} \left[D + 2 \left[\frac{1}{K_p} - 1 \right] \right] \qquad (41)$$

where $D = \frac{\overline{\nu(\nu-1)}}{\bar{\nu}^2}$ = Diven factor, $\$ = \frac{K-1}{\beta K}$.

It was shown (Appendix G, p. 172) that the quantity $\bar{c}^2 - \bar{c}^2$ is the correlated count variance and the random count variance (white noise) is $\bar{c}$. In the same manner as Equation G19, the coherence function can now be derived from Equation 41 and is written as

$$\rho = \frac{\frac{W}{\beta^2} \frac{1}{(1-\$)^2} \left[D + 2 \frac{1}{K_p} - 1 \right]}{1 + \frac{W}{\beta^2} \frac{1}{(1-\$)^2} \left[D + 2 \frac{1}{K_p} - 1 \right]} . \qquad (42)$$

Applying the above coherence function to the reference state 1 and a measured subcritical state $\$_2$, $\$_2$ is found to be

$$\$_2 = 1 - (1-\$_1) \left(\frac{\beta_1}{\beta_2} \right) \left(\frac{W_2}{W_1} \right)^{\frac{1}{2}} \left(\frac{\rho_1}{1-\rho_1} \times \frac{1-\rho_2}{\rho_2} \right)^{\frac{1}{2}} C'^{\frac{1}{2}}$$

$$\text{where} \quad C' = \frac{D + 2\left(\frac{1}{K_{p_2}} - 1\right)}{D + 2\left(\frac{1}{K_{p_1}} - 1\right)} \quad . \tag{43}$$

Equation 43 is the inference relation derived from the modified Rossi-Alpha--Variance-to-mean method. At the near critical state, i.e. $K_{p_2} \simeq K_{p_1} \simeq 1$, the correction factor C' is almost one and Equation 43 reduces to the simpler form of Equation 14. If the measured state is far subcritical, e.g. $K_{p_2} \simeq 0.90$, then the correction factor can modify the result of $\$_2$ by 13%.

To conclude, Equation 43 was derived by accounting for the pairing of counts from different generations of fissions which have a common ancestor in the same chain. The derivation did not account for the effect of the presence of an extraneous neutron source and the fluctuation of the fission rate.

D. The Noise Equivalent Source Approach

A neutron noise equivalent source in the form of a spectral density was defined by Cohn [41] to be:

$$\langle |S_o|^2 \rangle = \sum_i \bar{q}_i'^2 \, m_i \tag{44}$$

where $\langle |S_o|^2 \rangle$ = noise equivalent source (NES) in neutron^2/sec

q_i' = number of neutrons produced (or lost) in reaction type i

m_i = rate of reaction type i.

Since both the probability of neutrons produced and the reaction rates are statistical quantities, the noise equivalent source consequently exhibits fluctuation. Analytical treatment of the fluctuation of the noise equivalent source would yield the expression for the correlated count rate (the so-called pile noise) and the random count rate (uncorrelated count rate). An expression for the coherence function can then be defined by the correlated count rate and the random count rate. With the coherence function defined for both the reference state and the measured state, a new inference relation for subcritical reactivity $\$_2$ can be obtained. Thus, from this approach, the effect of the fluctuation of the noise equivalent source on the inferred subcritical reactivity can be examined.

From the standard technique of Fourier analysis for a band-limited white noise, the spectral density can be written in the form

$$<|S_x|^2> = \frac{\delta_x^2}{\Delta f} \tag{45}$$

where δ_x^2 = variance of the time domain signal, x, and

Δf = band frequency in Hz.

It can be shown that the neutron production and loss rate are "white" in the frequency range of 10-200 Hz for a fast reactor.[1] Thus, defining the quantity x to be the neutron production and loss rate

$$x = \sum_i q_i' m_i \tag{46}$$

where q_i' and m_i are defined in Equation 43.

Equations 44 and 46 describe the same physical quantity, the noise equivalent source.

Consider the case where the only two types of reactions are fission and parasitic absorption (neutron-capture). Accordingly, the following parameters are defined:

parasitic absorption: $m_1 = \frac{n}{\ell} \frac{\Sigma_c}{\Sigma_c + \Sigma_f}$; $q_1 = -1$

fission: $m_2 = \frac{n}{\ell} \frac{\Sigma_c}{\Sigma_c + \Sigma_f}$; $q_2 = \sum_{N=1}^{\infty} P_N(N-1)$

where n_o = steady state neutron density in neutrons/cm^3 (at zero frequency)

ℓ = neutron life-time in sec

---

[1] By referring to the neutron production and loss rate as "white," it is meant that their spectral densities are constant with respect to the specified range of frequency. Here it is meant by sweeping between the frequencies of 10 to 200 Hz, the cross power spectral densities are constant. It is interesting to note that this frequency range corresponds to the time span long enough to cover the chain history but short enough to preclude the delayed neutron precursors.

$\frac{n_o}{\ell}$ = neutron absorption (capture and fission) rate

Σ_f = macroscopic fission cross section in cm^{-1}

Σ_c = macroscopic parasitic absorption cross section in cm^{-1}

P_N = probability of N neutron released per fission.

Substituting the above expressions into Equation 46 yields

$$x = \left(\frac{n_o}{\ell} \frac{\Sigma_c}{\Sigma_c + \Sigma_f}\right)(-1) + \left(\frac{n_o}{\ell} \frac{\Sigma_c}{\Sigma_c + \Sigma_f}\right) \sum_{N=1}^{\infty} P_N(N-1). \quad (47)$$

Applying the classical propagation of error techniques to Equation 46 results in

$$\delta_x^2 = \left(\frac{\partial x}{\partial m_1}\right)^2 \delta_{m_1}^2 + \left(\frac{\partial x}{\partial m_2}\right)^2 \delta_{m_2}^2 + \left(\frac{\partial x}{\partial q_1}\right)^2 \delta_{q_1}^2 + \left(\frac{\partial x}{\partial q_2}\right)^2 \delta_{q_2}^2 . \quad (48)$$

For a Poisson probability distribution, the variance of the reaction rate is equal to the reaction rate. Therefore, it follows that

$$\delta_{m_1}^2 = \frac{n_o}{\ell} \frac{\Sigma_c}{\Sigma_c + \Sigma_f} \quad ; \quad \delta_{m_2}^2 = \frac{n_o}{\ell} \frac{\Sigma_c}{\Sigma_c + \Sigma_f} . \quad (49)$$

Substituting the above results into Equation 48, the expression for the variance of the signal x is

$$\delta_x^2 = \frac{n_o}{\ell} \frac{\Sigma_c}{\Sigma_c + \Sigma_f}(-1)^2 + \frac{n_o}{\ell} \frac{\Sigma_c}{\Sigma_c + \Sigma_f} \sum_{N=1}^{\infty} P_N (N-1)^2$$

$$+ \left(\frac{n_o}{\ell} \frac{\Sigma_c}{\Sigma_c + \Sigma_f}\right)^2 \delta_{q_1}^2 + \left(\frac{n_o}{\ell} \frac{\Sigma_f}{\Sigma_c + \Sigma_f}\right)^2 \delta_{q_2}^2 . \qquad (50)$$

It can be seen that the last two terms of Equation 50 vanish since the variance of the mean number of neutrons lost and produced are zero. As a result, Equation 50 can be simplified to the following expression

$$\delta_x^2 = \frac{n_o}{\ell}\left(\frac{\Sigma_c}{\Sigma_c + \Sigma_f} + \frac{\Sigma_c}{\Sigma_c + \Sigma_f} \sum_{N=1}^{\infty} P_N (N-1)^2\right) . \qquad (51)$$

For an infinite neutron multiplying medium, the multiplication factor is related to the property of the medium by

$$K = \nu \frac{\Sigma_f}{\Sigma_c + \Sigma_f} \qquad (52)$$

where ν = number of neutrons released per fission.

Combining Equation 51 and 52 yields the following expression for the variance of the signal:

$$\delta_x^2 = \frac{n_o}{\ell}\left(\left(\frac{\overline{\nu^2} - 2\bar{\nu}}{\bar{\nu}}\right) K + 1\right) \qquad (53)$$

where $\overline{\nu^2} = \sum_{N=1}^{\infty} P_N N^2$; $\bar{\nu} = \sum_{N=1}^{\infty} P_N N$.

Substituting Equations 53 into 45, a new expression for the noise equivalent source expressed in terms of the multiplication factor K, is obtained

$$\langle |S_x|^2 \rangle = \frac{\frac{n_o}{\ell}\left(\left[\frac{\overline{\nu^2} - 2\bar{\nu}}{\bar{\nu}}\right] K + 1\right)}{\Delta f} \quad . \tag{54}$$

The neutron density fluctuations resulting from the driving function represented by the noise equivalent source, can be defined by the input-output relation of the classical transfer function technique

$$\langle |n(\omega)| \rangle^2 = |H(\omega)|^2 \langle |S_x|^2 \rangle \tag{55}$$

where $\langle |n(\omega)| \rangle^2$ = power spectral density of the neutron density fluctuation at frequency ω

$|H(\omega)|^2$ = square modulus of subcritical source transfer function

$$= \left[\frac{\ell}{1 - K(1-\beta)}\right]^2 \text{ at } \omega << \alpha^1; \ \alpha = \frac{\beta}{\ell}$$

Application of the expressions for the transfer function and the noise equivalent source to Equation 55 yields

---

[1]For ZPPR assembly 3 phase 1B core, α is 5427.9 rad/sec (863.9 Hz). The plateau frequency ($\sim$ 100 Hz) where the NES is "white" is much less than α. Therefore $\omega << \alpha$, and the expression for the transfer function is valid.

$$<|n(\omega)|>^2 = \left(\frac{n_o \ell}{(1-\$)^2 (K\beta)^2} \left[\left(\frac{\overline{\nu^2} - 2\bar{\nu}}{\bar{\nu}} \right) K + 1 \right] \right) \Big/ \Delta f \qquad (56)$$

where $\$ = \frac{K-1}{K\beta}$.

The fluctuation of the neutron density at the plateau frequency can be observed experimentally. In particular, the neutron detectors respond to the fluctuation of the neutron density and convert it to a fluctuating current at the corresponding frequency. The power spectral density for the detector current is

$$<|I_p(\omega)|^2> = \left(\frac{W K \bar{q}}{\nu \ell} \right)^2 <|n(\omega)|^2> , \qquad (57)$$

where $<|I_p(\omega)|^2>$ = power spectral density of the detector current at frequency ω

W = detector efficiency in counts per fissions

$\bar{q}$ = average charge released per detection.

As can be discerned from Equation 57, $<|I_p(\omega)|^2>$ is the "output" due to the "input" $<|n(\omega)|^2>$. Due to the fact that $<|n(\omega)|^2>$ is the direct result of the intrinsic nature of the reactor "pile," it is referred to as "pile noise" in the early literature [41]. As opposed to the pile noise, there exists an ever present detector current due to the incidence of the steady state neutrons. This results in the random detections

of neutrons uncorrelated in fission history. It is written as

$$\langle |I_w|^2 \rangle = \left(\frac{WK}{\nu}\right) \overline{q^2} \frac{n_o}{\ell} / \Delta f \tag{58}$$

$\langle |I_w|^2 \rangle$ is quite often referred to as the "white noise."

The coherence function can be defined in terms of the pile noise and the detection noise. Specifically, the pile noise is the cross power spectral density of the detector current. The sum of the white noise and the pile noise is the auto power spectral density of the detector current. Assuming a two-channel detector experiment where the detector efficiencies and the electronic network are identical in both channels, it follows that

$$\Phi_{xy}(\omega) = \langle |I_p(\omega)| \rangle^2 = \left(\frac{WK\bar{q}}{\nu\ell}\right)^2 \left[\frac{n_o \ell}{(1-\$)^2 (K\beta)^2} \left[\left(\frac{\overline{\nu^2} - 2\bar{\nu}}{\bar{\nu}} \right) K+1 \right] \right] \Big/ \Delta f \tag{59}$$

and

$$\Phi_{ii}(\omega) = \langle |I_w| \rangle^2 + \langle |I_p(\omega)| \rangle^2$$

$$= \left[\left(\frac{WK}{\nu}\right) \overline{q^2} \frac{n_o}{\ell} + \left(\frac{WK\bar{q}}{\nu\ell}\right)^2 \frac{n_o \ell}{(1-\$)^2 (K\beta)^2} \left[\left(\frac{\overline{\nu^2} - 2\bar{\nu}}{\bar{\nu}} \right) K+1 \right] \right] \Big/ \Delta f \tag{60}$$

$i = x, y.$

With the cross and auto power spectral densities defined, the coherence function is obtained as

$$\rho = \frac{W\left[\left(\frac{\overline{\nu^2} - \bar{\nu}}{\bar{\nu}^2}\right) + \left(\frac{1}{K} - 1\right)\frac{1}{\nu}\right]}{Q\,\bar{q}^2(1-\$)^2\,\beta^2 + W\left[\left(\frac{\overline{\nu^2} - \bar{\nu}}{\bar{\nu}^2}\right) + \left(\frac{1}{K} - 1\right)\frac{1}{\nu}\right]} \qquad (61)$$

where $Q = \overline{q^2}/\bar{q}^2$ = Bennett factor.

Applying the above relation for the coherence function to a reference state 1 and a measured state 2 the inference relation for the subcritical reactivity is

$$\$_2 = 1 - (1-\$_1)\left(\frac{\beta_1}{\beta_2}\right)\left(\frac{W_2}{W_1}\right)^{\frac{1}{2}}\left(\frac{\rho_1}{1-\rho_1} \times \frac{1-\rho_2}{\rho_2}\right)^{\frac{1}{2}} C'^{\frac{1}{2}} \qquad (62)$$

where $$C' = \left[\frac{D + \left(\frac{1}{K_{p_2}} - 1\right)\frac{1}{\nu}}{D + \left(\frac{1}{K_{p_1}} - 1\right)\frac{1}{\nu}}\right]$$

$$D = \frac{\overline{\nu^2} - \bar{\nu}}{\bar{\nu}^2} = \text{Diven factor.}$$

From Equation 62, it is observed that at near critical state, for $K_{p_2} \simeq K_{p_1} \simeq 1$, the correction factor C' becomes unity and the inference relation reduces to Equation 14. For a far subcritical state of $K_{p_2} = 0.90$, $\$_2 \simeq -30$, the correction

factor can increase the calculated subcriticality by 3%.

It should be noted that if the infinite neutron multiplying medium is treated as delayed critical, i.e. Equation 52 = 1, then the inference relation is that of the conventional form, namely Equation 14. This was the approach taken by Cohn [41] in his early application of the concept of the noise equivalent source.

To summarize, the noise equivalent source can be used to derive the inference relation of subcritical reactivity. With proper constraints on the treatments on the detector signals, the inference relation of Equation 62 is obtained. The derivation assumes the absence of an extraneous neutron source such as Pu-240 and/or Cf-252. Equation 62 is therefore not strictly applicable to ZPPR subcritical reactivity measurements.

In concluding this section on the proposed correction of the inference relation for subcritical reactivity, a set of tables that illustrate the origins and the magnitude of the correction is in order.

Table 8 summarizes the correction for the inference relation for subcritical reactivity for each method. It shows the physical variances which each method has accounted for. From this table, it is noted that five different expressions of the correction factor, C', are obtained from the five approaches used for deriving it. The differences in the expression for the correction factor may be explained by the fact that each

Table 8. A summary on the proposed modifications of the inference relation for subcritical reactivity from coherence function measurements

General form of inference relation: $\$_2 = 1 - (1-\$_1)\left(\frac{\beta_1}{\beta_2}\right)\left(\frac{W_2}{W_1}\right)^{\frac{1}{2}}\left(\frac{\rho_1}{1-\rho_1} \times \frac{1-\rho_2}{\rho_2}\right)^{\frac{1}{2}} C'^{\frac{1}{2}}$

Technique of analysis	Correction factor C'[a]	Effects accounted for: Fluctuation of fission neutrons released in one generation	Fluctuation of fission neutrons released in all generations of the chain	Fluctuation of the fission rate	Extraneous source	Correction due to extraneous source	Correction of $\$_2$ at $K_{p_2} = 0.9$
Conventional approach[b]	1	yes	no	no	no	NA	0
Fission probability approach[c]	Eq. 63	yes	yes	yes	yes	minor	18%
Binary source approach	Eq. 64	yes	yes	no	yes	minor	7%
Rossi-Alpha variance-to-mean approach	Eq. 65	yes	yes	no	no	NA	13%
Noise equivalent source approach	Eq. 66	yes	no	yes	no	NA	3%

[a]The various expressions of C', Eq. 63-64, are shown on p 121.

[b]Developed by Seifritz [2] and modified by Ackerman et al. [34] and Danofsky et al. [6].

[c]Developed by Carpenter [35].

approach has accounted for different degrees of fluctuations. The process from the birth of a neutron to its detection as a member of a fission chain consists of several forms of fluctuation. For example, there are fluctuations in the number of fission neutron emitted in a generation and in the whole fission chain; fluctuations in the fission rate of the whole reactor; fluctuation in the number of fissions per chain; fluctuations in the random count rate and finally, fluctuations in the charge released per detection. These fluctuations have not been accounted for consistently by the five different derivations. Consequently, the expression of the correction factor, C', are different for each case.

Using the appropriate inference relations, the various modified subcritical reactivities of ZPPR assembly 3 were calculated. Tables 9, 10 and 11 show the intercomparison between the results of the source multiplication method and the "uncorrected" and "corrected" polarity coherence reactivities. It should be noted that the effect of spatial dependency was minimal in the intercomparison of these measurements. This is due to the fact that the detectors for the source multiplication method and the polarity coherence function method were located in the core center. They are situated axially 6 inches from the midplane, i.e. 12 inches nominal distance between the detectors of the two methods.

Table 9. Corrected rod worth by the modified inference relations for measurements in phase 1A of ZPPR assembly 3

Subcritical source mult.[a] $	K_{p_2}	Polarity coherence		Measurement $ ± $\delta_{\$}$[b]		
		Conventional form Eq. 14	Fission prob. approach Eq. 63	Binary source approach Eq. 64	Rossi-Alpha approach Eq. 65	Noise equivalent source approach Eq. 66
-1.34	0.9957	-1.36±0.01	-1.37±0.01	-1.36±0.01	-1.37±0.01	-1.36±0.01
-1.41	0.9956	-1.39±0.01	-1.40±0.01	-1.39±0.01	-1.40±0.01	-1.39±0.01
-3.37	0.9894	-3.40±0.03	-3.45±0.03	-3.41±0.03	-3.43±0.03	-3.41±0.01
-1.14	0.9965	-1.12±0.01	-1.13±0.01	-1.12±0.01	-1.13±0.01	-1.12±0.01
-2.98	0.9905	-3.05±0.03	-3.09±0.03	-3.07±0.03	-3.08±0.03	-3.06±0.01
-4.52	0.9856	-4.64±0.05	-4.72±0.05	-4.69±0.05	-4.70±0.05	-4.68±0.05
-9.42	0.9721	-9.11±0.09	-9.44±0.09	-9.30±0.09	-9.38±0.09	-9.21±0.09
-30.20	0.9344	-22.3 ±0.60	-24.24±0.62	-23.2 ±0.61	-23.7 ±0.62	-22.9 ±0.60
-18.80	0.9535	-15.5 ±0.30	-16.44±0.32	-16.0 ±0.32	-16.1 ±0.32	-15.8 ±0.30
-9.90	0.9722	-9.10±0.09	-9.43±0.09	-9.31±0.09	-9.37±0.09	-9.21±0.09

[a]Fission counter at core center, half 2, 6 inches from midplane.

[b]Li-6 detector pair at core center, half 1, 6 inches from midplane.

Table 10. Corrected rod worth by the modified inference relation for measurements in phase 1B of ZPPR assembly 3

Subcritical source mult.[a] $\$ \pm \delta_{\$}$	K_{p_2}	Polarity coherence measurement $\$ \pm \delta_{\$}$[b]				
		Conventional form Eq. 10	Fission prob. approach Eq. 63	Binary source approach Eq. 64	Rossi-Alpha approach Eq. 65	Noise equivalent source approach Eq. 66
-3.69±0.02	0.9885	-3.60±0.02	-3.65±0.02	-3.63±0.02	-3.65±0.02	-3.62±0.02
-4.94±0.02	0.9847	-4.74±0.02	-4.83±0.02	-4.76±0.02	-4.82±0.02	-4.76±0.02
-4.34±0.02	0.9865	-4.29±0.02	-4.36±0.02	-4.34±0.02	-4.36±0.02	-4.33±0.02
-6.44±0.04	0.9801	-6.44±0.04	-6.60±0.04	-6.55±0.04	-6.58±0.04	-6.51±0.02
-20.53±0.14	0.9393	-18.61±0.40	-20.10±0.42	-19.20±0.41	-19.80±0.42	-18.90±0.40
-29.28±0.21	0.9157	-24.39±0.69	-27.17±0.74	-25.12±0.71	-26.43±0.74	-24.87±0.69
-43.58±0.30	0.8795	-31.45±0.80	-36.75±1.10	-32.95±0.92	-35.47±1.10	-32.39±0.83
-28.33±0.20	0.9186	-23.77±0.40	-26.37±0.42	-25.27±0.41	-25.96±0.42	-24.43±0.40
-27.47±0.17	0.9205	-23.20±0.22	-25.68±0.28	-24.72±0.24	-25.14±0.28	-23.82±0.22
-14.88±0.08	0.9553	-13.63±0.11	-14.42±0.13	-14.18±0.12	-14.27±0.13	-13.90±0.11
-22.20±0.14	0.9352	-19.76±0.31	-21.46±0.37	-20.26±0.34	-20.84±0.37	-20.13±0.31
-14.01±0.07	0.9578	-14.80±0.18	-15.61±0.23	-15.30±0.20	-15.41±0.23	-15.10±0.18

[a] Fission counter at core center, half 2, 6 inches from midplane.

[b] Li-6 detector at core center, half 1, 6 inches from midplane.

Table 11. Corrected rod worth by the modified inference relations for measurements in phase 2 of ZPPR assembly 3

Subcritical source mult.[a] $\$ \pm \delta_{\$}$	K_{p_2}	Polarity coherence measurement $\$ \pm \delta_{\$}$[b]				
		Conventional form Eq. 10	Fission prob. approach Eq. 63	Binary source approach Eq. 64	Rossi-Alpha approach Eq. 65	Noise equivalent source approach Eq. 66
-1.73±0.01	0.9946	-1.76±0.01	-1.77±0.01	-1.76±0.01	-1.77±0.01	-1.76±0.01
-5.76±0.04	0.9822	-5.84±0.03	-5.97±0.03	-5.90±0.03	-5.93±0.03	-5.87±0.03
-7.40±0.05	0.9773	-7.73±0.05	-7.93±0.05	-7.80±0.05	-7.86±0.05	-7.78±0.05
-13.01±0.09	0.9607	-14.05±0.11	-14.78±0.11	-14.31±0.11	-14.57±0.11	-14.19±0.11
-13.88±0.10	0.9582	-13.46±0.17	-14.19±0.18	-13.64±0.17	-13.92±0.18	-13.47±0.17
-13.03±0.09	0.9606	-12.50±0.09	-13.14±0.11	-12.77±0.11	-12.96±0.11	-12.61±0.10
-27.43±0.19	0.9206	-23.05±0.40	-25.51±0.42	-24.27±0.40	-25.12±0.42	-23.22±0.40

[a]Fission counter at core center, half 2, 6 inches from midplane.

[b]Li-6 detector pair at core center, half 1, 6 inches from midplane.

The 12 inches separation in between them in the axial direction tends to minimize any effective neutronic shadowing. In addition, due to the symmetry of their geometric positions, the two sets of detectors should experience the same magnitude of neutron flux, and thus have the same efficiency.

$$C' = \frac{K_{p_2}^2 M_2 + (1-K_{p_2})(1-K_{p_2}+RK_{p_2})^2}{(1-K_{p_2}+RK_{p_2})K_{p_2}^2} \times \frac{(1-K_{p_1}+RK_{p_1})K_{p_1}^2}{K_{p_1}^2 M_1 + (1-K_{p_1})(1-K_{p_1}+RK_{p_1})^2} \tag{63}$$

where $M_i = DRK_p + D'(1-K_p)R^2 + \left[\frac{1-K_p}{K_p}\right]R + R(1-R)(1-K_p)$

$i = 1, 2.$

$$C' = \frac{DK_{p_2} + (1-K_{p_2})D'R}{1 - K_{p_2}(1-R)} \times \frac{1 - K_{p_1}(1-R)}{DK_{p_1} + (1-K_{p_1})D'R} . \tag{64}$$

$$C' = \frac{D + 2\left[\frac{1}{K_{p_2}} - 1\right]}{D + 2\left[\frac{1}{K_{p_1}} - 1\right]} . \tag{65}$$

$$C' = \frac{D + \left[\frac{1}{K_{p_2}} - 1\right]\frac{1}{\nu}}{D + \left[\frac{1}{K_{p_1}} - 1\right]\frac{1}{\nu}} . \tag{66}$$

Three states of subcriticality for intercomparison are important to note in the tables: approximately -1$, -7$, and -30$. These states of subcriticality are significant because of the following:

1. Other techniques, such as inverse kinetics (by rod drop or source jerk) and source multiplication, are calibrated near -1$.
2. -7$ represents the lower limit of applicability of most kinetic techniques due to reactivity and efficiency problems.
3. -30$ is a good approximation of the full shutdown of a typical liquid metal fast breeder reactor (LMFBR).

In general, all the coherence function $'s from the proposed modified inference reactions agree with the source multiplication method within ±2% around -1$, and ±5% around -7$. Between -7$ and -30$, the degree of disagreement increases even with the proposed modifications in the inference relation. The disagreement between the modified coherence function reactivity and the result of the source multiplication method may be as high as 20% at -30$. (In the LMFBR program plan, requirements were established for an accuracy of 20% for measurements of more than 15$ subcritical.) [1].

Since the treatment of the fission probability approach (Equation 63) has accounted for the most fluctuating effects.

It is considered that the correction expression from this approach is most accurate among the five proposed forms. Close examination of Tables 9, 10 and 11 supports this view. In each core of the ZPPR assembly 3, it was observed that in the range of $<-7, the correction by Equation 63, i.e. the fission probability approach, results in the closest agreement with the subcritical source multiplication method. However, it should be pointed out that, even with the correction factor of the fission probability approach, i.e. Equation 63, there are still considerable differences in the magnitude of $\$_2$ in the far subcritical range. In particular, in the phase 1B core of ZPPR assembly 3 at -43.58$, the "corrected" polarity coherence reactivity is 16% less subcritical. Such discrepancy at this range has not been satisfactorily explained.

VII. CONCLUSION

Few experimental and numerical results have been reported on the spatial dependency of the coherence function reactivity in a fast critical assembly. This study provided some data in this area.

It has been found from experiments conducted in the ZPPR assembly 3 phase 3 core that the coherence function is spatially dependent. The inferred subcriticalities from the coherence functions measured in the radial blanket exhibited a deviation of about 7% at -7$. It appears the source of this deviation is the change of detector efficiency ratio (due to neutron shadowing) in the different measurement locations. It was also noted from experimental observations that the insertion or removal of the strong extraneous source has little effect on the inferred subcritical reactivities.

It has been shown that the computer code TASK, utilizing the transfer and scattering matrices, can be used to compute the coherence function reactivity for different detector placements. Results of the numerical mockup of ZPPR assembly 3 phase 1B core indicated that the coherence function is spatially dependent. Specifically, the coherence function decreases very drastically in the area of control rod and blanket. The inferred subcriticality at different radial positions also exhibit some deviations among themselves. The

disagreement due to the detector placement at the core center and the blanket is approximately 26% at -14$. The inferred subcriticality near the core center is most accurate when compared to the lamda-mode reactivity. It appears that part of the source of this disagreement is the change of detector efficiency ratio (due to neutron shadowing) in the different detector locations. In addition, there may be a spatial effect, not shown in terms of the detector efficiency ratio, which may account for the total deviation of the coherence functional reactivity.

The disagreement between the results of the source multiplication method and the polarity coherence function method is significant at far subcritical range, approximately 20% at -30$. Modifications of the conventional inference relation were shown to be warranted. Four different approaches to modify the inference relation were discussed. These modifications account for different forms of fluctuation in the neutron multiplication and detection process. The modification results in correction from +18% to +3% at -30$ for the inferred coherence function reactivity.

VIII. SUGGESTION FOR FUTURE STUDY

The use of the coherence function to infer the subcritical reactivity appears to be a promising method to be applied to future LMFBR's. As has been shown, experimental measurements and numerical simulation can, under the proper conditions, be used to determine the subcriticality in an accurate and reliable way. The accuracy can be confirmed by comparing with the lamda-mode reactivity or with the results of the subcritical source multiplication method.

Further work can be done to improve the technique for inferring the coherence function reactivity. Specifically, the following areas are suggested:

1. Use a high-energy-sensitive Pu-240 detector for the coherence function reactivity study. Note the energy dependence effects by comparing the result with those of a low-energy-sensitive detector such as Li-6 scintillation counter or U-235 fission counter.[1]
2. Extend the frequency-dependent flux calculation to the break frequency range (800-1200 Hz for ZPPR). Obtain the subcritical reactivity by examining the slope and the magnitude of the roll-off frequency.

---

[1]Recent study by Buhl et al. [57] indicated that there exists some energy effect in the determination of the coherence function reactivity.

This serves as another comparison with the coherence function reactivity.

3. Use the Californium-252 as a randomly pulsed neutron source to determine the prompt-neutron decay constant and hence the subcritical reactivity of ZPPR.[1]

---

[1]Recent study by Mihalezo [21] indicated that the modified version of the Rossi-Alpha method may be quite suitable for determining subcriticality of LMFBR.

IX. LITERATURE CITED

1. Argonne National Laboratory. 1968. Liquid metal fast breeder reactor program plan. USAEC Reports WASH-1104 and WASH-1109.

2. Seifritz, W. 1969. The polarity correlation of reactor noise in the frequency domain. Nucl. Appl. Tech. 7: 513-522.

3. Nabavian, M. 1973. Reactor noise measurement in the UTR-10 using the polarity correlation method. Unpublished M.S. thesis, Iowa State University.

4. Lehto, W. K., J. M. Larson, R. W. Goin and J. E. Hutton. 1971. A polarity-correlation system for fast reactor noise studies. Nucl. Instr. Method 97: 507-519.

5. Lehto, W. K. 1971. ZPPR noise studies. Reactor development program progress report. ANL-7783 (Argonne National Laboratory, Idaho Falls, Idaho) 11 pp.

6. Danofsky, R. A., J. M. Larson, S. G. Carpenter and J. M. Gasidlo. 1972. Polarity coherence function reactivity measurements in ZPPR assembly 3, phase 1A. ANL-8010 (Argonne National Laboratory, Idaho Falls, Idaho).

7. Bennett, E. F., S. G. Carpenter, C. E. Cohn and D. H. Shaftmen. 1973. Argonne experience in measurement for reactivity of subcritical fast reactor systems. Trans. Am. Nucl. Soc. 16: 290-291.

8. Ackerman, N. J. 1971. Subcritical measurement in an LMFBR. Nucl. Saf. 12(6): 583-590.

9. Seber, R. 1945. The definition of neutron multiplication. LA-335 (Los Alomos Scientific Laboratory, Los Alomos, New Mexico).

10. Kaiser, R. E. 1973. Calculated corrections for phases 1B and 2 multiple control rod and configurations. ZPR-TM-134 (Argonne National Laboratory, Idaho Falls, Idaho) 4 pp.

11. Samstad, G. I. and C. L. Larson. 1972. LMFBR in-core instrumentation and in-vessel surveillance systems. GEAP-13825-4 (General Electric Atmoic Power, Sunnyvale, Calif.).

12. Fleischman, R. M. 1973. Subcritical reactivity surveillance procedures for the Fast Flux Test Facility. HEDL-TME-73-43 (Hanford Engineering Development Laboratory, Hanford).

13. Fleischman, R. M. 1972. Shutdown reactivity measurement in FTR in critical experiment evaluation. HEDL-TME-72-22 (Hanford Engineering Development Laboratory, Hanford).

14. Albrecht, R. W. and G. M. Hess. 1971. A comparison of inverse kinetics and polarity spectrum reactivity measurement in FTR-3. Trans. Am. Nucl. Soc. 14: 45-46.

15. Carpenter, S. G., A. L. Hess and J. M. Gasidlo. 1971. Control rod worth measurements in the ZPPR-2 benchmark core. Trans. Am. Nucl. Soc. 14: 27-29.

16. Cohn, C. E. 1972. Simulation studies of subcriticality measurement by rod drop. Trans. Am. Nucl. Soc. 15: 522-523.

17. Carpenter, S. G. 1972. Statistical errors in rod drop measurements of subcriticality. ANL-8010 (Argonne National Laboratory, Idaho Falls, Idaho).

18. Amundson, P. I., S. G. Carpenter and J. M. Gasidlo. 1972. Subcritical worth measurements of simulated control rod banks in the LMFBR demonstration plant benchmark critical. Trans. Am. Nucl. Soc. 15: 931-933.

19. Lehto, W. K. 1968. Pulsed neutron measurement in ZPR-3. ANL-7518 (Argonne National Laboratory, Idaho Falls, Idaho) 22 pp.

20. Orndoff, J. D. 1957. Prompt neutron periods of metal critical assemblies. Nucl. Sci. Eng. 2: 450-460.

21. Mihalezo, J. T. 1974. The use of Californium-252 as a randomly pulsed neutron source for prompt-neutron decay measurement. Nucl. Sci. Eng. 53: 393-414.

22. Feyman, M. P., F. DeHoffman and R. Seber. 1956. Dispersion of the neutron emission in U-235 fission. J. Nucl. Energy 3: 64-75.

23. Thie, J. A. 1963. Reactor Noise. AEC monograph. Rowman and Littlefield, New York.

24. Urig, R. E. 1970. Random noise technique in nuclear reactor systems. Ronald Press, New York.

25. Balcomb, J. 1963. Noise analysis in nuclear systems. Proceedings of the Symposium, Gainsville, Florida. 183 pp.

26. Stern, T. E. 1963. Noise analysis in nuclear systems. Proceedings of the Symposium, Gainsville, Florida. 203 pp.

27. Valat, J. 1963. Noise analysis in nuclear systems. Proceedings of the Symposium, Gainsville, Florida. 219 pp.

28. Cohn, C. E. 1959. Determination of reactor kinetic parameters by pile noise analysis. Nucl. Sci. Eng. 5: 331-340.

29. Boardman, F. D. 1963. Noise analysis in nuclear systems. Proceedings of the Symposium, Gainsville, Florida. 469 pp.

30. Dragt, J. B. 1966. Neutron noise, wave, and pulse propogation. Transactions of Symposium, Gainsville, Florida. 47 pp.

31. Rajagopal, V. 1962. Determination of reactor transfer functions by statistical correlation method. Nucl. Sci. Eng. 12: 218-224.

32. Bradgley, R. and R. Urig. 1964. Power-spectral-density measurements in a subcritical nuclear reactor. Nucl. Sci. Eng. 19: 158-163.

33. Balcomb, J., H. Demuth and E. Gyftopoulous. 1961. A cross correlation method for measuring the impulse response of reactor systems. Nucl. Sci. Eng. 11: 159-166.

34. Ackerman, N. J., A. R. Buhl and R. C. Kryter. 1971. An analytical and experimental evaluation of detection efficiency dependence of subcritical measurements by the polarity spectral coherence method. Trans. Am. Nucl. Soc. 14: 44-45.

35. Carpenter, S. G. 1973. Fast critical facilities measurement technique development. ANL-RDP-16 (Argonne National Laboratory, Idaho Falls, Idaho) 8.21 pp.

36. Ebert, D. D., J. D. Clement and W. M. Stacey, Jr. 1974. Interpretation of coherence function measurements in zero-power coupled-core reactors. Nucl. Sci. Eng. 55: 368-387.

37. Daly, T. A., G. K. Leaf and A. S. Kennedy. 1972. The ARC system: Two dimensional diffusion theory capability, DARC 2D. ANL-7716 (Argonne National Laboratory, Lemont, Ill.).

38. Engle, W. W. 1967. A user's mannual for ANISN, a one-dimensional discrete ordinates transport code with aniostropic scattering. ORGDEP-K-1693 (Oak Ridge Gaseous Diffusion Plant, Oak Ridge, Tenn.).

39. Cohn, C. E., R. J. Johnson and R. N. Macdonald. 1966. Calculating space-dependent reactor transfer function using static techniques. Nucl. Sci. Eng. 26: 198-206.

40. Dodd, H. L., J. C. Robinson and A. R. Buhl. 1972. The formulation and application of the transfer-scattering matrix method to space-, energy-, and angular-dependent fast reactor kinetics. Nucl. Sci. Eng. 47: 262-274.

41. Cohn, C. E. 1960. A simplified theory of pile noise. Nucl. Sci. Eng. 7: 472-485.

42. Stenberg, C. G. and A. Lindeman. 1973. The ARC system cross-section generation capabilities, ARC-MC^2. ANL-7722 (Argonne National Laboratory, Lemont, Ill.).

43. Grasseschi, G. 1972. ZPPR Internal Memorandum (Argonne National Laboratory, Idaho Falls, Idaho).

44. Carpenter, S. G. 1973. The space dependence of the polarity coherence function and its effect on the determination of the subcriticality. Part 2. ANL-RDP-21 (Argonne National Laboratory, Idaho Falls, Idaho) 6.22 pp.

45. Laworski, H. 1968. Zero power plutonium reactor facility. Nucl. News 11(2): 47-50.

46. Gasidlo, J. M. 1973. Worth measurements of single B_4C rod in ZPPR assembly 3, phase 3. ANL-RDP-17 (Argonne National Laboratory, Idaho Falls, Idaho) 6.5 pp.

47. Hess, A. L. 1973. Measurements of control-rod group worths in ZPPR assembly 3 phase 3. ANL-RDP-17 (Argonne National Laboratory, Idaho Falls, Idaho) 6.1 pp.

48. Koo, N. H. and S. G. Carpenter. 1973. The space dependence of the polarity coherence function and its effect on the determination of the subcriticality. Part 1. ANL-RDP-21 (Argonne National Laboratory, Idaho Falls, Idaho) 6.19 pp.

49. Kryter, R. C., N. J. Ackermann Jr., and A. R. Buhl. 1971. Measurement of subcriticality in large fast reactors by combining noise and multiplication technique. Trans. Am. Nucl. Soc. 14: 42-43.

50. Hess, A. L. 1972. Measurements of control rod group worths in ZPPR assembly 3 phase 2. ZPR-TM-134 (Argonne National Laboratory, Idaho Falls, Idaho) 8 pp.

51. Hess, G. M. and R. W. Albrecht. 1969. Polarity spectral analysis reactivity errors. Trans. Am. Nucl. Soc. 12: 738-739.

52. Buhl, A. R., R. A. Lillie, H. L. Dodds, Jr., O. W. Hermann, J. C. Robinson and R. J. Hinton. 1972. A generalized one-dimensional transport and diffusion kinetics code. ORNL-TM-3811 (Oak Ridge National Laboratory, Oak Ridge, Tenn.).

53. Sheff, J. R. and R. W. Albrecht. 1966. The space dependency of reactor noise, I-theory. Nucl. Sci. Eng. 24: 246-259.

54. Kaiser, R. E. 1973. Evaluation of detector efficiency and source worth correction for ZPPR-3 subcritical reactivity measurements. ZPR-TM-137 (Argonne National Laboratory, Idaho Falls, Idaho).

55. Carpenter, S. G. 1973. Fast critical facilities measurement technique development. ANL-RDP-21 (Argonne National Laboratory, Idaho Falls, Idaho) 6.19 pp.

56. Borgwaldt, H. and D. Stegemann. 1965. A common theory for neutronic noise analysis experiments in nuclear reactors. Nukleonik 7: 313-325.

57. Buhl, A. R., J. C. Robinson and E. T. Tomlison. 1974. Intercomparison of nonperturbing techniques for inferring the reactivity of fast reactors. Nucl. Tech. 21: 67-74.

58. Terrel, J. 1957. Distributions of fission neutron numbers. Phys. Rev. 108(3): 783-789.

X. ACKNOWLEDGEMENT

The author wishes to thank Dr. R. A. Danofsky for his many valuable suggestions, assistances and guidances in this investigation. The many enlightening thoughts and encouragement from him have been greatly helpful in the course of this research.

The author would like to express his sincere appreciation to the experimental and theoretical support staff of Applied Physics Division, Argonne National Laboratory (Idaho). Their assistance and cooperation had made this experimental and numerical study possible. Special thanks are due for Dr. S. G. Carpenter who developed the original concept of the fission probability approach for the modified inference relation. The author also benefited from the many professional discussions with S. G. Carpenter and J. M. Gasidlo.

The author wishes to express his gratitude to Drs. Glenn Murphy, R. G. Brown, D. M. Roberts and R. J. Lambert, who together with Drs. R. A. Danofsky and S. G. Carpenter, form his graduate committee.

Finally, the author wants to thank Dr. Glenn Murphy whose guidance and assistance have been most helpful during his graduate study in Iowa State University.

XI. APPENDIX A: RELATION OF COHERENCE FUNCTION AND SUBCRITICAL REACTIVITY

Assuming a prompt[1] point reactor kinetic model, one can infer the subcritical state (usually written in unit of dollar, \$) from the measurement of the coherence function, ρ, of this state. The inference relation can be derived from the coherence function defined in Equation 1. For band limited neutron detector signals $x(\omega,t)$ and $y(\omega,t)$, it can be shown that the cross power spectral density of these two signals is:

$$\Phi_{xy}(\omega) = \bar{q}_x \bar{q}_y \, F \, \frac{W_x \, W_y \, D \, K_{eff}^2}{\ell^2 (\alpha^2 + \omega^2)} \qquad (A1)$$

where $\Phi_{xy}(\omega)$ = cross power spectral density of signal x and y

$\bar{q}_i$ = average charge per detected neutron for detector i

F = fission rate, fission/sec

W_i = detector efficiency (detection/fission) for detector i

D = Diven factor = $\frac{\overline{\nu(\nu-1)}}{\bar{\nu}^2}$[2], ν = number of neutrons released per fission

---

[1] By a "prompt" model, it is meant that to the time span considered is sufficiently short such that the birth of delayed neutron can be precluded.

[2] The Diven factor is a measure of the relative width of the neutron multiplicity distribution [58].

K_{eff} = effective multiplication factor, including delayed neutrons

ℓ = prompt neutron life-time

β = total delayed neutron fraction

α = break frequency (roll-off frequency)

$$= \frac{1 - K(1-\beta)}{\ell} .$$

For the measurement of the polarity coherence function in a fast breeder reactor to determine the subcritical state, the band limiting filter frequency is much less than the break frequency, i.e. $\omega << \alpha$. Furthermore, if the two neutron detectors are experiencing the same magnitude of neutron flux and their instrumentation responses are the same, then $q = q_x = q_y$ and $W = W_x = W_y$. Equation A1 can therefore be simplified to:

$$\Phi_{xy}(\omega) = \frac{\bar{q}^2 \, FW^2 D \, K^2}{\ell^2 \alpha^2} = \frac{\bar{q}^2 \, FW^2 D}{\beta^2 (1-\$)^2} \qquad \text{(A2)}$$

where $\$$ = reactivity in dollar = $\frac{K-1}{K\beta}$.

Equation A2 is the expression for the cross power spectral density for correlated pile noise signals from two detectors. It is shown in section IV that the correlated pile noise signals are, conceptually, the neutron detections from the same fission chain (so-called chain related neutron

detections). For a single detector system, the auto power spectral density is obtained:

$$\Phi_{xx}(\omega) = \bar{q}^2 \; F \; W \; Q \left[1 + \frac{WD}{Q} \left(\frac{1}{1-\$} \right)^2 \right] \tag{A3}$$

where $\Phi_{ii}(\omega)$ = auto power spectral density of detector i

$$Q = \text{Bennett factor} = \frac{\overline{q^2}}{\bar{q}^2} .$$

The Bennett factor is the factor accounting for the statistical fluctuations of the ionization phenomena in the detector chamber. The auto power spectral density is due to the detection of two sources of signals. The first term in Equation A3 describes the contribution of the uncorrelated white noise (nonchain related neutron detection) and the second term describes the effect of the correlated pile noise signal (chain-related neutron detection). Substitution of Equation A2 and A3 into 1 yields the following:

$$\rho(\omega) = \frac{\frac{D}{R\beta^2} W}{(1-\$)^2 + \frac{D}{R\beta^2} W} . \tag{A4}$$

With suitable manipulation of Equation A4, it follows that

$$\frac{\rho}{1-\rho} = \frac{\frac{D}{R\beta^2} W}{(1-\$)^2} . \tag{A5}$$

Applying Equation A5 to a calibrated near-critical state 1 and a measurement subcritical state 2, the inference relation from the coherence functions to the subcritical $\$_2$ is obtained as

$$\$_2 = 1 - (1-\$_1)\left(\frac{W_2}{W_1}\right)^{\frac{1}{2}}\left(\frac{\beta_1}{\beta_2}\right)\left(\frac{1-\rho_2}{\rho_2}\cdot\frac{\rho_1}{1-\rho_1}\right)^{\frac{1}{2}}, \qquad \text{(A6)}$$

where subscripts 1 and 2 refer to the reference state and measured state respectively.

The detector efficiency ratio $\left(\frac{W_2}{W_1}\right)$ and the delayed neutron fraction ratio $\left(\frac{\beta_1}{\beta_2}\right)$ can be obtained by numerical computation [53]. Some early work in coherence function measurement treated these two ratios to be unity [2].

With the parameters of the calibrated near-critical state 1 and the measurement of the coherence function at state 2, the subcritical reactivity at state 2 can be inferred by Equation A6. It should be pointed out that a modification is needed when the measured state 2 is far subcritical (about -30$). This modification of Equation A6 may account for the discrepancy between the results of the source multiplication method and the polarity coherence function method in the far subcritical range. The proposed modification of Equation A6 is treated in detail in section IV.

XII. APPENDIX B: THE ALGORITHM OF THE TASK (Transfer And Scattering Kinetics) PROGRAM [52]

Consider the one-dimensional time dependent diffusion equation with G energy group and M delayed neutron groups:

$$v^{-1}\frac{\partial \underline{\phi}(x,t)}{\partial t} + \frac{\partial \underline{J}(x,t)}{\partial x} + \underline{\underline{\Sigma}}(x)\,\underline{\phi}(x,t) = (1-\beta)\underline{\chi}[\underline{\nu\Sigma_f}(x)]^T\underline{\phi}(x,t) + \underline{\underline{\Sigma_s}}(x)\underline{\phi}(x,t) + \sum_{i=1}^{M}\lambda_i\,\underline{\gamma_i}C_i(x,t) + \underline{S}(x,t) \tag{B1}$$

$$\frac{\partial C_i(x,t)}{\partial t} + \lambda_i C_i(x,t) = \beta_i[\underline{\nu\Sigma_f}(x)]^T\underline{\phi}(x,t) \quad \text{for } i = 1,2,\ldots M \tag{B2}$$

$$\underline{\underline{D}}^{-1}\,\underline{J}(x,t) = -\frac{\partial \underline{\phi}(x,t)}{\partial x} \tag{B3}$$

where x,t = independent variable of space and time

$\underline{\phi}$ = G x 1 column vector of neutron flux

$\underline{J}$ = G x 1 column vector of neutron current

C_i = precursor concentration of the i^{th}-group delayed neutron

$\underline{\chi}$ = column vector for the prompt neutron fission energy spectrum

$\underline{\gamma_i}$ = column vector for the delayed neutron energy spectrum of the i^{th}-group precursor

$\underline{\underline{\Sigma}}$ = diagonal matrix whose diagonal elements are the total cross section

$\underline{S}$ = volumetric source vector

λ_i = precursor decay constant of i^{th}-group delayed neutron

β_i = delayed neutron fraction of the i^{th}-group

ν = number of neutron released per fission

$[\underline{\nu\Sigma_f}]^T$ = transpose of a column vector of ν times the fission cross section, Σ_f

and $\underline{\underline{V}}^{-1}$, $\underline{\underline{\Sigma_s}}$ and $\underline{\underline{D}}^{-1}$ are matrices whose elements are

$$\underline{\underline{V}}^{-1} = \begin{bmatrix} \frac{1}{V_1} & 0 & \cdots & 0 \\ 0 & \frac{1}{V_2} & 0 & \vdots \\ 0 & 0 & \ddots & \vdots \\ \vdots & \vdots & & \vdots \\ 0 & 0 & \cdots & \frac{1}{V_G} \end{bmatrix}, \quad V_j = \text{mean neutron velocity of group } j$$

$$\underline{\underline{\Sigma_s}} = \begin{bmatrix} \Sigma_s^{1\to1} & \Sigma_s^{2\to1} & \cdots & \Sigma_s^{G\to1} \\ \Sigma_s^{1\to2} & \Sigma_s^{2\to2} & & \vdots \\ \vdots & & \ddots & \vdots \\ \Sigma_s^{1\to G} & \cdots & & \Sigma_s^{G\to G} \end{bmatrix}, \quad \Sigma_s^{i\to j} = \text{scattering cross section from group i to group j}$$

$$\underline{\underline{D}}^{-1}=3 \begin{bmatrix} \Sigma_{t_r}^1 & & & Q \\ & \Sigma_{t_r}^2 & & \\ & & \ddots & \\ Q & & & \Sigma_{t_r}^G \end{bmatrix}, \quad \Sigma_{t_r}^j = \text{transport cross section of group j.}$$

Applying the Fourier transform to Equations B1, B2 and B3, and eliminating C_i in Equations B1 from B2, the following is obtained

$$\frac{\partial}{\partial x}\underline{J}(x,\omega)+[\omega\underline{\underline{V}}^{-1}+\underline{\underline{\Sigma}}-(1-\beta)\ \underline{\chi}(\underline{\nu\Sigma_f})^T-\underline{\underline{\Sigma_s}}-\sum_{i=1}^{M}\frac{\lambda_i\beta_i}{S+\lambda_i}\ \underline{\gamma_i}(\underline{\nu\Sigma_f})^T]\underline{\phi}(x,\omega)$$

$$= \underline{S}(x,\omega) \qquad \text{(B4)}$$

$$\frac{\partial}{\partial x}\underline{\phi}(x,\omega) + \underline{\underline{D}}^{-1} J(x,\omega) = 0 \qquad \text{(B5)}$$

Equations B4 and B5 are now in the frequency domain. $\underline{S}(x,\omega)$ is the square root of the "noise equivalent source" as defined by Cohn [41] and Sheff and Albrecht [53]. If one defines the matrix $A(\omega)$ to be:

$$\underline{\underline{A}}(\omega) = \omega \underline{\underline{V}}^{-1} + \underline{\underline{\Sigma}} - (1-\beta)\, \underline{\chi}\, (\nu\underline{\Sigma_f})^T - \underline{\underline{\Sigma_s}} - \sum_{i=1}^{M} \frac{\lambda_i \beta_i}{S+\lambda_i}\, \underline{\gamma_i}\, (\nu\underline{\Sigma_f})^T, \tag{B6}$$

then Equations B4 and B5 can be combined to become:

$$\frac{\partial}{\partial x}\begin{bmatrix} \underline{J}(x,\omega) \\ \underline{\phi}(x,\omega) \end{bmatrix} + \begin{bmatrix} \underline{\underline{0}} & \underline{\underline{A}}(\omega) \\ \underline{\underline{D}}^{-1} & \underline{\underline{0}} \end{bmatrix} \begin{bmatrix} \underline{J}(x,\omega) \\ \underline{\phi}(x,\omega) \end{bmatrix} = \begin{bmatrix} \underline{S}(x,\omega) \\ \underline{0} \end{bmatrix} \tag{B7}$$

where $\underline{\underline{0}}$ is the null matrix and $\underline{0}$ is the null vector. Equation B7 can be written in the abbreviated form of:

$$\frac{\partial}{\partial x}\, \underline{\psi}(x,\omega) + \underline{\underline{B}}(\omega)\, \underline{\chi}(x,\omega) = \underline{Z}(x,\omega) \tag{B8}$$

where $\underline{\psi}(x,\omega)$, $\underline{\underline{B}}(\omega)$ and $\underline{Z}(x,\omega)$ are respectively the state vector, the coefficient matrix and the source vector in the frequency domain. Their definitions are evident from Equation B7. The state vector $\underline{\psi}(x,\omega)$ and source vector $\underline{S}(x,\omega)$ are $2G \times 1$ column vectors and $\underline{\underline{B}}(\omega)$ is a $2G \times 2G$ matrix. They can be viewed as the fluctuations about the steady state case.

One way to obtain the solution of Equation B8 efficiently is by using the transfer and scattering matrices. Expanding

the state vector in Taylor series yields

$$\psi(x+\Delta x,\omega)=\chi(x,\omega)+\frac{d}{dx}\psi(x,\omega)\Delta x+\frac{1}{2!}\frac{d^2}{dx^2}\psi(x,\omega)\Delta x^2+\ldots+\frac{1}{n!}\frac{d^n}{dx^n}\psi(x,\omega)\Delta x^n. \quad (B9)$$

With the assumption that $\underline{\underline{B}}(\omega)$ and $\underline{Z}(x,\omega)$ are constant over Δx and that ψ is a continuously differentiable function of x, repeated differentiation of Equation B8 will yield expressions for the derivatives of ψ which can be substituted into Equation B9. The final result is:

$$\psi(x+\Delta x,\omega) = \Lambda^{(1)}(\Delta x,\omega)\psi(x,\omega) + \Lambda^{(2)}(\Delta x,\omega)Z(x,\omega) \quad (B10)$$

where

$$\Lambda^{(1)}(\Delta x,\omega) = 1-B(\omega)\Delta x + \frac{1}{2!}[B(\omega)]^2(\Delta x)^2+\ldots+\frac{1}{n!}[B(\omega)]^n(\Delta x)^n+\ldots$$

$$= \sum_{n=1}^{\infty}\frac{(-1)^n(B(\omega)\Delta x)^n}{n!}$$

$$\Lambda^{(2)}(\Delta x,\omega) = \Delta x\left(1 - \frac{1}{2!}B(\omega)\Delta x + \frac{1}{3!}[B(\omega)]^2(\Delta x)^2-\ldots\right)$$

$$= \Delta x\sum_{n=1}^{\infty}\frac{(-1)^n(B(\omega)\ x)^n}{(n+1)!}\ .$$

Because $\Lambda^{(1)}(\Delta x)$ relates ψ at space point x to ψ at space point $x + \Delta x$, $\Lambda^{(1)}(\Delta x)$ is called the "transfer matrix."

In principle, Equation B10 can be applied along with appropriate boundary conditions to determine the state vector at all points of interest. This procedure will usually fail in a two point boundary value problems (i.e. problems in which half of the boundary conditions are known at one space point and the other half are known at another space point)[40]. This difficulty can be circumvented by changing from the transfer matrix format to the scattering matrix formulism. This can be done by rewriting Equation B10 in the form of:

$$\psi(x + \Delta x,\omega) = \Lambda^{(1)}(\Delta x,\omega)\psi(x,\omega) + F(\Delta x,\omega) \qquad \text{(B11)}$$

where $F(\Delta x,\omega) = \Lambda^{(2)}(\Delta x,\omega)Z(x,\omega)$.

Partitioning Equation B11 into the upper half and lower half of the matrices and vectors, one obtains:

$$\begin{bmatrix} \psi_U(x+\Delta x,\omega) \\ \psi_L(x+\Delta x,\omega) \end{bmatrix} = \begin{bmatrix} \Lambda_{11}^{(1)}(\Delta x,\omega) & \Lambda_{12}^{(1)}(\Delta x,\omega) \\ \Lambda_{21}^{(1)}(\Delta x,\omega) & \Lambda_{22}^{(1)}(\Delta x,\omega) \end{bmatrix} \begin{bmatrix} \psi_U(x,\omega) \\ \psi_L(x,\omega) \end{bmatrix} + \begin{bmatrix} F_U(\Delta x,\omega) \\ F_L(\Delta x,\omega) \end{bmatrix}. \qquad \text{(B12)}$$

Subscripts U and L stand for upper and lower half of the matrices of vectors. $\Lambda_{11}^{(1)}$, $\Lambda_{12}^{(1)}$, $\Lambda_{21}^{(1)}$ and $\Lambda_{22}^{(1)}$ are G x G matrices and ψ_U, ψ_L, F_U and F_L are G x 1 vectors.

Rearranging Equation B12 in the scattering matrix formalism, it follows that

$$\begin{bmatrix} \psi_U(x+\Delta x,\omega) \\ \psi_L(x,\omega) \end{bmatrix} = \begin{bmatrix} G_{11}(\Delta x,\omega) & G_{12}(\Delta x,\omega) \\ G_{21}(\Delta x,\omega) & G_{22}(\Delta x,\omega) \end{bmatrix} \begin{bmatrix} \psi_U(x,\omega) \\ \psi_L(x+\Delta x,\omega) \end{bmatrix} + \begin{bmatrix} S_U(\Delta x,\omega) \\ S_L(\Delta x,\omega) \end{bmatrix}, \tag{B13}$$

where the coefficient matrix $\underline{\underline{G}}$ and the source vector $\underline{S}$ are given by:

$$G_{11}(\Delta x,\omega) = \Lambda_{11}^{(1)}(\Delta x,\omega) - \Lambda_{12}^{(1)}(\Delta x,\omega)\left[\Lambda_{22}^{(1)}(\Delta x,\omega)\right]^{-1}\Lambda_{21}^{(1)}(\Delta x,\omega)$$

$$G_{12}(\Delta x,\omega) = \Lambda_{12}^{(1)}(\Delta x,\omega)\left[\Lambda_{22}^{(1)}(\Delta x,\omega)\right]^{-1}$$

$$G_{21}(\Delta x,\omega) = -\left[\Lambda_{22}^{(1)}(\Delta x,\omega)\right]^{-1}\Lambda_{21}^{(1)}(\Delta x,\omega)$$

$$G_{22}(\Delta x,\omega) = \left[\Lambda_{22}^{(1)}(\Delta x,\omega)\right]^{-1}$$

$$S_U(\Delta x,\omega) = F_U(\Delta x,\omega) - \Lambda_{12}^{(1)}(\Delta x,\omega)\left[\Lambda_{22}^{(1)}(\Delta x,\omega)\right]^{-1}F_L(\Delta x,\omega)$$

$$S_L(\Delta x,\omega) = -\Lambda_{22}^{(1)}(\Delta x,\omega)^{-1}\, F_L(\Delta x,\omega).$$

The $\underline{\underline{G}}$ matrix of Equation B13 is called the scattering matrix (or the response matrix). The submatrices G_{11} and G_{22} are called transmission matrices and G_{12} and G_{21} the reflection matrices. For a slab material of thickness Δx, the vector composed of $\psi_U(x,\omega)$ and $\psi_L(x+\Delta x,\omega)$ is the radiation input state vector into the slab and the vector composed of $\psi_U(x+\Delta x,\omega)$ and $\psi_L(x,\omega)$ is the radiation output state vector emerging from the

slab.

With proper input of boundary conditions, Equation B13 can be used to compute the frequency dependent neutron flux at different space points of the reactor. The computer code, TASK [52], employs the relation of Equation B13 for calculation of the neutron flux distribution. This neutron flux distribution is then folded in with the detector cross section to obtain the detector response (as defined in Equation 4, p. 14). With the detector response, one can calculate the coherence function by Equation 1 and the subcritical reactivity ($\$_2$) can then be inferred from Equation 3.

XIII. APPENDIX C: THE STANDARD DEVIATION ($\delta_{\$_2}$) OF THE INFERRED SUBCRITICAL REACTIVITY ($\$_2$) DETERMINED BY A PAIR OF NEUTRON DETECTORS OF EQUAL EFFICIENCY

The inferred subcritical reactivity in $\$_2$ is expressed by Equation 3 as:

$$\$_2 = 1 - (1-\$_1)\left(\frac{\beta_1}{\beta_2}\right)\left(\frac{W_2}{W_1}\right)^{\frac{1}{2}}\left(\frac{1-\rho_2}{\rho_2} \times \frac{\rho_1}{1-\rho_1}\right)^{\frac{1}{2}} \tag{C1}$$

In functional form, Equation C1 can be written as:

$$\$_2 = f\left(\$_1,\ \rho_2,\ \rho_1,\ \frac{\beta_1}{\beta_2},\ \frac{W_2}{W_1}\right) . \tag{C2}$$

The variance of $\$_2$ can be obtained by applying the classical propagation of error-analysis techniques to Equation C2 with the assumption that the functional quantities are independent. Thus, one writes:

$$\delta^2_{\$_2} = \left(\frac{\partial f}{\partial \$_1}\right)^2 \delta^2_{\$_1} + \left(\frac{\partial f}{\partial \rho_1}\right)^2 \delta^2_{\rho_1} + \left(\frac{\partial f}{\partial \rho_2}\right)^2 \delta^2_{\rho_2} + \left(\frac{\partial f}{\partial B}\right)^2 \delta^2_{B} + \left(\frac{\partial f}{\partial \varepsilon}\right)^2 \delta^2_{\varepsilon} \tag{C3}$$

where $B = \frac{\beta_1}{\beta_2}$ and $\varepsilon = \frac{W_2}{W_1}$.

The partial derivatives of $f(\$_1, \rho_2, \rho_1, B, \varepsilon)$ in Equation C3 can be obtained by taking the differentials of Equation C1 with respect to the various quantities concerned. After suitable differentiating and manipulation of Equation C1, the

following expressions are obtained:

$$\frac{\partial f}{\partial \$_1} = \frac{1-\$_2}{1-\$_1} \tag{C4}$$

$$\frac{\partial f}{\partial \rho_1} = -\frac{1}{2}\frac{1-\$_2}{\rho_1(1-\rho_1)} \tag{C5}$$

$$\frac{\partial f}{\partial \rho_2} = \frac{1}{2}\frac{1-\$_2}{\rho_2(1-\rho_2)} \tag{C6}$$

$$\frac{\partial f}{\partial B} = \frac{\beta_2}{\beta_1}(1-\$_2) \tag{C7}$$

$$\frac{\partial f}{\partial \varepsilon} = -\frac{1}{2}\frac{W_1}{W_2}(1-\$_2) \tag{C8}$$

Substituting Equation C4-C8 into Equation C3, the following result is obtained:

$$\delta_{\$_2} = (1-\$_2)\left\{\frac{\delta^2_{\hat{\$}_1}}{(1-\$_1)^2} + \frac{1}{4}\frac{\delta^2_{\hat{\rho}_1}}{\rho_1^2(1-\rho_1)^2} + \frac{1}{4}\frac{\delta^2_{\hat{\rho}_2}}{\rho_2^2(1-\rho_2)^2}\right.$$

$$\left. + \left(\frac{\beta_2}{\beta_1}\right)^2\delta^2_B + \frac{1}{4}\left(\frac{W_1}{W_2}\right)^2\delta^2_\varepsilon\right\}^{\frac{1}{2}} \tag{C9}$$

Close examination of the magnitude of each term in the above equation reveals the following: Of the five terms on the RHS, the second and third term, i.e. the $\delta^2_{\rho_1}$ and $\delta^2_{\rho_2}$ terms, are the dominate ones. For example, a typical set of measurement [54, 46] showed the following data:

$$\rho_1 = 0.484 \qquad \rho_2 = 0.058$$

$$\$_1 = -1.608 \qquad \$_2 = -9.240$$

$$\frac{\beta_2}{\beta_1} = 0.997 \qquad \frac{W_1}{W_2} = 1.047 \quad .$$

Applying these data in Equation C9 results in the following expression:

$$\delta_{\$_2} = 10.240\{0.148\ \delta^2_{\$_1} + 4.008\ \delta^2_{\rho_1} + 79.360\ \delta^2_{\rho_2} + 0.994\ \delta^2_B + 0.262\ \delta^2_\varepsilon\}^{\frac{1}{2}} \quad . \qquad \text{(C10)}$$

It is known from experience that all of the variances on the RHS of the above equation are of the same order of magnitude. Therefore, it appears from the example of Equation C10 that if the uncertainties in $\delta_{\$_i}$, δ_B and δ_ε are neglected, the accuracy of Equation C10 would not be affected by more than 2%. Thus, the simplified expression is obtained:

$$\delta_{\$_2} = \frac{(1-\$_2)}{2}\left[\frac{\delta^2_{\rho_1}}{\rho_1^2(1-\rho_1)^2} + \frac{\delta^2_{\rho_2}}{\rho_2^2(1-\rho_2)^2}\right]^{\frac{1}{2}} \qquad \text{(C11)}$$

Equation C11 is the same as Equation 7. This equation was implemented in the ZPPR mini-computer for on-line calculation of the standard deviation of $\$_2$.

XIV. APPENDIX D: THE DERIVATION OF SUBCRITICAL REACTIVITY INFERRED FROM THE COHERENCE FUNCTION BY A PAIR OF NEUTRON DETECTORS OF DIFFERENT EFFICIENCIES

Two neutron detectors (x and y) are used to determine the coherence function for a given configuration of the nuclear reactor. The two detectors may have different efficiencies, i.e. $W_x \neq W_y$. In case I, we consider the hypothetical situation where the efficiency of the reference state and the measured state (of the same detector) are identical, i.e. $W_{x1} = W_{x2}$, $W_{y1} = W_{y2}$. In case II, we consider the practical situation where the efficiency of the reference state differs from that of the measured state, i.e. $W_{x1} \neq W_{x2}$, $W_{y1} \neq W_{y2}$.

Case I: Detector efficiency unchanged for the reference state and the measured state ($W_{x1} = W_{x2}$, $W_{y1} = W_{y2}$; $W_x \neq W_y$)

The coherence function is defined in Equation 1 to be 2:

$$\rho(\omega) = \frac{\Phi_{xy}(\omega)}{[\Phi_{xx}(\omega)\ \Phi_{yy}(\omega)]^{\frac{1}{2}}} \quad . \tag{D1}$$

Assuming a prompt point reactor kinetic model and using the same notations as Equation 2, Equation D1 becomes:

$$\rho(\omega) = \left[\frac{Q_x(\omega)\ Q_y(\omega)}{[1 + Q_x(\omega)][1 + Q_y(\omega)]}\right]^{\frac{1}{2}} \tag{D2}$$

where $Q_n(\omega) = \frac{Q_{n,i}}{(1-\$_i)^2 + \left(\frac{\omega}{\alpha_c}\right)^2}$ = ratio of correlated to uncorrelated noise contribution (signal-to-noise ratio) in channel n (n = x, y) (D3)

$Q_{n,i} = \frac{D}{R\beta_i^2} W_{n,i}$ = maximum signal-to-noise ratio of channel n at state i and low frequency ($\omega << \alpha_c$). (D4)[1]

Rewriting Equation D2 by utilizing Equations D3 and D4 yields

$$\rho(\omega) = \left(\frac{Q_{y,}^2 \varepsilon}{[(1-\$_i)^2 + Q_{y,i}\ \varepsilon + \left(\frac{\omega}{\alpha_c}\right)^2][(1-\$_i)^2 + Q_{y,i} + \left(\frac{\omega}{\alpha_c}\right)^2]} \right)^{\frac{1}{2}} \quad \text{(D5)}$$

where $\varepsilon = \frac{Wx}{Wy}$.

For purpose of measuring the polarity coherence function to determine the subcritical reactivity, the frequency of the band limited amplifier is set in the range of 10-200 Hz. Thus, the quantity $\frac{\omega}{\alpha_c}$ is negligible in Equation D5. After suitable manipulation of Equation D5 and applying it to the measured state 2 yields

---

[1]Assuming that the detector efficiency $W_{n,i}$ and the delayed neutron fraction β_i are the same for the reference state and the measured state, then $Q_{n,i}$ is constant.

$$\rho_2 = \left[\frac{Q_{y,2}^2 \, \varepsilon}{(1-\$_2)^4 + (1-\$_2)^2 \, Q_{y,2}(\varepsilon+1) + Q_{y,2}^2 \, \varepsilon} \right]^{\frac{1}{2}} . \qquad \text{(D6)}$$

One of the solution of Equation D6 is

$$\$_2 = 1 - \left[Q_{y,2} \times \frac{[(1-\varepsilon)^2 \rho_2^2 + 4\varepsilon] - \rho_2(1+\varepsilon)}{2\rho_2} \right]^{\frac{1}{2}} . \qquad \text{(D7)}$$

Consider the case of delayed critical, then $\$_c = \$_2 = 0$ and Equation D7 becomes:

$$Q_{y,c} = Q_{y,2} = \rho_c \frac{\rho_c(1+\varepsilon) + [(1-\varepsilon)^2 \rho_c^2 + 4\varepsilon]^{\frac{1}{2}}}{2\varepsilon(1-\rho_c^2)} \qquad \text{(D8)}$$

where the subscript c refers to the critical state, and W_{ni} and β_i are assumed constant for the two states.

Substitution of Equations D8 into D7 yields the following expression:

$$\$_2 = 1 - \left[\rho_c \frac{\rho_c(1+\varepsilon) + [(1-\varepsilon)^2 \rho_c^2 + 4\varepsilon]^{\frac{1}{2}}}{2\varepsilon(1-\rho_c^2)} \times \frac{[(1-\varepsilon)^2 \rho_2^2 + 4\varepsilon]^{\frac{1}{2}} - (1+\varepsilon)\rho_2}{2\rho_2} \right] . \qquad \text{(D9)}$$

Equation D9 was published by Seifritz [2]. Note that if $\varepsilon = 1$, i.e. the two detectors are of same efficiency $W_x = W_y$, then Equation D9 reduces to the simple form of:

$$\$_2 = 1 - \left(\frac{\rho_c}{1-\rho_c} \times \frac{1-\rho_2}{\rho_2}\right)^{\frac{1}{2}} . \qquad \text{(D10)}$$

Case II: Detector efficiency changes for the reference state and the measured state ($W_{n1} \neq W_{n2}$, $n = x,y$; $W_x \neq W_y$) and the reference state is not delayed critical ($\$_1 \neq 0$).

Similar to the derivation of case I, the analogy of Equation D7 for the reference state 1 and the measured state 2 is

$$1 - \$_1 = \left(Q_{y,1} \frac{[(1-\varepsilon_1)^2\rho_1^2 + 4\varepsilon_1]^{\frac{1}{2}} - \rho_1(1+\varepsilon_1)}{2\rho_1}\right)^{\frac{1}{2}} , \qquad \text{(D11)}$$

$$1 - \$_2 = \left(Q_{y,2} \frac{[(1-\varepsilon_2)^2\rho_2^2 + 4\varepsilon_2]^{\frac{1}{2}} - \rho_2(1+\varepsilon_2)}{2\rho_2}\right)^{\frac{1}{2}} \qquad \text{(D12)}$$

where $\varepsilon_i = \frac{W_{xi}}{W_{yi}}$, $i = 1, 2$

$\varepsilon_1 \neq \varepsilon_2$.

Taking the ratio of Equations D12 and D11

$$\frac{1-\$_2}{1-\$_1} = \left(\frac{Q_{y,2}}{Q_{y,1}} \times \frac{\rho_1}{\rho_2} \times \frac{[(1-\varepsilon_2)^2\rho_2^2 + 4\varepsilon_2]^{\frac{1}{2}} - \rho_2(1+\varepsilon_2)}{[(1-\varepsilon_1)^2\rho_1^2 + 4\varepsilon_1]^{\frac{1}{2}} - \rho_1(1+\varepsilon_1)}\right)^{\frac{1}{2}} . \qquad \text{(D13)}$$

The terms $Q_{y,2}$ and $Q_{y,1}$ are defined in Equation D4 and their ratio is

$$\frac{Q_{y,2}}{Q_{y,1}} = \frac{\frac{D}{R\beta_2^2} W_{y2}}{\frac{D}{R\beta_1^2} W_{y1}} = \left(\frac{\beta_1}{\beta_2}\right) \frac{W_{y2}}{W_{y1}} \qquad \text{(D14)}$$

Substitution of Equation D14 into D13 yields the expression:

$$1 - \$_2 = (1-\$_1)\left(\frac{\beta_1}{\beta_2}\right)\left(\frac{W_{y2}}{W_{y1}} \times \frac{\rho_1}{\rho_2} \times \frac{[(1-\varepsilon_2)^2\rho_2^2+4\varepsilon_2]^{\frac{1}{2}}-\rho_2(1+\varepsilon_2)}{[(1-\varepsilon_1)^2\rho_1^2+4\varepsilon_1]^{\frac{1}{2}}-\rho_1(1+\varepsilon_1)}\right)^{\frac{1}{2}} \qquad \text{(D15)}$$

With proper rationalization of the denominator of Equation D15 and manipulation, the final form for the subcritical reactivity $\$_2$ is obtained as

$$\$_2 = 1 - (1-\$_1)\left(\frac{\beta_1}{\beta_2}\right)\left(\frac{W_{y2}}{W_{y1}}\right)^{\frac{1}{2}}\left(\rho_1 \times \frac{[(1-\varepsilon_1)^2\rho_1^2+4\varepsilon_1]^{\frac{1}{2}}+\rho_1(1+\varepsilon_1)}{2\varepsilon_1(1-\rho_1^2)} \times \frac{[(1-\varepsilon_2)^2\rho_2^2+4\varepsilon_2]^{\frac{1}{2}}-\rho_2(1+\varepsilon_2)}{2\rho_2}\right)^{\frac{1}{2}} \qquad \text{(D16)}$$

It is appropriate to review the conditions under which Equation D16 is true. These conditions are:

i. the two detectors have different efficiency, $W_x \neq W_y$.

ii. the two subcritical states 1 and 2 induce a change in the delayed neutron fraction, $\beta_1 \neq \beta_2$, and the detector efficiency $W_{n1} \neq W_{n2}$, n = x, y.

iii. the reference state 1 is not the critical state, i.e. $\$_1 \neq 0$.

If the reference state 1 is the critical state, i.e. $\$_1 = \$_2 = 0$, and that β_i and W_{ni} are the same for the two states, then Equation D16 reduces to Equation D10 of case I.

The measurement of the polarity coherence function in ZPPR was conducted at a reference state slightly subcritical $\$_1 \sim -1.6$. The detector efficiency, in general, does change as the subcriticality changes from state 1 to 2, i.e. $W_{n1} \neq W_{n2}$. Thus, application of Equation D16 is more adequate than D10.

XV. APPENDIX E: THE STANDARD DEVIATION ($\delta_{\$_2}$) OF THE INFERRED SUBCRITICAL REACTIVITY ($\$_2$) DETERMINED BY A PAIR OF NEUTRON DETECTORS OF DIFFERENT EFFICIENCIES

It was shown in Appendix D that the inference relation from the coherence function to the subcritical reactivity for a pair of neutron detectors of different efficiencies is

$$\$_2 = 1 - (1-\$_1)\left(\frac{\beta_1}{\beta_2}\right)\left(\frac{W_{y2}}{W_{y1}}\right)^{\frac{1}{2}}\left\{\rho_1 \times \frac{[(1-\varepsilon_1)^2\rho_1^2+4\varepsilon_1]^{\frac{1}{2}}+\rho_1(1+\varepsilon_1)}{2\varepsilon_1(1-\rho_1^2)} \times \frac{[(1-\varepsilon_2)^2\rho_2^2+4\varepsilon_2]^{\frac{1}{2}}-\rho_2(1+\varepsilon_2)}{2\rho_2}\right\}^{\frac{1}{2}} \tag{E1}$$

where ρ_i = coherence function at state i measured by the cross correlation of detector x and y

ε_i = detector efficiency ratio at state i = $\frac{W_{xi}}{W_{yi}}$

W_{ni} = detector efficiency at state i of n channel (n = x, y)

i = 1, 2.

It should be pointed out that the detector efficiency ratio, ε_1 and ε_2 can be obtained by the lengthly process of solving the multi-group diffusion equation of the system. It can also be obtained by employing the following relation:

$$\varepsilon_i = \left(\frac{\rho_{xi}}{1-\rho_{xi}}\right)\left(\frac{1-\rho_{yi}}{\rho_{yi}}\right) \tag{E2}$$

where ρ_{ni} = coherence function at state i measured by a pair of n channel detectors (n = x, y).

Equation E2 was derived directly from Equation D5. It is valid in the low frequency range. In the evaluation of the standard deviation $\delta_{\$_2}$ in this section, ε_1 and ε_2 are calculated according to Equation E2.

Applying the classical propagation of error-analysis technique to Equation E1, the following expression is obtained:

$$\delta_{\$_2} = \left(\left(\frac{\partial \$_2}{\partial \$_1}\right)^2 \delta^2_{\$_1} + \left(\frac{\partial \$_2}{\partial \rho_1}\right)^2 \delta^2_{\rho_1} + \left(\frac{\partial \$_2}{\partial \rho_2}\right)^2 \delta^2_{\rho_2} + \left(\frac{\partial \$_2}{\partial \varepsilon_1}\right)^2 \delta^2_{\varepsilon_1} + \left(\frac{\partial \$_2}{\partial \varepsilon_2}\right) \delta^2_{\varepsilon_2}\right)^{\frac{1}{2}} \tag{E3}$$

The partial derivatives in the above equation can be obtained by taking the differentials of Equation E1 with respect to the five quantities concerned. After the proper differentiation and manipulation of Equation E1, the following relations are obtained:

$$\frac{\partial \$_2}{\partial \$_1} = \frac{1-\$_2}{1-\$_1}\ , \tag{E4}$$

$$\frac{\partial \$_2}{\partial \rho_1} = (1-\$_2)\left\{\frac{1}{\rho_1} \times \frac{1}{(1+\varepsilon_1)\rho_1+[(1-\varepsilon_1)^2\rho_1^2+4\varepsilon_1]^{\frac{1}{2}}}\right.$$

$$\left. \times \frac{\rho_1(1+\varepsilon_1)[(1-\varepsilon_1)^2\rho_1^2+4\varepsilon_1]^{\frac{1}{2}}+(1-\varepsilon_1)^2\rho_1^2+2\varepsilon_1(1+\rho_1^2)}{(1-\rho_1^2)^2[1-\varepsilon_1^2)\rho_1^2+4\varepsilon_1]^{\frac{1}{2}}}\right\}, \qquad \text{(E5)}$$

$$\frac{\partial \$_2}{\partial \rho_2} = (1-\$_2)\left\{\frac{2\varepsilon_2}{\rho_2[(1-\varepsilon_2)^2\rho_2^2+4\varepsilon_2]^{\frac{1}{2}}} \times \frac{1}{[(1-\varepsilon_2)^2\rho_2^2+4\varepsilon_2]^{\frac{1}{2}}-(1+\varepsilon_2)\rho_2}\right\}$$

(E6)

$$\frac{\partial \$_2}{\partial \varepsilon_1} = \frac{1-\$_2}{2} \times \left\{\frac{\varepsilon_1}{(1+\varepsilon_1)\rho_1+[(1-\varepsilon_1)^2+4\varepsilon_1]^{\frac{1}{2}}}\right.$$

$$\left. \times \frac{2-\rho_1[(1-\varepsilon_1)^2\rho_1^2+4\varepsilon_1]^{\frac{1}{2}}-2(1-\varepsilon_1)^2\rho_1^2-4\varepsilon_1}{\varepsilon_1^2[(1-\varepsilon_1)^2\rho_1^2+4\varepsilon_1]^{\frac{1}{2}}}\right\}, \qquad \text{(E7)}$$

$$\frac{\partial \$_2}{\partial \varepsilon_2} = \frac{1-\$_2}{2} \times \left\{\frac{2-(1-\varepsilon_2)\rho_2^2}{[(1-\varepsilon_2)^2\rho_2^2+4\varepsilon_2]^{\frac{1}{2}}} - \rho_2\right\}$$

$$\times \left\{\frac{1}{[(1-\varepsilon_2)^2\rho_2^2+4\varepsilon_2]^{\frac{1}{2}}-(1+\varepsilon_2)\rho_2}\right\}. \qquad \text{(E8)}$$

Of the five partial derivatives defined in Equations E4-E8, $\left(\frac{\partial \$_2}{\partial \rho_1}\right)$ and $\left(\frac{\partial \$_2}{\partial \rho_2}\right)$ are the dominate ones. As an example, taking the data from run 686 and 684 of Table 2, the following parameters are obtained

$$\$_1 = -1.834 \qquad \$_2 = -5.874$$

$$\rho_1 = 0.4379 \qquad \rho_2 = 0.1149$$

$$\rho_{x1} = 0.6667 \qquad \rho_{x2} = 0.2211$$

$$\rho_{y1} = 0.2979 \qquad \rho_{y2} = 0.0749$$

$$\varepsilon_1 = \left(\frac{\rho_{x1}}{1-\rho_{x1}}\right)\left(\frac{1-\rho_{y1}}{\rho_{y1}}\right) = 4.842$$

$$\varepsilon_2 = \left(\frac{\rho_{x2}}{1-\rho_{x2}}\right)\left(\frac{1-\rho_{y2}}{\rho_{y2}}\right) = 3.516 \ .$$

Substituting these values into Equations E4-E8 yields the following results:

$$\frac{\partial \$_2}{\partial \$_1} = (1-\$_2)(0.705),$$

$$\frac{\partial \$_2}{\partial \rho_1} = (1-\$_2)(3.172),$$

$$\frac{\partial \$_2}{\partial \rho_2} = (1-\$_2)(4.233),$$

$$\frac{\partial \$_2}{\partial \varepsilon_1} = (1-\$_2)(0.129),$$

$$\frac{\partial \$_2}{\partial \varepsilon_2} = (1-\$_2)(0.034).$$

To calculate the standard deviation of $\$_2$, substitute the above values into Equation E3:

$$\delta_{\$_2} = (6.874)\left(0.493\delta^2_{\$_1} + 10.046\delta^2_{\rho_1} + 17.822\delta^2_{\rho_2} + 0.017\delta^2_{\varepsilon_1} + 0.012\delta^2_{\varepsilon_2}\right). \qquad \text{(E9)}$$

Since the various standard deviations are all of the same order of magnitude, it is concluded that the uncertainties due to ρ_1 and ρ_2, i.e. the $\left(\frac{\partial \$_2}{\partial \rho_1}\right)$ and $\left(\frac{\partial \$_2}{\partial \rho_2}\right)$ terms, are the predominate causes of the uncertainty in $\$_2$.

Since the terms $\left(\frac{\partial \$_2}{\partial \$_1}\right)$, $\left(\frac{\partial \$_2}{\partial \varepsilon_1}\right)$, and $\left(\frac{\partial \$_2}{\partial \varepsilon_2}\right)$ are negligible in Equation E3, it can be simplified to:

$$\delta_{\$_2} = \left(\left(\frac{\partial \$_2}{\partial \rho_1}\right)\delta^2_{\rho_1} + \left(\frac{\partial \$_2}{\partial \rho_2}\right)\delta^2_{\rho_2}\right)^{\frac{1}{2}}. \qquad \text{(E10)}$$

Equation E10 was used in the calculation of $\delta_{\$_2}$ for Tables 1 and 2. It was implemented in an algorithm, run on the IBM 360/75 digital computer.

XVI. APPENDIX F: THE LIMITATION OF ONE-DIMENSIONAL NUMERICAL REACTOR MODELS

It should be mentioned here that there is an implicit limitation in one-dimensional codes such as TASK. Specifically, the azimuthal heterogeneity of nuclear properties can not be modeled adequately.

Consider the cross-sectional view of the ZPPR assembly in Figure 18. Four identical neutron detectors (1, 2, 3 and 4) are located at the same radius and subtended by different polar angles. In the one-dimensional model (which reduces Figure 18 into the slab geometry of Figure 19), there is no distinction between the four detectors. If the core is homogeneous in the azimuthal direction within each radial zone, then the four detectors experience the same magnitude of neutron flux. In as much as the calculated detector response (the detector white noise and the PSD's) are concerned, they are the same for the four detectors. Under such circumstances, the cross power spectral density between detector pair 1-2, 1-3, 1-4, 2-3, 2-4 and 3-4 are the same.

In an experimental setup, the CPSD for pair 1-3 may be measured. In the one-dimensional model, the CPSD for pair 1-2 may be calculated instead. Under the condition that there is no azimuthal heterogeneity in all the radial zones, the CPSD for pair 1-2 and 1-3 are the same. In this special case, the one-dimensional model is adequate.

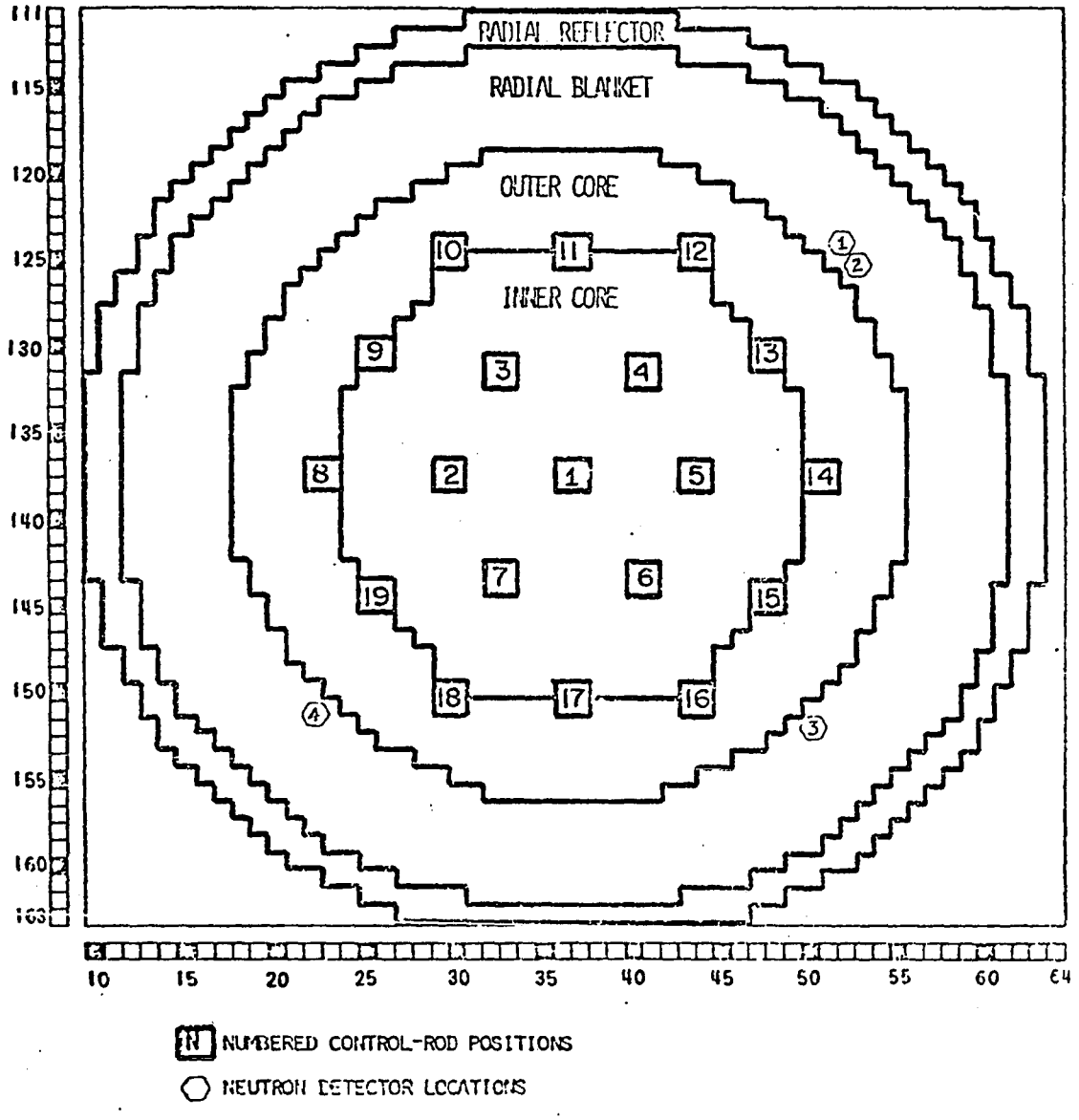

Figure 18. A cross-sectional view of detector and control rod locations

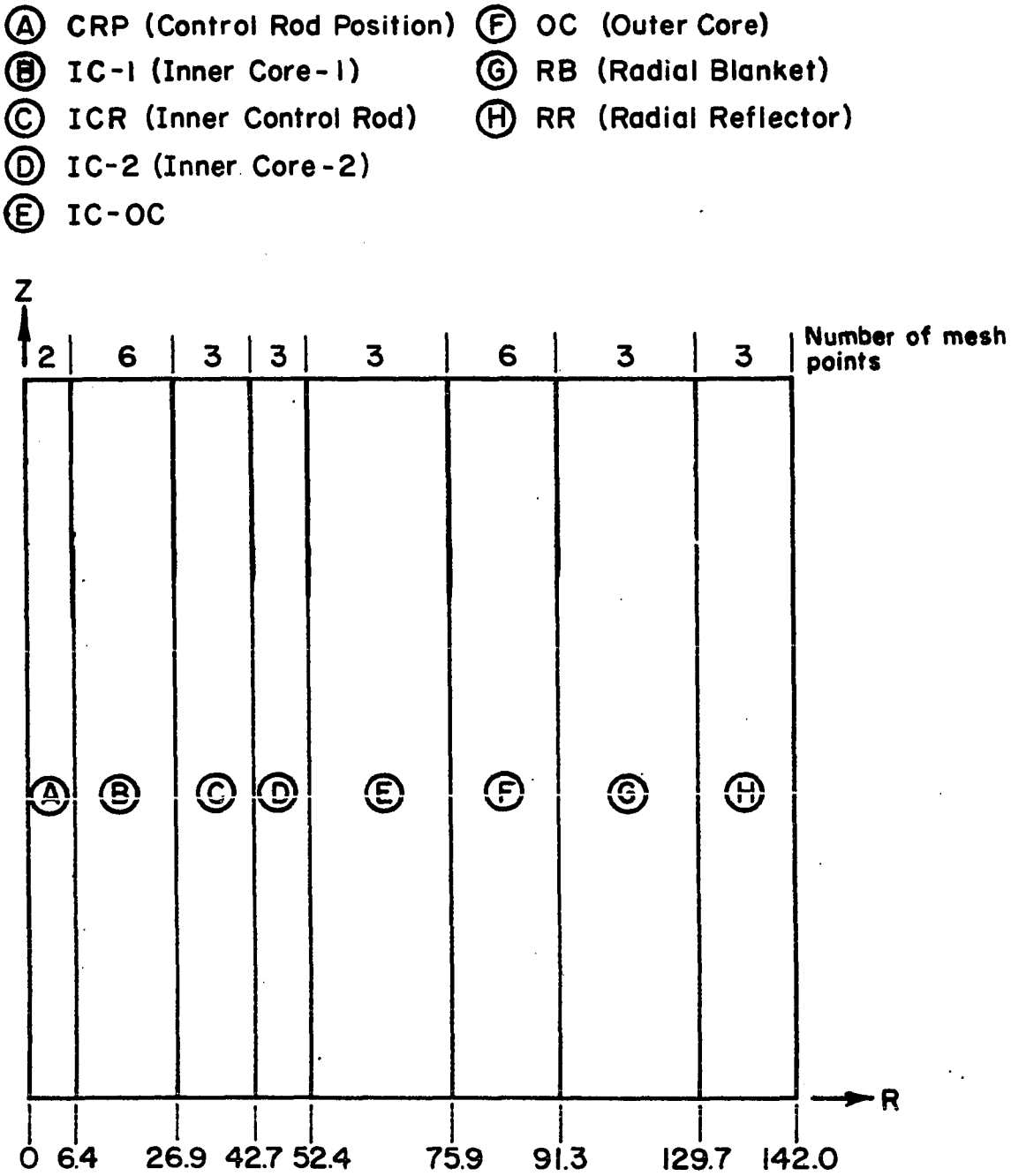

Figure 19. The slab model of ZPPR assembly 3 (all dimensions in cm)

However, if there is any azimuthal heterogeity in the radial zones, then the response of detector 1, 2, 3 and 4 may not be the same. The one-dimensional model does not account for this heterogeneous effect. Consequently, the calculated detector responses at different radial zones may not reflect the experimental conditions of the reactor core.

As an example, consider the experimental data of Table 3, p. 55, for run 5, 6, 7 and 8. The control rod was in the core center, i.e. CRP-1. There is no nuclear heterogeneity in each radial zone. Consequently, the 1-dimensional model is adequate in describing the various detector responses of the ZPPR core configuration. For run 3, 4, 9, 10, and 11, the control rod is in CRP-7 or CRP-17. As can be observed from Figure 18, such a core configuration is heterogeneous in the control rod zone. In particular, the one-dimensional model cross section for the ICR zone and the IC-OC zone were obtained by homogenizing (smearing out) the control rod cross section over the whole radial zone. Consequently, the calculated detector responses do not reflect those of detector 1, 2, 3 and 4. For these cases, the one-dimensional model for the ZPPR core is inadequate.

It should be pointed out that in a real physical reactor consisting of azimuthally homogeneous medium, the initiation and propagation of the fission chain may not be azimuthally symmetric at any given time. This is due to the statistical

nature of the fission process. Consequently, the correlations of the responses by detectors at the same radius but different polar angles are different also. The correlation decreases as the subcriticality increases. The reason being that the departure of the neutron flux distribution becomes more significant at far subcritical states. One dimensional neutronic codes such as TASK do not account for this effect. Therefore, computation by the one dimensional cylindrical geometry model of TASK does not accurately describe the system for far subcritical states.

XVII. APPENDIX G: THE FISSION PROBABILITY APPROACH [35, 55]

The polarity coherence function method is based on the fluctuation property of the detected signals. The fluctuation of the detected signal is the resultant of the fluctuation (variance) of the number of fissions in a chain, the fluctuation (variance) of the fission rate and the fluctuation (variance) of the count rate. By properly accounting for these three kinds of variances and relating them to the coherence function, a modified inference relation can be obtained that could explained the discrepancy between the results of the source multiplication method and the coherence function method mentioned previously.

Consider a reactor consisting of both Pu-239 and Pu-240. A fission chain can be initiated by either a delayed neutron or a fission neutron from Pu-240 spontaneous fission. For a near critical state, most fission chains are started by delayed neutrons whereas in the far subcritical states, spontaneous fission (sf) induced fission chains can predominate. The ratio of Pu-240 sf induced chains to delayed neutron induced fission chain is about -$. As an example, for the ZPPR core at -22$ subcritical, approximately 22 fission chains are started by Pu-240 spontaneous fission to every fission chain started by delayed neutron.

Let R be defined as:

$$R = \frac{\bar{\nu}'}{\bar{\nu}}$$

where ν' = number of neutrons emitted in a Pu-240 spontaneous fission

ν = number of neutrons emitted in a Pu-239 fission

Suppose a spontaneous fission of Pu-240 takes place, ν' neutrons are emitted in the manner of a pulse. This pulse of neutrons has a probability of initiating fission chain(s) upon the absorption by Pu-239. Assuming a point reactor kinetic model and ignoring the delayed neutron (of the spontaneous fission), the average number of fissions in the chain is:

$$N = 1 + \frac{RK_p}{1-K_p} \qquad \text{(G1)}$$

where N = average number of fissions in a chain

K_p = prompt multiplication factor = $(1-\beta)K$.

The one on the R.H.S. of Equation G1 refers to the starting event, i.e. the spontaneous fission, and the second term is the number of fissions from the first generation on to the termination of the chain. Derivation of Equation G1 is shown in Appendix H.

Let p_i be the probability of i fission in the first generation. The quantity $\sum_{i=o}^{\infty} p_i\, i$ is therefore the average number of fission in the first generation. One can further reason that the number of fissions in a chain is the summation of the propagation of fissions of all possible i (the number of fission in the first generation). Thus, it can be written

$$N = 1 + \sum_{i=o}^{\infty} p_i (i + kK_p + iK_p^2 + iK_p^3 + \ldots)$$

$$= 1 + \sum_{i=o}^{\infty} p_i \left(i + \frac{iK_p}{1-K_p} \right) . \qquad \text{(G2)}$$

Equations G1 and G2 are describing the same physical quantity. Combining these two equations yields the expression:

$$\sum_{i=o}^{\infty} p_i\, i = R\, K_p . \qquad \text{(G3)}$$

It is also necessary to consider the quantity $\sum_{i=o}^{\infty} p_i\, i^2$. This quantity can be interpreted as the mean square number of fissions in the first generation. It can be expressed as:

$$\sum_{i=o}^{\infty} p_i\, i^2 = K_p + K_p^2 \left(\frac{\overline{\nu^2} - \bar{\nu}}{\bar{\nu}^2} \right) . \qquad \text{(G4)}$$

Detailed derivation of Equations G3 and G4 are shown in Appendix I.

With the quantities $\sum_{i=o}^{\infty} p_i\, i$ and $\sum_{i=o}^{\infty} p_i\, i^2$ determined, the variance of the number of fissions in a chain can be defined.

Physically speaking, the variance of the number of fissions in a chain is due to two causes: (1) the fluctuation of the number of first generation fission(s), i and (2) the fluctuation of the number of fissions thereafter of the i first generation fission(s). The former can be written, in reference to Equations G1 and G2, as:

$$\delta_N'^2 = \overline{N^2} - \bar{N}^2 = \sum_{i=o}^{\infty} p_i \left[i + \frac{iK_p}{1-K_p} \right]^2 - \left[\frac{RK_p}{1-K_p} \right]^2 . \qquad \text{(G5)}$$

The latter is the variance of the number of fissions resulting from i first generation fission(s). It is therefore written as:

$$\delta_N''^2 = \left[\sum_{i=o}^{\infty} p_i\, i \right] \delta_N^2 \qquad \text{(G6)}$$

where δ_N = standard deviation of the number of fission in a Pu-239 delayed neutron initiated chain.

Equations G5 and G6 are referring to two independent fluctuations. The total fluctuation is therefore the sum of their quadrature, namely,

$$\delta_x^2 = \sum_{i=o}^{\infty} p_i \left(\left(i + \frac{iK_p}{1-K_p} \right)^2 - \left(\frac{RK_p}{1-K_p} \right)^2 + i\,\delta_N^2 \right) \qquad \text{(G7)}$$

where δ_x = standard deviation of the number of fissions of Pu-240 spontaneous fission initiated chain.

For purpose of simplification, consider a purely Pu-239 system, then R = 1 and Equation G7 reduces to:

$$\delta_N^2 = \frac{1}{1-K_p} \left[\sum_{i=o}^{\infty} p_i \left(i + \frac{i}{1-K_p} \right)^2 - \left(\frac{K_p}{1-K_p} \right)^2 \right] . \qquad \text{(G8)}$$

The derivation of the equivalent of Equation G8 and the subsequent correction of $\$_2$ for a mixed system of Pu-239 and Pu-240 is shown in Appendix J.

By applying the forgoing relation for $\sum_{i=o}^{\infty} p_i\, i$ and $\sum_{i=o}^{\infty} p_i\, i^2$ (Equations G3 and G4) and after suitable manipulation of Equation G8, the result follows

$$\delta_N^2 = \frac{K_p^2}{(1-K_p)^3} \left(\frac{1}{K_p} - 1 + \frac{\overline{\nu^2} - \bar{\nu}}{\bar{\nu}^2} \right) . \qquad \text{(G9)}$$

Equation G9 relates the variance of the number of fissions in a delayed neutron initiated chain to the prompt multiplication factor K_p (which determines the subcriticality). The variance of the fission rate as a result of the variance of

the number of fission per chain will be determined next.

For a delayed neutron initiated chain, let

N = number of fissions in a chain = $\frac{1}{1-K_p}$

F = number of fission per sec (of the whole reactor)

δ_N^2 = variance of number of fissions in a chain

$Z = F(1 - K_p)$ = number of chain generated per sec (of the whole reactor).

From the above definitions, it can be written

$$F = ZN \tag{G10}$$

i.e. fission rate = chain rate x number of fissions per chain.

From the classical technique of error propagation, the fission rate variance is

$$\delta_F'^2 = \left(\frac{\partial F}{\partial N}\right)^2 \delta_N^2 + \left(\frac{\partial F}{\partial Z}\right)^2 \delta_Z^2 = [\bar{F}(1-K_p)]^2 \delta_N^2 + \frac{\bar{F}}{1-K_p} \tag{G11}$$

where the relation of the variance of chain rate, $\delta_Z^2 = \bar{Z} = \bar{F}(1-K_p)$, has been employed.

For a real detection system, the fission rate variance consists of the "chain related" (correlated) fission rate variance and the "random" (uncorrelated) fission rate variance. The "chain related" fission rate variance is referring to the fissions that are from the same chain. Equation G11 describes the fission rate variance of the whole reactor, i.e. of all

chains. To reduce Equation G11 to describe the "chain related" property, the first term on the R.H.S. should be divided by the chain rate, namely $\bar{F}(1-K_p)$. The second term of Equation G11, i.e. $\bar{F}/(1-K_p)$, describes the "random" fission rate variance. This variance is due to all the chains that are present in the reactor. Thus, there is no need to divide this term by the chain rate. Applying the forgoing reasoning, the fission rate variance as "experienced" by the neutron detector is:

$$\delta_F^2 = [\bar{F}(1-K_p)]\delta_N^2 + \frac{\bar{F}}{1-K_p} \quad . \tag{G12}$$

Substituting Equation G9 into G12, the true fission rate variance is

$$\delta_F^2 = \bar{F}\,\frac{K_p^2}{(1-K_p)^2}\left[\frac{\overline{\nu^2} - \bar{\nu}}{\bar{\nu}^2} + \frac{1}{K_p^2} - 1\right] \tag{G13}$$

With the applicable fission rate variance defined in the above equation, the count rate variance may be determined.

By definition, the relation between the count rate and the fission rate is:

$$\dot{C} = WF \tag{G14}$$

$\dot{C}$ = counts/sec

F = fissions/sec

W = detector efficiency in counts rate/fission rate

The count rate variance due solely to the fission rate variance can be derived from Equation G14 and is written as:

$$\delta_1^2 = W\bar{\dot{C}} \frac{\delta_F^2}{\bar{F}} \tag{G15}$$

where δ_1^2 = correlated count rate variance (pile noise variance).

Substitution of Equation G13 to G15 yields:

$$\delta_1^2 = W\bar{\dot{C}} \frac{K_p^2}{(1-K_p)^2} \left[\frac{\overline{\nu^2} - \bar{\nu}}{\bar{\nu}^2} + \frac{1}{K_p^2} - 1 \right] \tag{G16}$$

Equation G16 can be viewed as the variance of correlated count rate.

In addition to the correlated count rate variance (which is due to the fission rate variance), there is an additional variance that is due to the inherent random statistical nature of the count rate. This variance (which is due to statistical uncertainty) is analogous to the variance of a Poisson distribution which characterizes the decay of radioactive nuclei. It is equal to the mean count rate:

$$\delta_2^2 = \bar{\dot{C}} \tag{G17}$$

where δ_2^2 = "random" count rate variance (white noise variance).

Equations G16 and G17 are two independent variables. The total count rate variance is therefore the sum of their quadratures:

$$\delta_C^2 = \delta_1^2 + \delta_2^2 = \bar{c} \left[1 + W \frac{K_p^2}{(1-K_p)^2} \left(\frac{\overline{\nu^2} - \bar{\nu}}{\bar{\nu}^2} + \frac{1}{K_p^2} - 1 \right) \right] . \quad \text{(G18)}$$

From the definition of coherence function (Equation 1) and the pile noise theory [41], the following relation between the coherence function and the count rate variances can be derived

$$\rho = \frac{\delta_1^2}{\delta_1^2 + \delta_2^2} . \quad \text{(G19)}$$

Rearranging the above equation and using the relation of Equations G16 and G17, Equation G19 becomes:

$$\left(\frac{\rho}{1-\rho} \right)^{\frac{1}{2}} = W^{\frac{1}{2}} \frac{(1-\beta)}{(1-\$)\beta} \left(\frac{\overline{\nu^2} - \bar{\nu}}{\bar{\nu}^2} + \frac{1}{K_p} - 1 \right)^{\frac{1}{2}} \quad \text{(G20)}$$

where $\$ = \frac{K-1}{K\beta}$.

Applying Equation G20 for a reference state 1 and a sub-critical state 2, the modified inference relation is obtained

$$\$_2 = 1 - (1-\$_1) \left(\frac{\beta_1}{\beta_2} \right) \left(\frac{W_2}{W_1} \right)^{\frac{1}{2}} \left(\frac{\rho_1}{1-\rho_1} \times \frac{1-\rho_2}{\rho_2} \right)^{\frac{1}{2}} C'^{\frac{1}{2}} \quad \text{(G21)}$$

$$\text{where} \quad C' = \frac{\dfrac{\overline{\nu^2} - \bar{\nu}}{\bar{\nu}^2} + \dfrac{1}{K_{p_2}^2} - 1}{\dfrac{\overline{\nu^2} - \bar{\nu}}{\bar{\nu}^2} + \dfrac{1}{K_{p_1}^2} - 1} \quad .$$

Without the presence of the correction factor $C'^{\frac{1}{2}}$, Equation G21 is identical to the more familiar form of the inference relation, Equation 14. For near critical measurements, $K_{p_2} \simeq K_{p_1} \simeq 1$, the correction $C'^{\frac{1}{2}}$ factor is almost unity. Equation G21 therefore reduces to Equation 14. If the measured state 2 is far subcritical (e.g. $K_{p_2} = 0.90$, $\$ \simeq -30$ for ZPPR), the correction factor $C'^{\frac{1}{2}}$ can modified the result ($\$_2$) by 14%.

XVIII. APPENDIX H: DERIVATION OF THE AVERAGE NUMBER OF FISSIONS IN A SPONTANEOUS FISSION INITIATED CHAIN

Consider the situation where a Pu-240 spontaneous fission takes place at time t = 0. The kinetic equation that describes the prompt neutron time behavior is:

$$\frac{dn}{dt} = \frac{K_p - 1}{\ell} n + \overline{\nu'} \delta(t) \tag{H1}$$

where ν' = number of neutron emitted in a Pu-240 spontaneous fission

ℓ = neutron lifetime.

The solution to Equation H1 is of the form of an exponential decay:

$$n(t) = \overline{\nu'} \; e^{\frac{K_p - 1}{\ell} t} . \tag{H2}$$

The fission rate of the reactor can be expressed as

$$F(t) = \delta_f \phi(t) = \frac{n}{\ell} \frac{K_p}{\bar{\nu}} \tag{H3}$$

where $\phi(t)$ = neutron flux in n/cm^2 sec

ν = number of neutrons emitted in a Pu-239 fission

δ_f = microscopic fission cross section.

Combination of Equations H2 and H3 yields:

$$F(t) = \frac{K_p}{\bar{\nu}} \overline{\nu'} \, e^{\frac{K_p - 1}{\ell} t} \quad . \tag{H4}$$

The number of fissions in a chain is the integral of the fission rate with respect to time. Therefore,

$$N = \int_o^\infty F(t)dt = \frac{RK_p}{1-K_p} \tag{H5}$$

where $R = \frac{\overline{\nu'}}{\bar{\nu}}$.

In addition to the number of fissions described above, there is the initiation fission that gives off the pulse of prompt neutron $\overline{\nu'}$. Therefore, the total number of fissions in a Pu-240 spontaneous fission initiated chain is:

$$N = 1 + \frac{RK_p}{1-K_p} \quad . \tag{H6}$$

XIX. APPENDIX I: DERIVATION FOR THE NUMBER OF FISSIONS IN A CHAIN AND THE QUANTITY $\sum_{i=o}^{\infty} p_i\, i^2$

Consider a pulse of fast prompt neutrons given off by a Pu-240 spontaneous fission. This pulse of fast neutrons then causes i first generation fission when captured by Pu-239. By definition of the prompt multiplication factor K_p, the number of fission in the second generation is $i\,K_p$, the third generation iK_p^2 etc. The n-th generation number of fissions is iK_p^{n-1}. Thus, the total number of fission (including the initiating event of the Pu-240 s.f.) is the summation of all possible i for all generations:

$$N = 1 + \sum_{i=o}^{\infty} p_i (i + iK_p + iK_p^2 + \ldots + iK_p^n + \ldots)$$

$$= 1 + \sum_{i=o}^{\infty} p_i \left[i + \frac{iK_p}{1-K_p} \right]. \qquad (I1)$$

The expression for $\sum_{i=o}^{\infty} p_i\, i^2$ will now be derived.

Physically, for every fission chain, the starting event (whether a Pu-240 spontaneous fission or a delayed neutron induced Pu-239 fission) has a certain distribution for the number of neutrons released. For example, Terrel [58] found that the neutron yield from a fission follows an exponentially

decreasing function. For purpose of clarity of symbols, the following are designated:

p_i = probability of i fission in the first generation

g_N = probability of N neutrons released in the starting event of a Pu-240 spontaneous fission or delayed neutron induced fission of Pu-239

ρ_f = probability of fission in the reactor when a neutron is released from the starting point.

To have a first generation fission, two dependent events have to happen: (1) one or more than one neutrons are emitted in the starting event, i.e. $N \geq 1$, (2) at least one of the neutrons from the starting event induces a fission in Pu-239. Thus, p_i is the end result of the dependent events of g_n and ρ_f.

Consider the following case: If K neutrons are chosen from a population of N neutrons for inducing fissions, then the probability of fission for a certain set of K and N is characterized by the binomial frequency function:

$$B(N,K) = \frac{N!}{K!(N-K)!} \rho_f^K (1-\rho_f)^{N-K} . \qquad (I2)$$

The summation of all allowable K neutrons in the above function B(N,K) is the binomial distribution:

$$C(N) = \sum_{K=1}^{N} B(N,K) = \sum_{K=1}^{N} \frac{N!}{K!(N-K)!} \rho_f^K (1-\rho_f)^{N-K} . \qquad (I3)$$

From the above consideration, the quantity $p_i\, i^2$ can be written as the square of the number of first generation fissions weighted by the binomial distribution. Accordingly, it follows that

$$\sum_{i=1}^{\infty} p_i i^2 = \sum_{N=1}^{\infty} g_N \sum_{K=1}^{N} K^2 \frac{N!}{K!(N-K)!} \rho_f^K (1-\rho_f)^{N-K} . \qquad (I4)$$

Expanding Equation I4 and rearranging as follows yields Equation I5,

$$\sum_{i=1}^{\infty} p_i i^2 = \sum_{N=1}^{\infty} g_N \left[(1)^2 \frac{N!}{1!(N-1)!} \rho_f^1 (1-\rho_f)^{N-1} + \sum_{K=2}^{N} K^2 \frac{N!}{K!(N-K)!} \rho_f^K (1-\rho_f)^{N-K} \right]$$

$$= \sum_{N=1}^{\infty} g_N \left(\frac{N!}{(N-1)!} \rho_f (1-\rho_f)^{N-1} + \sum_{K=2}^{N} \frac{N!}{(N-K)!} \rho_f^K (1-\rho_f)^{N-K} \left[\frac{1}{(K-1)!} + \frac{1}{(K-2)!} \right] \right)$$

$$= \sum_{N=1}^{\infty} g_N \left[\sum_{K=o}^{N-1} \rho_f^{K+1} (1-\rho_f)^{N-K-1} \frac{N!}{K!(N-K-1)!} \right.$$

$$\left. + \sum_{K=o}^{N-2} \rho_f^{K+2} (1-\rho_f)^{N-K-2} \frac{N!}{(N-K-2)!} \right]$$

$$\sum_{i=1}^{\infty} p_i i^2 = \sum_{N=1}^{\infty} g_N [\rho_f N + \rho_f^2 N(N-1)] \quad . \tag{I5}$$

Using the relations: $\bar{\nu} = \sum_{N=1}^{\infty} g_N N$, $\overline{\nu^2} = \sum_{N=1}^{\infty} g_N N^2$ and $\rho_f = \frac{\Sigma_f}{\Sigma_a} = \frac{K_p}{\bar{\nu}}$

where Σ_f = macroscopic fission cross section of the reactor

Σ_a = macroscopic absorption cross section of the reactor.

Equation I5 becomes:

$$\sum_{i=1}^{\infty} p_i i^2 = K_p + K_p^2 \frac{\overline{\nu^2} - \bar{\nu}}{\bar{\nu}^2} = K_p + K_p^2 D \tag{I6}$$

where D = Devin factor for Pu-239 $\simeq$ 0.8.

Equation I6 was derived based on the assumption that the $\bar{\nu}$ of the starting event is the same as those of the fission chain. This is true for a delayed neutron induced Pu-239 fission chains in ZPPR. For a chain that is started by a Pu-240 spontaneous fission, the following equation is obtained

$$\sum_{i=1}^{\infty} p_i i^2 = K_p \frac{\overline{\nu'}}{\bar{\nu}} + K_p^2 \frac{\overline{\nu'^2} - \overline{\nu'}}{\bar{\nu}^2}$$

$$= K_p R + K_p^2 R^2 D' \qquad \text{(I7)}$$

where D' = Diven factor for Pu-240 $\simeq 0.8$

$$R = \frac{\overline{\nu'}}{\bar{\nu}} \quad .$$

XX. APPENDIX J: CORRECTION FOR SUBCRITICAL REACTIVITY FOR A MIXED SYSTEM OF Pu-239 AND Pu-240

Consider a fission chain that is started by a Pu-240 spontaneous fission that releases ν' neutrons to cause i first generation fission (of Pu-239). The variance of the number of fissions for such a chain is expressed by Equation G7:

$$\delta_x^2 = \sum_{i=o}^{\infty} p_i \left(\left(i + \frac{iK_p}{1-K_p} \right)^2 - \left(\frac{RK_p}{1-K_p} \right)^2 + i\delta_N^2 \right) \qquad \text{(J1)}$$

where $_x$ = standard deviation of the number of fissions in a Pu-240 spontaneous fission initiated chain

$_N$ = standard deviation of the number of fissions in a delayed neutron initiated fission chain

$$R = \frac{\overline{\nu'}}{\bar{\nu}}$$

From Equation G9, the relation for δ_N^2 was found to be:

$$\delta_N^2 = \frac{K_p^2}{(1-K_p)^3} \left[\frac{1}{K_p} - 1 + \frac{\overline{\nu^2} - \bar{\nu}}{\bar{\nu}^2} \right]. \qquad \text{(J2)}$$

From Equation G3 and I7, the following relations were derived for a Pu-240 spontaneous fission initiated chain:

$$\sum_{i=o}^{\infty} p_i i = R K_p \qquad \text{(J3)}$$

$$\sum_{i=o}^{\infty} p_i i^2 = R\,K_p + R^2 K_p^2 \left(\frac{\overline{\nu'^2} - \bar{\nu}'}{\bar{\nu}'^2} \right) \tag{J4}$$

Substituting Equations J2, J3 and J4 into Equation J1 yields

$$\delta_x^2 = \frac{K_p^2}{(1-K_p)^3} \left[\frac{\overline{\nu^2} - \bar{\nu}}{\bar{\nu}^2} R\,K_p + \frac{\overline{\nu'^2} - \bar{\nu}'}{\bar{\nu}'^2}(1-K_p)R^2 + R\left(\frac{1-K_p}{K_p}\right) + R(1-R)(1-K_p) \right] \tag{J5}$$

In the same manner as the variance of the fission rate of a purely Pu-239 system was determined in Equation G13, it is found that

$$\delta_F^2 = \bar{F} \left[\frac{K_p^2}{(1-K_p)^2} \frac{1}{(1-K_p + RK_p)} M + \frac{1-K_p + RK_p}{1-K_p} \right]$$

where

$$M = \frac{\overline{\nu^2} - \bar{\nu}}{\bar{\nu}^2} R\,K_p + \frac{\overline{\nu'^2} - \bar{\nu}'}{\bar{\nu}'^2}(1-K_p)R^2 + R\left(\frac{1-K_p}{K_p}\right) + R(1-R)(1-K_p) \tag{J6}$$

The first term of Equation J6 describes the "correlated fission rate variance" that is due to the same fission chain only. The second term of Equation J6 describes the "random" fission rate variance that is due to all the fission chains

present. These two components of the total fission rate variance are independent.

With the fission rate variance defined, the count rate variance can be determined. Using the same relation and notation of Equations G13 and G14 yields

$$\delta_1^2 = \bar{\dot{W}}\bar{\dot{C}} \left[\frac{K_p^2}{(1-K_p)^2} \frac{1}{(1-K_p + RK_p)} M + \frac{1-K_p + RK_p}{1-K_p} \right] \qquad \text{(J7)}$$

where δ_1^2 = correlated count rate variance (pile noise variance).

In addition to the pile noise variance, there is the constant background of the white noise variance. The white noise variance is due to the random statistical nature of the count rate and is expressed as:

$$\delta_2^2 = \bar{\dot{C}} \qquad \text{(J8)}$$

where δ_2^2 = uncorrelated count rate variance (white noise variance).

With the same line of reasoning as in Equations G19 and G20, it follows that the inference relation for a mixed system of Pu-239 and Pu-240 is

$$\$_2 = 1 - (1-\$_1) \left(\frac{\beta_1}{\beta_2} \right) \left(\frac{W_2}{W_1} \right)^{\frac{1}{2}} \left[\frac{\rho_1}{1-\rho_1} \times \frac{1-\rho_2}{\rho_2} \right]^{\frac{1}{2}} C'^{\frac{1}{2}}$$

$$\text{where} \quad C' = \frac{K_{p_2}^2 M_2 + (1-K_{p_2})(1-K_{p_2}+RK_{p_2})^2}{(1-K_{p_2}+RK_{p_2})K_{p_2}^2} \times \frac{(1-K_{p_1}+RK_{p_1})K_{p_1}^2}{K_{p_1}^2 M_1 + (1-K_{p_1})(1-K_{p_1}+RK_{p_1})^2} \qquad (J9)$$

and M_1, M_2 are defined in Equation J6.

If $\nu' = \nu$, $R = 1$ (i.e. a purely Pu-239 system), then Equation J9 reduces to Equation G21. If both the reference state and the measured state is near critical, i.e. $K_{p_2} \simeq K_{p_1} \simeq 1$, then $M_2 \simeq M_1 = D$ and the correction factor C reduces to unity. Thus, for near critical cases, Equation J9 becomes the more familiar form of Equation 14. At the far subcritical case cf $K_{p_2} = 0.9$, $\$_2 \simeq -30$, the correction factor C' would modify the result ($\$_2$) by approximately 18%.

To conclude, in as much as the inference of subcritical reactivity is concerned, the presence of the spontaneous fission source (Pu-240) in the multiplying medium of Pu-239 causes no noticeable effect at near critical states. At far subcritical states, the presence of Pu-240 in a mixed system of Pu-239 and Pu-240 causes the inferred subcriticality to be larger than for a purely Pu-239 system.

XXI. APPENDIX K: DERIVATION OF THE MODIFIED INFERENCE RELATION BY THE BINARY SOURCE APPROACH

Consider a two-channel neutron noise analysis system in a reactor. The cross-correlation of the two-channel detector signals is shown schematically in Figure 20. The instrumentation in the two channels are assumed to be identical.

For a given binary source, $S_2(r_1, r_2)$, the cross-correlation of the signals can be written as:

$$\overline{x \cdot y} = \bar{x} \cdot \bar{y} + 2 \int dr_1 dr_2 \, S_2(r_1, r_2) \times \int dt \, g(r_1,t) g(r_2,t) \tag{K1}$$

where $\overline{x \cdot y}$ = cross-correlation of output signal from channel x and y

$\bar{x}$, $\bar{y}$ = time-averaged output signal of channel x, y due to steady state, single neutron

$S_2(r_1, r_2)$ = binary source producing (r_1, r_2)-pairs of neutrons

$g(r_n, t)$ = signal response of the detection channel to the injection of one r_n neutron (i.e. convolution of the system response).

Applying the Fourier transformation to the above equation yields the power spectral density. Consequently, Equation K1 becomes:

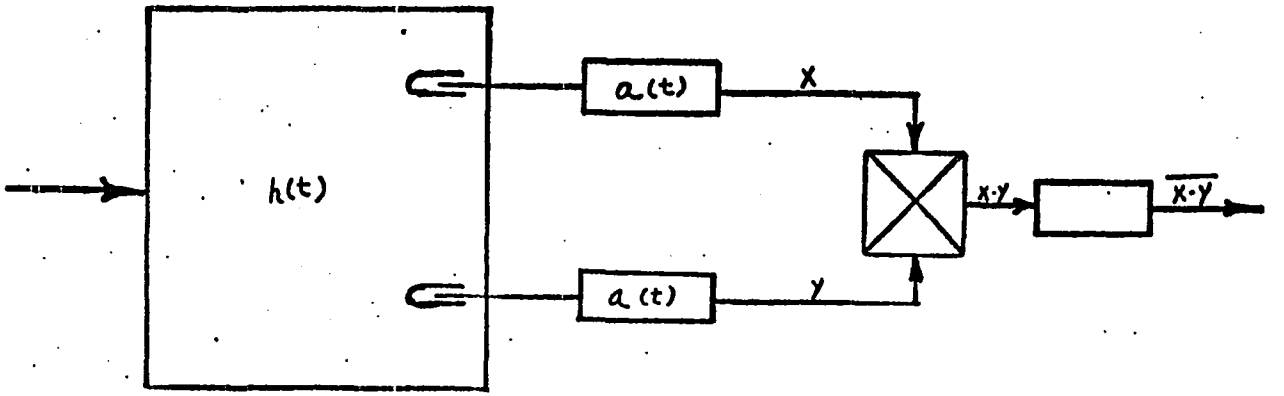

Figure 20. Schematic diagram of a correlation experiment with two channels

$$\Phi_{xy}(\omega) = \overline{x_\omega}\ \overline{y_\omega} + 2 \int dr_1 dr_2 S_2(r_1,r_2) \times \int \frac{d\omega}{2\pi} G(r_1,\omega)G(r_2,\omega) \qquad (K2)$$

where $\Phi_{xy}(\omega)$ = cross power spectral density of channel x and y

$\overline{x_\omega}$, $\overline{y_\omega}$ = Fourier-transformed output of the mean signal $\bar{x}$, $\bar{y}$

$G(r_n,\omega)$ = Fourier-transform of the response function $g(r_n,t)$.

With regard to the frequency analysis experiment, two assumptions can be made at this point to simplify the solution of Equation K2:

1) the point kinetic model is valid and therefore no spatial dependence effect are accounted for
2) the neutron sampling time is short enough (less than 10^{-2} sec) such that, for all practical purposes, there is no delayed neutron effect.

Accordingly, the response of the neutron population to the injection of a neutron into the reactor is described by the point kinetic equation:

$$\frac{d}{dt} h(t) = \frac{K(1-\beta)-1}{\ell} h(t) + \delta(t) \qquad (K3)$$

where β = total delayed neutron fraction

ℓ = prompt neutron life-time

$h(t)$ = response of neutron population to the injection of one prompt neutron

K = effective multiplication constant.

The Fourier transform of the response function is known as the reactor transfer function. It is written as:

$$H(\omega) = \frac{1}{\alpha + i\omega}$$

or

$$|H(\omega)|^2 = \frac{1}{\alpha^2 + \omega^2} \qquad \text{(K4)}$$

where $\alpha = \frac{1-K(1-\beta)}{\ell}$ = break frequency (roll-off frequency).

In the coherence function measurements, the selected frequency range is much less than the break frequency. Thus, $\alpha >> \omega$ and Equation K4 can be simplified to:

$$|H(\omega)|^2 = \frac{\ell^2}{(1-K_p)^2} \qquad \text{(K5)}$$

where $K_p = K(1-\beta)$.

The response function of the whole neutron multiplication and detection system can be written as

$$g(r_n,t) = \frac{WK_p}{\nu\ell} \int dt_1 h(t_1) a(t-t_1) \qquad \text{(K6)}$$

where W = neutron detector efficiency in detection per fission

ν = number of neutron released per fission

$a(t)$ = detection network response.

Equation K6 describes the response of the detector signal as one neutron is introduced into the reactor. The weighting function, $a(t-t_1)$, depends on the electronics of the detection system.

Application of the Fourier transform to Equation K6 yields

$$G(\omega) = \frac{WK}{\nu \ell} H(\omega)A(\omega) \tag{K7}$$

where $A(\omega)$ = detection transfer function.

The detection transfer function can be expressed as:

$$A(\omega) = qB(\omega) \tag{K8}$$

where q = charge released per detection

$B(\omega)$ = characteristics of the band pass filter.

In frequency analysis (and polarity coherence function) experiments, $B(\omega)$ is zero except in the limited band width range. Thus, the experimental conditions are:

$B(\omega)$ = constant $\neq 0$ for $\omega_1 < \omega < \omega_2$

$B(\omega) = 0$

$\Delta\omega = \omega_2 - \omega_1$ = band width of the tunable band limited filter.

It is recognized that the limited band pass filtered steady state signal $\bar{x}_\omega$, $\bar{y}_\omega$ are zero. Applying Equations K5, K7 and K8 to Equation K2 yields

$$\Phi_{xy}(\omega) = 2 \int dr_1 dr_2 \, S_2(r_1,r_2) \left(\frac{WK_p}{\nu\ell}\right)^2 \bar{q}^2 \left(\frac{\ell}{1-K_p}\right)^2 |B(\omega)|^2 \left(\frac{\Delta\omega}{2\pi}\right). \quad \text{(K9)}$$

In addition to the cross power spectral density described by Equation K9, there is the constant background of the white noise. The white noise is due to the random detection of the constant fission rate and is uncorrelated in the two channels. However, it does appear in the one-channel measurement. Therefore, for the auto power spectral density, it consists of the signal and the white noise and is often written as:

$$\Phi_{ii}(\omega) = WF\,\overline{q^2}|B(\omega)|^2\left(\frac{\Delta\omega}{2\pi}\right) + 2\int dr_1 dr_2 S_2(r_1,r_2) \left(\frac{\bar{W}\bar{K}}{\nu\ell}\right)^2 \bar{q}^2 |B(\omega)|^2\left(\frac{\Delta\omega}{2\pi}\right) \quad \text{(K10)}$$

where F = fission rate in the whole reactor

i = x, y.

Equation 27 defines a binary source that includes the three effects: (1) neutron pairing from a population of ν neutrons of the same fission, (2) neutron pairing from multiple generation neutrons of the same chain, and (3) the presence of

extraneous spontaneous fission sources (Pu-240 and/or Cf-252). The total fission rate expressed by Equation 22 is:

$$F = S_o\left[\frac{K_p}{1-K_p}\cdot\frac{1}{\nu}+\frac{1}{\nu'}\right] . \qquad (K11)$$

Substitution of Equations 27, K11 into Equations K9 and K10 yields:

$$\Phi_{xy}(\omega) = \frac{W^2K_p^2}{(1-K_p)^2}\,\bar{q}^2\,S_o\left[\frac{K_p}{(1-K_p)\nu}D+\frac{R}{\nu}D'+\frac{\nu}{K_p}\right]\,|B(\omega)|^2\left(\frac{\Delta\omega}{2\pi}\right) \qquad (K12)$$

$$\Phi_{ii}(\omega) = S_o\,\overline{q^2}\,W\left[\left(\frac{K_p}{1-K_p}\frac{1}{\nu}+\frac{1}{\nu'}\right)+\frac{W\,K_p^2}{Q(1-K_p)^2}\left[\frac{K_p\,D}{(1-K_p)\nu}+\frac{RD'}{\nu}+\frac{\nu}{K_p}\right]\right]\,|B(\omega)|^2\left(\frac{\Delta\omega}{2\pi}\right)$$

$$i = x,\ y. \qquad (K13)$$

Referring to the definition of the coherence function, Equation 1, and using the relation of the power spectral densities of Equations K12 and K13, the new expression for the coherence function is:

$$\rho(\omega) = \frac{\dfrac{W}{\beta^2(1-\$)^2}\left[\dfrac{K_p}{(1-K_p)\nu}D+\dfrac{R}{\nu}D'+\dfrac{\nu}{K_p}\right]}{\left[Q\left(\dfrac{K_p}{1-K_p}\dfrac{1}{\nu}+\dfrac{1}{\nu'}\right)+\dfrac{W}{(1-\$)^2}\left[\dfrac{K_p\,D}{(1-K_p)\nu}+\dfrac{RD'}{\nu}+\dfrac{\nu}{K_p}\right]\right]} . \qquad (K14)$$

Applying the above equation a reference state 1 and a measured state 2, and combining the two equations yields

$$\$_2 = 1 - (1-\$_1)\left(\frac{\beta_1}{\beta_2}\right)\left(\frac{W_2}{W_1}\right)^{\frac{1}{2}}\left(\frac{\rho_1}{1-\rho_1} \times \frac{1-\rho_2}{\rho_2}\right)^{\frac{1}{2}} C'^{\frac{1}{2}} \qquad \text{(K15)}$$

where $$C' = \frac{DK_{p_2} + (1-K_{p_2})RD' + \left(\frac{1-K_{p_2}}{K_{p_2}}\right)}{DK_{p_1} + (1-K_{p_1})RD' + \left(\frac{1-K_{p_1}}{K_{p_1}}\right)} \times \frac{1-K_{p_1}(1-R)}{1-K_{p_2}(1-R)} .$$

To summarize, assuming a point kinetic model and no delayed neutron effect, an inference relation for $\$_2$ can be derived from a two-channel cross correlation experiment. By properly defining the binary source to account for the multiple generation of fissions and the extraneous source, a modified form of the inference relation as shown by Equation K15 can be obtained. This equation reduces to the conventional form of Equation 14 when the binary source consists only of one fission in each detection sampling.